Ozone Deposition, Scalar Budgets and Radiative Heating over Texas Coastal Forest and Ocean

By
Stephan Randolph Kawa

Department of Atmospheric Science
Colorado State University
Fort Collins, Colorado

Colorado State University

Department of Atmospheric Science

Paper No. 398

OZONE DEPOSITION, SCALAR BUDGETS AND RADIATIVE HEATING OVER TEXAS COASTAL FOREST AND OCEAN

by

Stephan Randolph Kawa

Research supported by the
National Science Foundation
under Grants ATM 8114575
and ATM 8312615.

Department of Atmospheric Science
Colorado State University
Fort Collins, Colorado

April 1986

Atmospheric Science Paper No. 398

ABSTRACT

This study reports the results from analysis of data obtained during a field experiment conducted near Houston, Texas, in June of 1982. The measurements were made from an instrumented aircraft flying in and above the planetary boundary layer. The available instrumentation made it possible to measure vertical fluxes of heat, moisture, momentum, and ozone using the eddy correlation technique, as well as to measure components of the net atmospheric radiative flux. The flight plan admitted calculation of the relevant ozone deposition parameters (surface flux, deposition velocity, and surface resistance), the significant terms in the budget of an atmospheric scalar variable including the net in situ source/sink term, and the divergence of the net radiative flux. The results from several flights are presented concentrating on those over open ocean water in the Gulf of Mexico and the extensive, vigorous forests in the area of the Big Thicket National Preserve in eastern Texas.

The results of the analysis for ozone deposition show that the forest surface is a very active sink for ozone during daytime convective conditions. The surface flux in three cases is near 1.0 $\mu g\ m^{-2}\ s^{-1}$. The deposition velocities are measured in the range of 11 to 12 $mm\ s^{-1}$ and surface resistances are 55 to 60 $s\ m^{-1}$. The flux of ozone to the ocean surface is found to be very near zero during conditions of low wind and nearly calm seas.

The analysis of budgets for three different cases indicates that the magnitude of the various terms may depend on the relative influence of differing air mass sources: urban, rural, and marine. For the marine case all the budget terms are small and the net source/sink term is near zero for sensible heat, water vapor, and ozone. For the forest case exhibiting rural characteristics the heat and ozone source/sink terms are relatively small. For the case over forest under fairly direct advection from the Houston urban area there is an in situ production of ozone of about 14 ppb hr^{-1} and a heat source of about 0.5 K hr^{-1}. The boundary layer heating rate implied by the measured divergence of the net radiative flux nearly balances the source calculated in the sensible heat budget for each case. This heating is attributed to absorption of sunlight by components of the atmospheric aerosol advected from the Houston area. The ozone source is attributed to photochemical production from precursors such as are found in an urban plume. Other results which are presented include examples of time series, mean vertical profiles, spectra and cospectra, vertical and horizontal flux profiles, radiation profiles calculated by a radiative transfer model, and comparison of the measured absorptances to those predicted by a model for various types of aerosol.

ACKNOWLEDGEMENTS

This material is based upon work supported by the National Science Foundation under Grants No. ATM 8114575 and ATM 8312615. Aircraft time and computer support were provided, respectively, by the Research Aviation Facility and the Scientific Computing Division of the National Center for Atmospheric Research. The National Center for Atmospheric Research is sponsored by the National Science Foundation.

TABLE OF CONTENTS

1. INTRODUCTION

The planetary boundary layer is the lowest layer of the atmosphere, generally a few tens to hundreds of meters in depth. As such, it is the atmosphere in which most living things live and breathe; it is our interface with the atmosphere. The processes that determine the state of the boundary layer in relation to temperature, chemical composition, radiation, humidity, and air motion are clearly of vital importance. One of the most important trace constituents of the boundary layer, due to its key role in photochemical smog production, is ozone. Ozone sources and sinks in the planetary boundary layer are a major factor in determining pollution control strategies. The rate of ozone destruction at the surface is a key parameter in the tropospheric ozone budget, in photochemical pollution modeling, and assessment of oxidant impact on crops and vegetation.

An area which merits special attention for its interaction with boundary layer ozone is forest. Forests cover about 8% of the earth's surface (Seiler and Crutzen, 1980) and are known to interact strongly with atmospheric processes involving radiation, moisture, momentum, and chemistry. Forests are sources of atmospheric hydrocarbons which may play an important part in pollution production in rural areas (Dimitriades, 1981; Zimmerman, 1979a, 1979b). On the other hand, the surface resistance of forest to ozone uptake may be as much as a factor of two lower than previously estimated (Lenschow, 1982) implying a very active sink for boundary layer ozone. Ozone budgets and deposition are

difficult to measure directly however, and reliable experimental data for these parameters are scarce, especially over forest and ocean surfaces. An additional topic of interest in the planetary boundary layer over forest for which measurements are scarce is the interaction of the polluted urban atmosphere and the components of the boundary layer radiative flux. The motivation for this research is the need for further experimental results to increase our understanding of these critical processes near the earth-atmosphere interface.

In June, 1982, a group from Colorado State University headed by Dr. R. Pearson, Jr. performed an experiment to measure certain atmospheric variables in the planetary boundary layer near the area of Houston, Texas. The measurements were made from an aircraft in conjunction with scientists and staff from the National Center for Atmospheric Research (NCAR). The instrumentation measured mean and turbulent fluctuations of winds, water vapor, temperature and ozone as well as mean components of the radiative flux, and various other parameters. The purpose of the experiment was to gather data for several applications, concentrating on the boundary layer over open ocean in the Gulf of Mexico and the extensive, vigorous forests of the coastal plain. One objective of the experiment was to extend the established set of measurements of ozone deposition parameters to the forest and ocean surfaces. Reliable measurements of this type, especially over forests, include very few cases as discussed in the background section below. In addition to ozone surface deposition, further information on the chemical and physical interactions between the forest biosphere and the atmosphere are needed. To this end, the experiment was designed to allow calculation of budgets for ozone, heat, and moisture in the boundary layer overlying the

forest. From these, the relative importance of the various terms including the sources and sinks of the scalars can be analyzed. The treatment of ozone as an atmospheric scalar variable has been demonstrated by Lenschow, et al. (1980a, 1981, 1982). The experiment also gathered information on the boundary layer processes of entrainment, advection, three-dimensional distribution and transport of scalar variables, and propagation and extinction of solar and terrestrial radiation.

The chief purpose of this paper is to present the results of the Texas experiment, concentrating on three of the more interesting cases. The principal results reported here are values for the ozone surface deposition parameters (surface flux, deposition velocity, and surface resistance), the scalar budgets of ozone, potential temperature, and absolute humidity, and the fluxes and divergences of the components of the radiative flux. Sections 2 and 3 discuss previous measurements related to this experiment and the methodology of the experiment. There is also a rather detailed exposition of the underlying theory and the methods used to calculate the various results. This Sec. 4 is intended to make it possible to see exactly how the calculations were done in order to judge their validity and to reproduce them if desired. The analysis of the radiative fluxes has been extended with the use of radiative transfer model calculations and has compared measured absorptances with those predicted by a model for aerosol optical properties. These results are also included in Sec. 5.

2. BACKGROUND

The importance of ozone in the troposphere has been recognized for many years. The earliest works considered that ozone was injected from the stratosphere, was transported passively through the troposphere, and was destroyed at the surface (Junge, 1962). Numerous studies support this view, for example Chatfield and Harrison, 1977; Singh, et al., 1978; Danielson and Mohnen, 1977. A significant photochemical production and destruction of ozone has also been proposed by a number of investigators (Chameides and Walker, 1973; Fishmen and Crutzen, 1977, 1978). Recent studies generally seem to favor the view that both photochemistry and transport control the distribution of ozone within the troposphere (Gidel and Shapiro, 1980; Liu, et al., 1980; and Levy, et al. 1985). The rate of ozone destruction at the surface is a key factor in determining the roles of both photochemistry and transport.

2.1 Ozone Deposition

During recent years there has been a considerable interest in the problem of determining the rate of destruction of atmospheric ozone at the earth's surface. The surface destruction rate parameter has important applications in a number of fields such as air pollution modeling and global atmospheric chemistry budgets, and the current literature reflects this importance. The measurement of ozone deposition remains, however, a difficult experiment to perform due to the extreme variability of surface and aerodynamic conditions near the earth-atmosphere

interface. The experiment has been performed in a number of different ways, over a wide variety of conditions with widely varying results. Review papers by McMahon and Denison (1979) and Sehmel (1980) have collected many of these measurements and the values differ greatly even for reports on similar surfaces. In this section we will examine some of the reported measurements, the different methods used to obtain them, and how the present set of measurements fits into this context.

There are, at present, three popular methods to measure the surface flux of ozone. The first of these, referred to as the "box method," measures the time rate of change of the ozone concentration within a fixed volume of air over the surface of interest. The volume and surface area are generally fixed by a container whose sides and top are constructed of material that is relatively inert toward ozone. Clearly the main shortcoming of this method is that conditions within the box are not likely to be representative of actual mixing conditions and possibly plant respirational process. The box method would not be practical to study a forest, although it has been widely used over other surfaces (Regener and Aldaz, 1969; Aldaz, 1969; Hill, 1971; Galbally and Roy, 1980).

The second widely used flux measurement technique, the profile method, uses a vertical array of sensors to measure the ozone concentration gradient above the surface and the vertical eddy diffusivity. The flux is then found using the integral of the familiar equation

$$F = -K_{O_3}(\partial \bar{O}_3/\partial z) \qquad (2.1)$$

Here F is the vertical ozone flux, positive upward, K_{O_3} is the eddy diffusivity for ozone and $\bar{O}_3$ is the mean ozone concentration at height z. This method is also referred to as K-theory or first order closure.

Discussion on the application of this method may be found in Panofsky and Dutton (1984), chapter 4 and Pielke (1984), chapter 7, and the references contained therein. Measurements of ozone deposition by the profile method are found in Galbally (1971), Van Dop et al. (1977), and Garland and Derwent (1979). While being fairly easy to set up, this type of measurement may encounter difficulty accurately measuring small vertical gradients within the constant flux layer and usually involves the use of some rather elaborate assumptions to determine K_{O_3} (Businger, 1985). This method also does become somewhat more difficult to deploy in a mature forest. Some of the difficulties in applying the profile method over forest are discussed in Raupach (1979) and Tajchman (1982).

The third method, the eddy correlation technique, has been used for the experiment related here. In this method the fast-response fluctuations of ozone and vertical wind are measured simultaneously. The product of the instantaneous departure from the mean of ozone and vertical velocity is averaged over an appropriate time period to give the flux. This method is described further in Sec. 4.3. The development of fast-response, high sensitivity measuring systems for ozone, winds, temperature, and water vapor has allowed this method to be applied with great success in many different conditions. The eddy correlation technique has been used to determine fluxes of momentum, heat, and water vapor for some time (Kaimal, et al., 1972; Dyer and Hicks, 1970; McBean and Miyake, 1972). The recent development of a very responsive ozone detector (Pearson and Stedman, 1980; Pearson, in preparation) and aircraft mounted wind gust probes (Lenschow et al., 1981) have made it possible to carry out eddy correlation measurements from an aircraft throughout the planetary boundary layer. This greatly increases the

range of surfaces we can represent and is particularly effective for measurements over forest. The data obtained in this experiment were all gathered using low level aircraft flight patterns.

Previous measurements of ozone deposition using the eddy correlation technique from an aircraft over forest may be found in Lenschow et al. (1982) and Greenhut et al. (1983). Other measurements over forest have been done using eddy correlation instruments on a stationary tower. Hicks et al. (1982) reported results from a pine plantation and Wesely et al. (1983) used a similar set up at a bare, wintertime deciduous forest. Results from these experiments are discussed in Sec. 5.5.

The eddy correlation flux measurement technique has been widely used to measure ozone deposition over vegetation other than forests. Aircraft measurements over Colorado short-grass prairie may be found in Lenschow et al. (1980a, 1981) and Pearson et al. (1982). Tower based measurements are reported by Wesely et al. (1978) over maize and Wesely et al. (1982) over soybeans. Finally, aircraft measurements over water are found in Lenschow et al. (1982) for the Gulf of Mexico and the North Pacific ocean while Wesely et al. (1981) report tower measurements over lake water, snow and bare soil. These results are also compared in Sec. 5.5.

It is difficult to compare ozone deposition parameters measured by different experiments since they are often referred to different measurement levels, mean ozone concentrations, stability conditions, and surface states. From the literature reviewed here, however, several conclusions may be drawn. First, modern instrumentation has made direct measurement by eddy correlation the most widely applicable technique and that which gives the most consistent results. Second, this technique

can be used effectively from an aircraft over a variety of surfaces including forests. Third, the values of deposition velocity and surface resistance measured in this experiment over Texas Gulf Coast forest fit into the range of previously measured values at a position of high deposition velocity and low surface resistance that would be expected for such vegetation.

2.2 Budgets

The reliable measurement of scalar budgets in the planetary boundary layer is a difficult experiment to perform and only a few cases are reported in the literature. Lenschow et al. (1980a) attempted to measure the ozone budget over Colorado grassland but were not able to measure all the terms accurately enough to estimate the residual source/sink term. Two later budget measurements over Colorado shortgrass prairie (Lenschow et al., 1981 and Pearson et al., 1982) were successful and gave very similar results. Lenschow et al. (1982) measured ozone budgets over the Gulf of Mexico and found source terms about an order of magnitude smaller than the grassland results.

Aircraft measurements of humidity as well as potential temperature (or sensible heat) budgets are reported in Lenschow et al. (1981) and Pearson et al. (1982). Other aircraft measurements of potential temperature budgets may be found in Lenschow et al. (1980b) and Lenschow (1970). It should be noted that each of these temperature budgets balances to a net source term of less than 0.1 mK s^{-1}.

2.3. Radiative Heating

The effect of aerosol on radiative processes has been widely studied by analysis of models and measurements. Actual measurements of the effects are relatively scarce, however. Roach (1961) measured solar radiation with an aircraft over the English Channel. He concluded that heating rates of 0.14 mK s^{-1} (0.5 °C hr^{-1}) may occur over heavily polluted areas and that heating in excess of 0.06 mK s^{-1} (0.2 °C hr^{-1}) were not uncommon over the English channel. He also inferred that large heating rates were due to absorption of sunlight by aerosol pollution from London. De Luisi et al. (1976) have measured the effects of aerosol haze on radiative flux in conditions where the aerosol is likely to be rural in origin and have concluded that the heating by aerosol absorption is about one half that by water vapor absorption in the arid Southwest U.S.. Idso (1981) has used measurements at Phoenix, AZ to show that the net aerosol effect on near surface temperature may depend on the particle concentration and is not clearly positive or negative, although warming is likely. Ackerman and Cox (1982) have found that the dust laden air over the Saudi Arabian desert exhibits a heating by net radiative energy convergence of up to 0.06 mK s^{-1} (0.2 °C hr^{-1}) due to aerosol absorption. Method and Carlson (1982) studied radiative heating rates in the St. Louis, MO area and concluded that the net aerosol effects were small, about 0.01 mK s^{-1} (0.04 °C hr^{-1}) near midday in the planetary boundary layer. Their results were an average, however, over 20 flights including boundary layer winds from all directions. Many of these flights probably sampled air of rural origin. Their maximum heating rate was about 0.03 mK s^{-1} (0.12 °C hr^{-1}).

Model results for aerosol-induced heating in the planetary boundary layer are more plentiful. Atwater (1971) did model calculations for aerosol and gaseous absorption. He found NO_2 and aerosol, characteristic of polluted conditions, to have the largest heating effect, approaching or exceeding heating rates due to water vapor absorption (about 0.03 mK s^{-1} or 0.1 °C hr^{-1} near noon). Mitchell (1971) included the effect of aerosol extinction on the eddy flux heating of the lower boundary layer along with the direct radiative heating and found that net heating or cooling depended on the ratio of aerosol absorption to backscatter as well as surface properties. Braslau and Dave (1975) found a maximum heating rate of about 0.04 mK s^{-1} (0.14 °C hr^{-1}) in the lower boundary layer near noon for absorption of solar radiation by partly absorbing aerosol of a "heavy" distribution. Liou and Sasamori (1975) did band-by-band radiative transfer calculations incorporating water vapor and aerosol absorption and found combined integrated heating rates as high as 0.06 mK s^{-1} (0.20 °C hr^{-1}) near noon with a surface albedo of 0.1. The optical properties of their aerosol had fairly rural characteristics. Halpern and Coulson (1976) used a model to show that the radiative flux divergence in the lower troposphere depends not only on the solar zenith angle and aerosol refractive index but also upon the height and size distribution of the aerosol. They concluded that aerosol shortwave absorption can be many times larger than gaseous absorption for realistic combinations of aerosol parameters. Welch and Zdunkowski (1976) used a fairly complete model including NO_2 absorption and relative humidity effects on the aerosol particles. The heating rates they calculated for pollution aerosol were the highest encountered in the literature, exceeding 1.11 mK s^{-1} (4.0 °C hr^{-1}) near the top of

the haze layer for a zenith angle of 45°. Several of their model runs averaged over 0.28 mK s^{-1} (1.0 °C hr^{-1}) heating through the boundary layer. Venkatram and Viskanta (1977) examined the radiative effects of aerosol absorption in a mixed layer planetary boundary layer model. They found the heating contribution by urban aerosol absorption reached about 0.08 mK s^{-1} (0.30 °C hr^{-1}) near noon.

3. EXPERIMENTAL DESIGN

3.1 Cases

The results presented below focus primarily on data collected for three cases during the experiment. These were flight R5 flown over the ocean on 17 June 1982, and two cases over forest, flight R10 on 23 June 1982 and R13 on 27 June 1982. The flight over open ocean water, R5, was carried out over the Gulf of Mexico approximately 240 km south of Houston, Texas. The forest flights were carried out in the area of the Big Thicket National Preserve, about 55 km east-northeast of Houston and 30 km northwest of Beaumont, Texas. In addition limited data from flight R12, 25 June 1982, over the forest has been used. Figure 1 is a schematic map showing the flight locations. Figure 2 is a larger scale map showing topographic features in the forest area.

3.2 Flight Patterns

The basic flight pattern for this experiment was designed to enable the calculation of the significant terms in the budget of an atmospheric scalar variable in the planetary boundary layer (Lenschow et al., 1980a, 1981, 1982). This basic pattern consists of a set of stacked horizontal "L-shaped" patterns at three different altitudes within the boundary layer (Figure 3). This set of three is duplicated at least twice during a flight. A leg is the straight, level portion on one side of the "L". The legs are designed to be as long as possible while still covering homogeneous terrain and remaining within the aircraft fuel allotment for

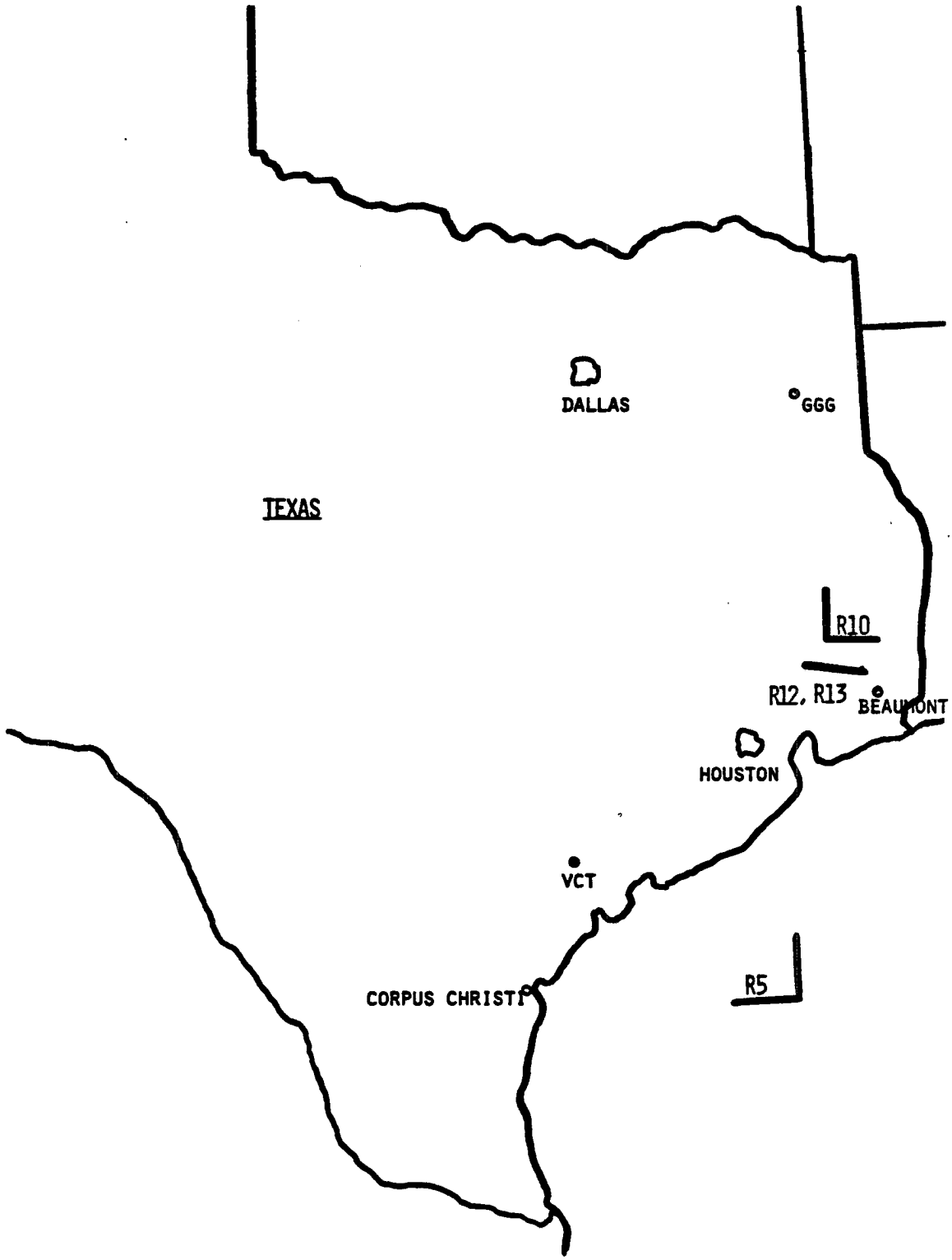

Fig. 1. Map of eastern Texas showing locations of research flights labeled R5, R10, R12, and R13. Rawinsonde stations are at Victoria (VCT) and Longview (GGG), Texas.

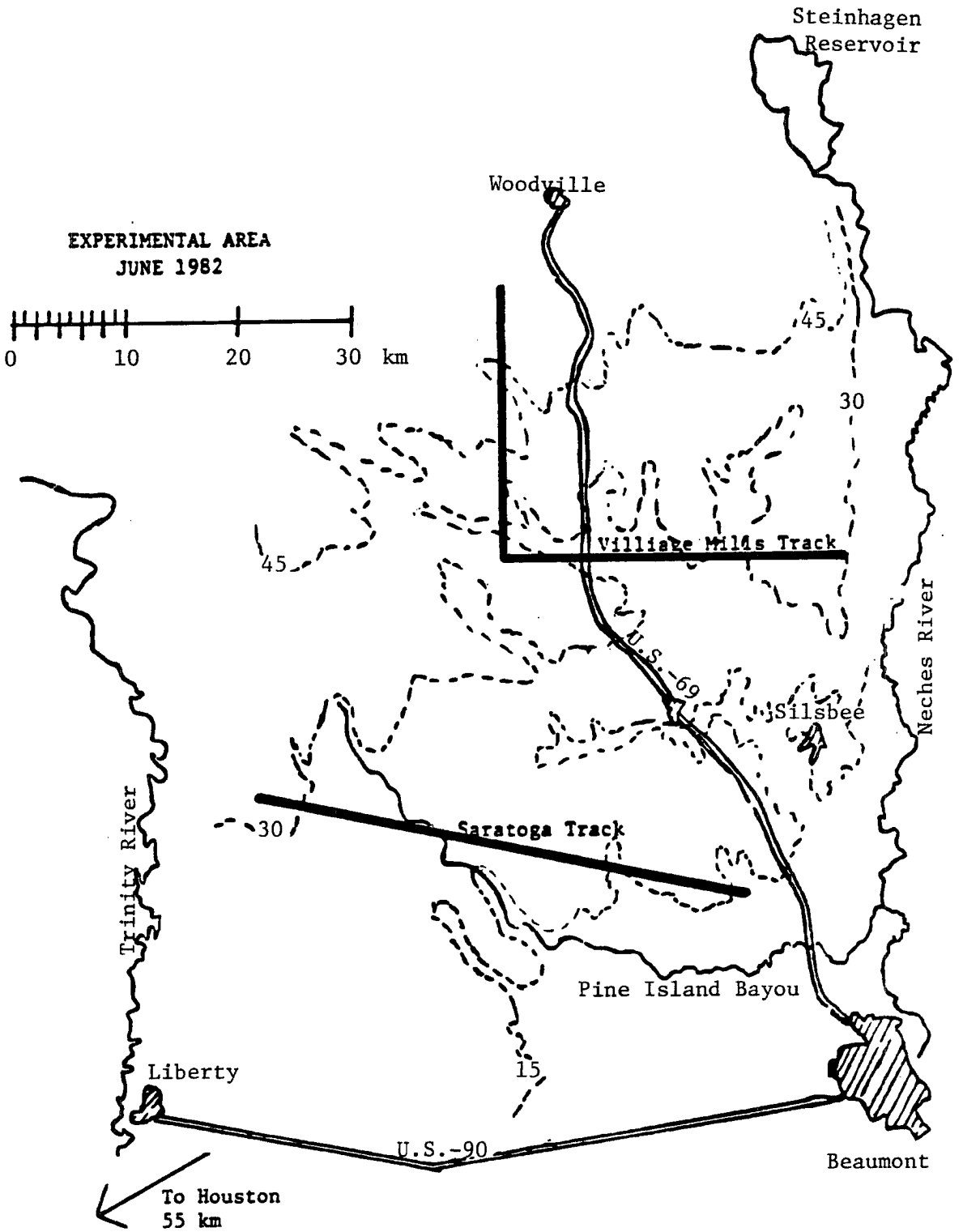

Fig. 2. Expanded map of Eastern Texas showing flight tracks over the forest and topographic features. Dashed lines are contour intervals of 15 m.

the flight. The length of legs in this experiment was about 6 to 10 minutes or 25 to 42 km at an average airspeed of 70 m s^{-1}. The ocean flight had the longer legs while terrain and obstacle restrictions limited the R10 forest flight to the shorter legs. The R13 forest flight consisted of level legs at four altitudes, 10 minutes long, in the direction of the mean wind only. No crosswind legs were flown. In addition to the level legs, slant soundings were flown to obtain profiles of the mean values of scalar variables. The sounding pattern consisted of flying the plane at constant heading and rate of climb (about 3 m s^{-1}) directly over the research area. Reverse heading (180°) turns were executed at the horizontal boundaries of the area to maintain the aircraft in position above the area. The pattern therefore looks like a vertical zig-zag. A sounding was generally taken near the middle of the flight and extended well above the depth of the boundary layer.

3.3 Big Thicket National Preserve

The Big Thicket National Preserve (BTNP) was chosen for the location of the forest flights. This area deserves some special description. The topography of this area is quite flat. The ground in the study area varied in elevation a maximum of only 20 m along the 40 km horizontal legs.

The region is special because of the wide variety and abundance of plant and animal life. The vegetation of the region is surveyed in Harcombe and Marks (1979). It is mainly mixed hardwood/pine forest with a largely closed canopy at heights up to 30 to 40 m. The combination of greater than 125 cm annual rainfall and abundant sunshine at 30 °N latitude, make it an area of rapidly growing, extremely dense vegeta-

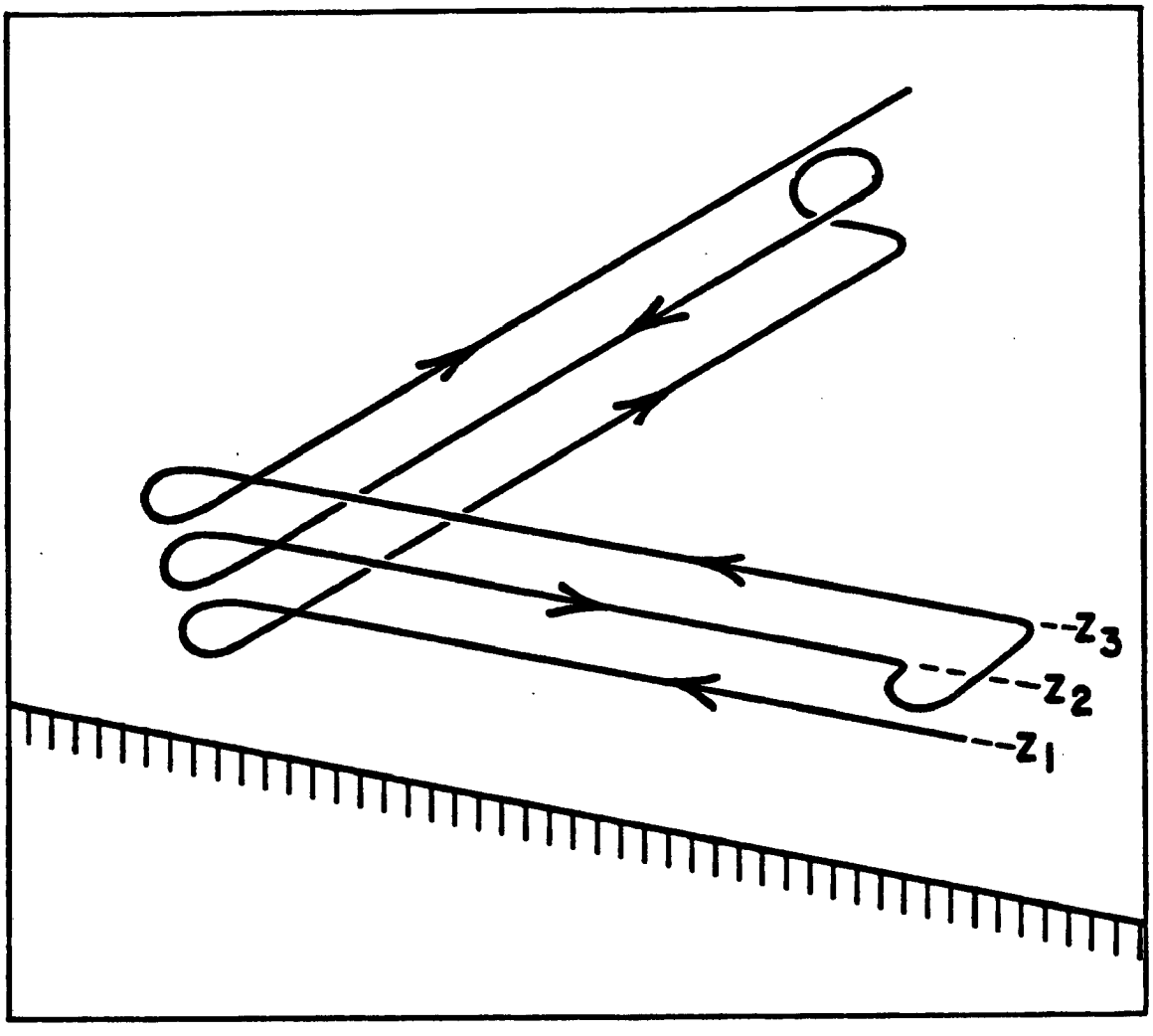

Fig. 3. Schematic flight plan designed to obtain scalar budget terms in the planetary boundary layer. This pattern is flown at least twice per budget.

tion. Hence the name Big Thicket. From the air, the tree canopy appears largely unbroken and uniform as far as the eye can see. Some areas of clear cut logging and pure pine plantations were encountered, but their areal extent was small. Work has been done in this region correlating vegetation types with LANDSAT photographic imagery (Nyquist and Cibula, in preparation) which indicates a variety of vegetation communities are detectable. This vegetative inhomogeneity may have an influence on the flux measurements.

3.4 Weather Conditions

The ideal weather conditions for this experiment are difficult to find, especially in a near-tropical summertime climate. Conditions must be convective to create turbulent fluxes but precipitation is unacceptable for most sensors. A well established steady-state boundary layer is best approached near local solar noon yet this is when cloudiness increases which greatly complicates interpretation of the radiation measurements. The flight days chosen were the best available.

The three cases were all obtained during generally fair weather conditions. The weather on the flight days was characterized by fairly weak synoptic flow, high temperatures and high dewpoints. Noontime surface weather reports from Beaumont and Houston had temperatures of 28 to 32 °C and dewpoints of 21 to 26 °C. Synoptic weather maps of the surface and 500 mb for the experimental period are shown in Figures 4 and 5.

Observations during flight R5 indicated scattered to broken stratocumulus at about 500 m MSL, haze, and calm seas. During R10, 10 to 50% moderate cumulus cover, haze, and unspecified cirrus were observed. The winds were light (0 to 2 m s^{-1}) and variable throughout the boundary

layer. During flight R13 the winds were moderate (4 to 10 m s^{-1}) from the west and a heavy, variable cirrus shield was noted. Haze and occasional small cumulus were also reported in the study area.

3.5 Instrumentation

The data from this experiment were collected using an airplane, a Beechcraft Queen Air, N306D, operated by the Research Aviation Facility (RAF) of the National Center for Atmospheric Research (NCAR). The aircraft was equipped with an inertial navigation system and resolver (Litton LTN-51 and APD 917055), an on-board data system (ARIS-IV) for data recording and real-time analysis, and high resolution, fast response sensors capable of measuring atmospheric variables including ozone mixing ratio. A partial list of the available sensors and their characteristics is given in Table 1. The fast response ozone monitor is used that described by Pearson (in preparation, 1984), Pearson and Stedman (1980), and Lenschow et al. (1981,1982). It operates on the principle of detection of the chemiluminescent reaction between ozone O_3 and nitric oxide NO

$$NO + O_3 \rightarrow NO_2^* + O_2 \qquad \text{I}$$

$$NO_2^* \rightarrow NO_2 + h\nu \qquad \text{II}$$

Here $h\nu$ represents the emission of photons in the red visible and near-infrared region of the spectrum. The rate of this reaction is sufficiently fast to enable construction of a detector with a 3 dB bandwidth of at least 20 Hz. The instrument output bandwidth is determined by a fourth order Butterworth low pass filter which has a 3 dB cutoff at 12.0 Hz ± 1% (Figs. 2 and 3, Pearson and Stedman, 1980). This response

Fig. 4. Surface weather maps and station weather for central and southeastern United States during the experimental period. The dates of the maps are 17 June 82 (A), 20 June 82 (B), 23 June 82 (C), and 27 June 82 (D). The time is 1200 z for each.

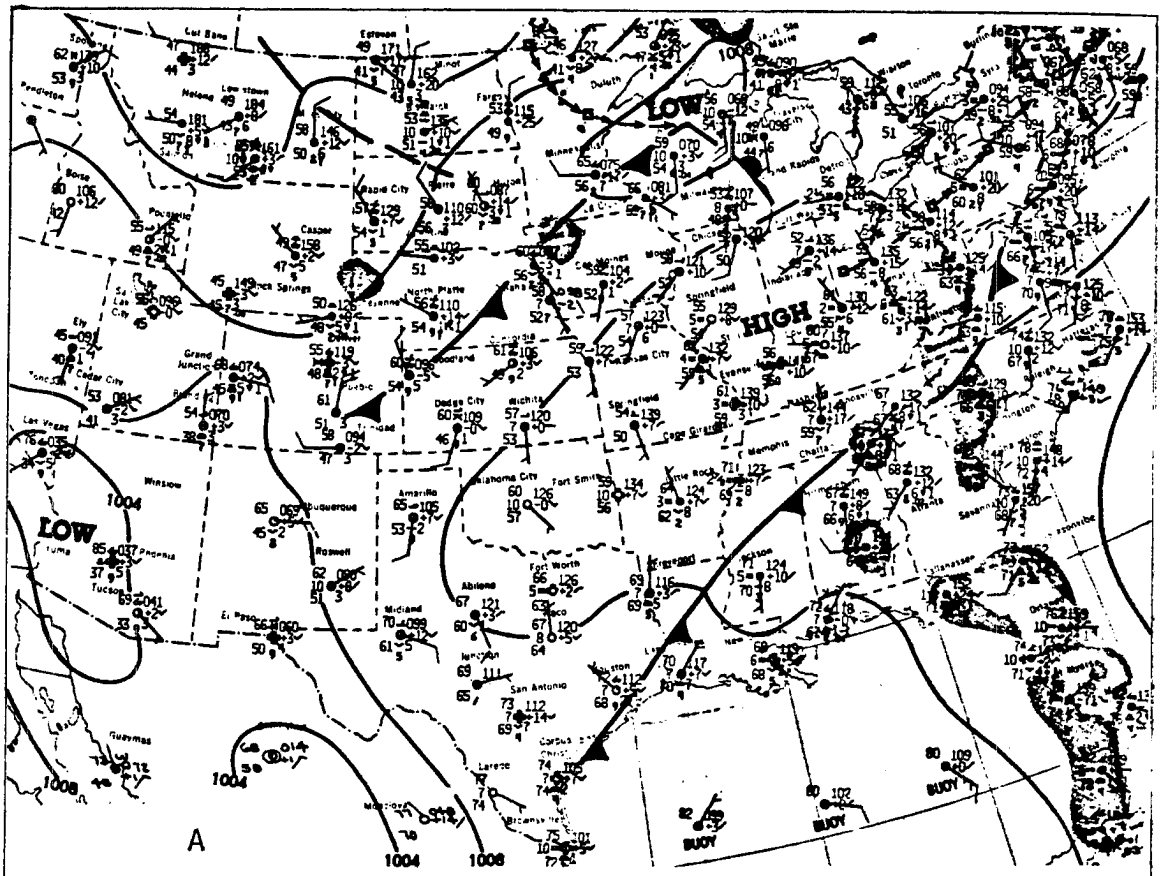
LOW
HIGH
LOW
1004
1004
1004
1008
BUOY
BUOY
A

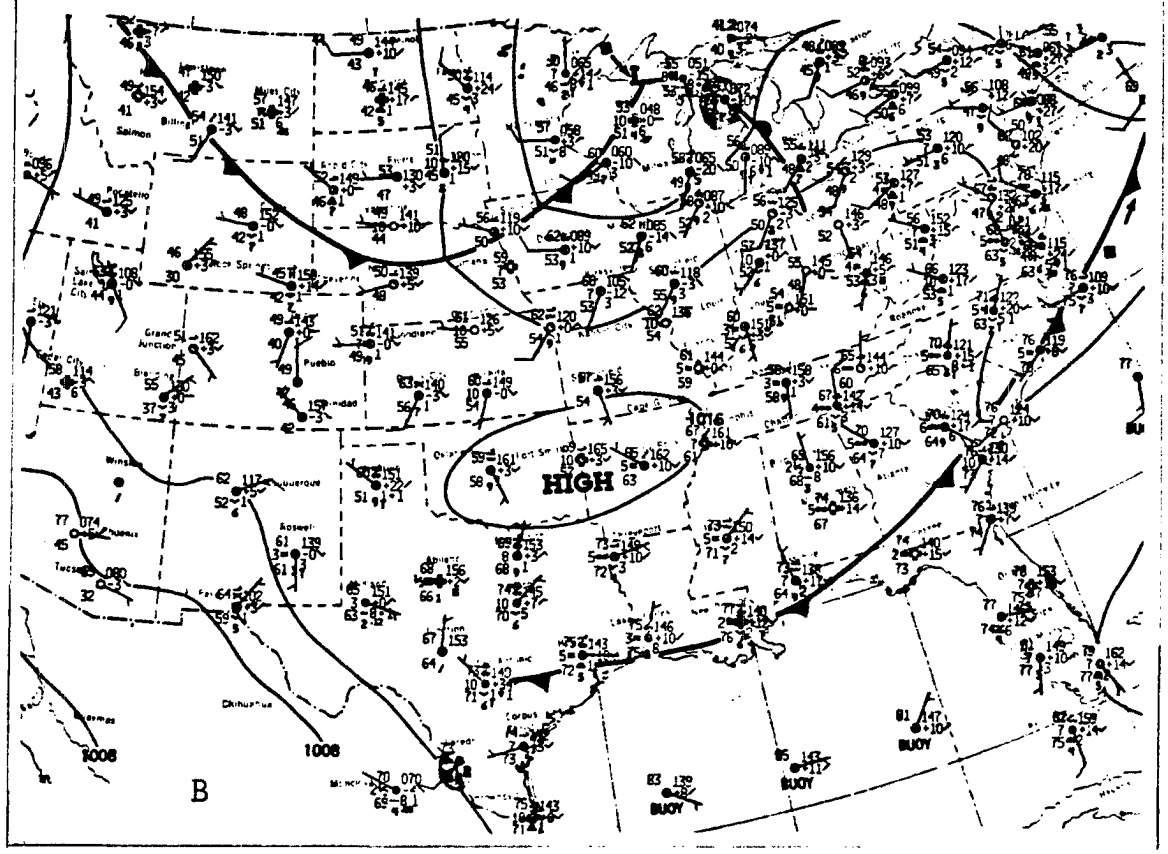
HIGH
1008
1008
BUOY
BUOY
BUOY
B

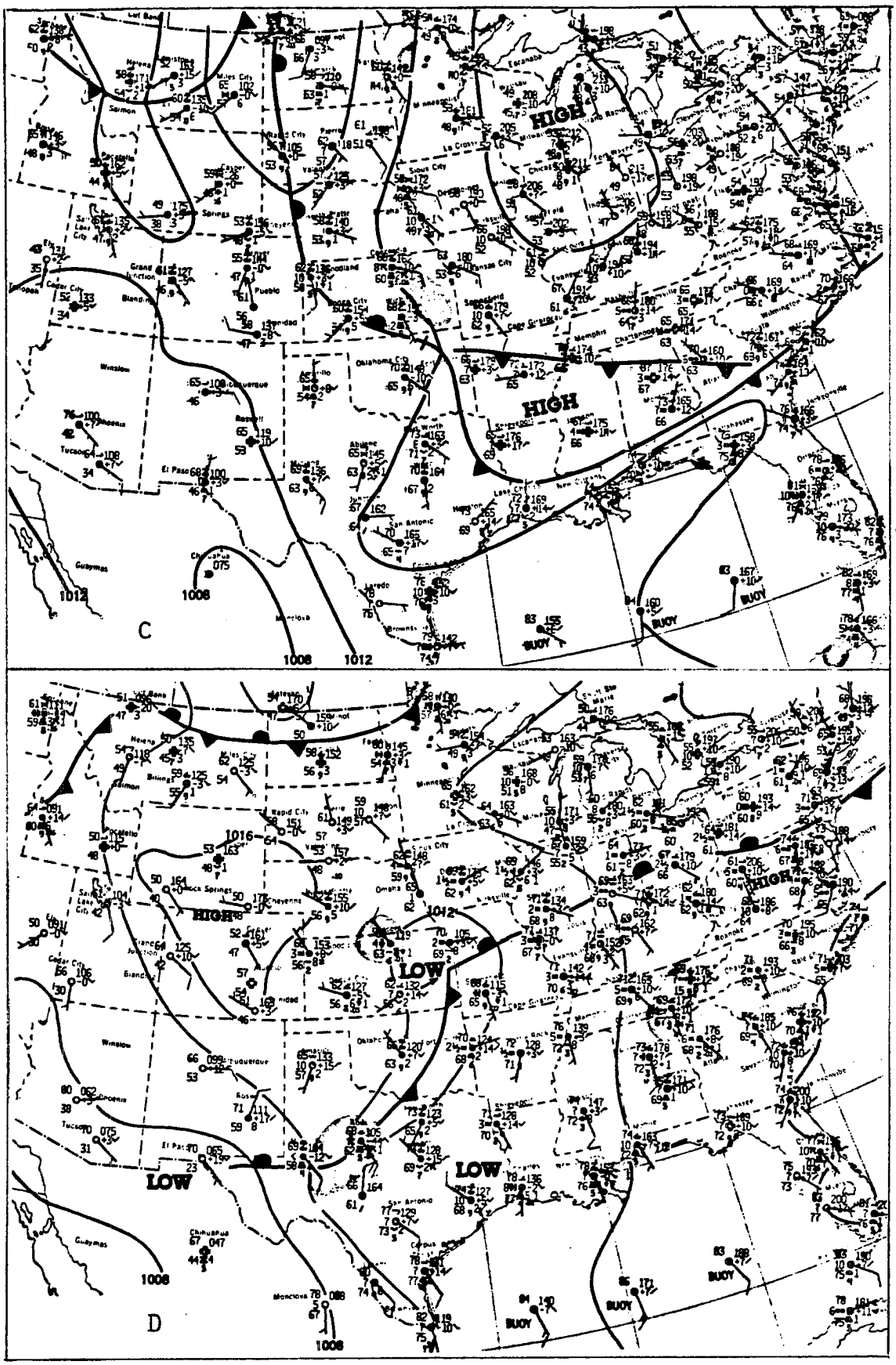
HIGH
HIGH
1012
1008
1008
1012
BUOY
BUOY
C
HIGH
1016
1012
LOW
LOW
LOW
1008
1008
BUOY
BUOY
BUOY
D

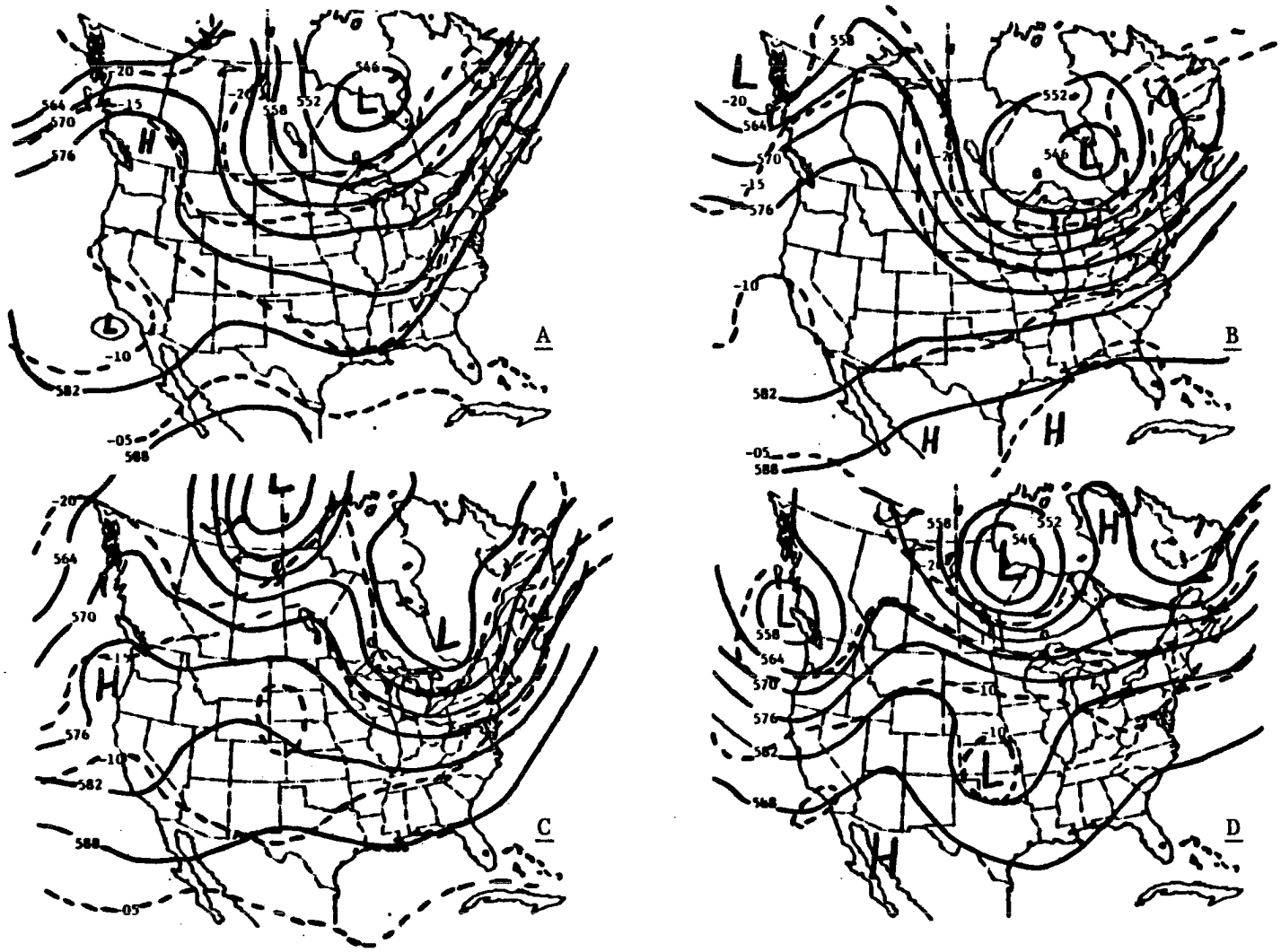

Fig. 5. Maps of constant 500-mb pressure for 17 June (A), 20 June (B), 23 June (C), and 27 June (D) 1982 at 1200 GMT. Solid lines are geopotential height (dm) and dashed lines are temperature (°C).

Table 1. Measurement capabilities and specifications of instruments available on NCAR Queen-Air N306D in June, 1982.

Parameter	Sensor type	Model	Rate	Reference	Range
Winds	Fixed vane	NCAR	20 s^{-1}	Lenschow, 1972	
Temperature	K-probe thermometer	NCAR	20 s^{-1}	Spyers-Duran & Baumgardner, 1983	-60 - + 40°C
Water vapor	Lyman-alpha hygrometer	NCAR LA-3	20 s^{-1}	Buck, 1980	-45 - + 30°C
Ozone	Chemiluminescent analyzer	CSU developed	20 s^{-1}	Pearson, Stedman, 1980	0 - 300 ppbv
Static pressure	Variable capacitance	Rosemount 1201 F	1 s^{-1}	See manufacturer's data	400 - 1035 mb
Dew point	Thermoelectric hygrometer	EG&G 137-C3-S3	1 s^{-1}	See manufacturer's data	-50 - + 50°C
Height above ground	Radio altimeter	Sperry Rand AA-220	1 s^{-1}	See manufacturer's data	0 - 762 m
Solar radiation	Pyranometer .285 - 2.8 μm	Eppley 2-WG7	1 s^{-1}	See manufacturer's data	0 - 1500 W m^{-2}
Infrared radiation	Pyrgeometer 4 - 45 μm	Eppley PIR	1 s^{-1}	See manufacturer's data	0 - 500 W m^{-2}
Surface temperature	Bolometric radiometer	Barnes Engineering Co. PRT - 5	1 s^{-1}	See manufacturer's data	-20 - + 75°C

is more than sufficient to resolve atmospheric fluctuations with a wavelength on the order of 10 m at typical research aircraft speeds of 100 m s^{-1}.

The sensitivity of the ozone instrument is sufficient to measure fluctuations of a few tenths of a ppb with an acceptable signal to noise ratio. Random statistical fluctuations in the rate of emission of photons from the reaction, called shot noise, is evident in these measurements. Their variance is proportional to the mean level of the signal and may reach a level equivalent to 1 to 2 $(ppb)^2$. This white noise is not correlated with the measured vertical velocity. Therefore there is no contribution of the noise to the mean covariance of ozone and vertical velocity, which is the vertical flux, when aver-aged over a sufficiently long period (Lenschow and Kristensen, 1984).

Other possible sources of ozone variance not related to atmospheric changes include changes in the instrument operating temperature, pressure, high voltage supply, and a slight interference from water vapor. The instrument operates at a low reaction chamber pressure (about 10 mb) and above ambient temperature (about 37°C) and is designed such that neither temperature nor pressure can change rapidly. The temperature, pressure, and power supplies are carefully regulated and monitored during flight. These readings are recorded as data and are checked for proper values. There are no known interferences from other light producing reactions. A slight negative interference due to water vapor quenching of the reaction in Eq. II occurs (Matthews et al., 1977). This is corrected for in the data processing according to the method outlined in Lenschow et al. (1981). An additional correction to the ozone data is done to account for the time lag between ozone and the

other sensors. The lag is about 0.2 s and is due both to the plumbing delays and to 6 m horizontal distance between the gust probe sensors and the ozone inlet.

4. THEORY AND METHOD OF CALCULATION

This section explains the methods used to calculate the various quantities involved in analysis of the data. Some definitions and discussion of the theoretical significance of the terms are also included here.

4.1 Definitions

Potential temperature Θ is the temperature a parcel of air would have if adiabatically expanded or compressed to a reference pressure level of 1000 mb. This definition is expressed by Poisson's equation,

$$\Theta = T\{1000/p\}^{(R/c_p)} \qquad (4.1)$$

where T is the parcel temperature (K), p is the pressure (mb), R is the specific gas constant for dry air, and c_p is the specific heat at constant pressure of dry air. This calculation is done using the fast response temperature (ATKP) data, $R/c_p = 0.286$, and the static pressure sampled at 1 Hz.

Virtual potential temperature Θ_v is the potential temperature dry air would have in order to have the same density as the moist parcel. This relation is expressed by the formula:

$$\Theta_v = \Theta\{p\,[p - (0.61 \times 10^{-5})\,RQT]^{-1}\} \qquad (4.2)$$

where Q is the absolute humidity ($g\ m^{-3}$) which, in this work, was

obtained from the Lyman-Alpha hygrometer. Calibration of this instrument was achieved by linearly fitting the raw output signal to Q derived from thermoelectric dew point (EG&G, Table I) during a sounding taken near the middle of each flight. This calibration was assumed to be constant throughout the flight, and is estimated to have an uncertainty of about 10% due, in part, to systematic changes in the instrument with time and to a small interference from oxygen absorption which depends on the air density (Buck, 1976).

Ozone values are expressed in parts per billion volume mixing ratio χ[ppbv] and mass concentration C[$\mu g\ m^{-3}$]. These quantities are related by the expression:

$$\chi[\text{ppbv}](\rho M_{o_3}/M_d) = C[\mu g\ m^{-3}] \qquad (4.3)$$

where ρ is the density of the parcel. The ratio of molecular weights is 1.657. SI units are used except when specified otherwise.

4.2 Profiles

The vertical profiles presented below represent data collected during soundings taken at constant heading to maintain good air motion measurements. The data are averaged into 10-m height bins and plotted against altitude above ground level (AGL). The aircraft rate of climb is usually about 3 m s^{-1} so about 60 points of the 20 Hz data go into each point plotted. Aircraft roll angles greater than 20° may give poor wind measurements, and are thus are rejected. Generally this removes only the 180° turns during the sounding.

4.3 Fluxes

The basis for calculation of fluxes lies in the principle of Reynold's decomposition (Pielke, 1984, Chapter 4). In this process any

record of a meteorological variable may be split into mean (overbar) and fluctuating (prime) components: $A = \overline{A} + A'$. The average quantities satisfy the Reynold's postulates that: 1) all primed quantities average to zero; 2) the correlation between averages and fluctuations must vanish; and 3) the average of an average must reproduce the same average. These conditions are expressed algebraically as:

$$\begin{aligned} \overline{A'} &= 0 \\ \overline{\overline{A}A'} &= 0 \\ \overline{\overline{A}} &= \overline{A} \end{aligned} \qquad (4.4a)$$

The average product of two variables is then written as:

$$\overline{AB} = \overline{A}\,\overline{B} + \overline{A'B'} \qquad (4.4b)$$

The last term is the covariance of two quantities, representing the product of the fluctuating components at any instant averaged over the chosen interval. The averaging operator represents a line average over a segment of the aircraft flight path. Vertical fluxes are obtained as the covariance between the variable of interest and the vertical component of the wind. In this experiment the mean vertical velocity cannot be measured and therefore is assumed to be negligible so: $\overline{w} = \overline{w'} = 0$. For each time interval, the mean and linear trend are obtained by linear regression. These are subtracted from the individual points to give the fluctuating component. For a scalar s, this new time series is then multiplied by the corresponding one for w and averaged to get the vertical flux $\overline{w's'}$. The normal sample rate for properties whose flux was of interest was 20 Hz.

4.3.1 Corrections to Measured Ozone Data

The ozone time series lags the other fast-response measurements due both to delays in the plumbing and the location of the sample inlet

which is about 6 m aft of the sensors which reside on the nose boom. Lenschow et al. (1981, 1982) have shown this lag is about 0.2 s for the instrument as it was used. The lag is removed by advancing the ozone time series four points (4/20 s) before the flux is calculated.

In addition, there is a small interference from water vapor arising from quenching of the chemiluminescence from O_3 and NO. Lenschow et al. (1981) used the data of Matthews et al. (1977) to the estimate the magnitude of the quenching as:

$$O_3 = O_{3m}(1 + \alpha r) \tag{4.5}$$

Here O_3 is the corrected ozone mixing ratio, O_{3m} is the measured ozone mixing ratio, r is the water vapor mixing ratio, and α is a constant of proportionality equal to 5.0 ± 1.0. They also showed that corrections to the fluxes could be estimated by

$$\overline{w'O_3'} = (1 + \alpha\bar{r})\ \overline{w'O_{3m}'} + \alpha\bar{O}_{3m}\ \overline{w'r'} \tag{4.6}$$

after neglecting higher order terms. Here, the water vapor flux was estimated from:

$$\overline{w'r'} \approx \overline{w'q'}/\bar{\rho} \tag{4.7}$$

This correction is typically less than 6% over land, but may be as high as 20% over warm water.

4.4 Budgets

The budget equation of an atmospheric scalar s may be written:

$$(\partial\bar{s}/\partial t) + \bar{u}(\partial\bar{s}/\partial x) + (\partial\overline{w's'}/\partial z) = Q_s \tag{4.8}$$

(Lenschow, 1981). Here x is chosen in the direction of the mean horizontal wind $\bar{u}$, z is the vertical coordinate, and Q_s is the net sum of the internal sources and sinks for s in the air sampled. The first term in Eq. (4.8) represents the local change of the mean quantity over time.

This term is calculated at each altitude by linear regression of the averages for each flight leg versus time of day. The rates of change at each altitude are then averaged to give $\partial\bar{s}/\partial t$ for the study area over the duration of the flight. This is done using the fast response sensor data for all variables except Q where the slower but more stable thermoelectric dewpoint sensor is used.

The second term in Eq. (4.8) is horizontal advection of the scalar by the mean wind. Where possible, the flight legs are oriented along and perpendicular to the mean wind. In this case, only the one advection term needs to be calculated. When this alignment is not feasible, horizontal advection is calculated from:

$$\underline{V} \cdot \nabla s = \bar{u}(\partial\bar{s}/\partial x) + \bar{v}(\partial\bar{s}/\partial y) \qquad (4.9)$$

The calculation of $\bar{u}(\partial\bar{s}/\partial x)$ is done for each flight leg and weighted by the depth of the boundary layer that each altitude represents.

The third term of Eq. (4.8) is the divergence of the vertical flux of the scalar. Assuming horizontal homogeneity, this term represents the net vertical transport into or out of the volume sampled. The fluxes are calculated for each segment and averaged to obtain the mean flux at that altitude. The 95% confidence limits on this flux based on the student-t distribution are calculated from the population of flux estimates from all segments at a given altitude. The slope $\partial(\overline{w's'})/\partial z$ is then calculated by linear regression.

The right-hand side of the budget equation, Q_s, cannot be measured in this work. Following Lenschow et al. (1981, 1982) it is calculated as the residual of the measured terms on the left side of Eq. (4.8).

4.5 Deposition Velocity and Surface Resistance

In order to estimate deposition, it is necessary first to select values for certain empirical constants charactertistic of the surface. The forest displacement height, or the effective height of the surface, is chosen to be 20 m AGL. This is about 2/3 of the height h_o of the large roughness elements, the trees. Panofsky and Dutton (1984) recommend using 0.7 to 0.8 of the height h_o. Wesely et al. (1978) have found 0.63 h_o to be typical for maize crops and Lamb et al. (1985) chose 0.7 h_o for forest based on other sources. The roughness length for the forest (z_o) is chosen as 1 m from Panofsky and Dutton (1984) and Lenschow et al. (1982). The value of the von Karman constant k is 0.4 to be consistent with of Wesely et al. (1981) and previous papers from that group.

The deposition velocity, v_d, for ozone is calculated from

$$v_d = (\overline{w'O_3'})_o/\bar{O}_3 \qquad (4.10)$$

Here $\bar{O}_3$ is the ozone volume mixing ratio. The surface flux $\overline{w'O_3'}$ is estimated by linear extrapolation of the measured flux profile down to the displacement height of the forest canopy. The mean concentration was that obtained at the lowest altitude sampled.

The surface resistance to ozone uptake is calculated by methods derived in Wesely et al. (1978) for ozone deposition to crops:

$$r_s = v_d^{-1} - r_a \qquad (4.11)$$

Here r_s is the surface resistance which is a property of the surface and the chemical or scalar species involved. The aerodynamic resistance r_a is a function of the flow field, temperature stratification, roughness length, and height. Following the discussion of Galbally and Roy

(1980), r_a is assumed to consist of two additive terms: a resistance of the turbulent layer from height z to the level of the momentum sink and a resistance across the roughness layer. The latter term depends on the flow characteristics and the molecular diffusivity of the species in question. It is usually parameterized by using a surface transfer function B^{-1} which depends on the thermal and molecular diffusivities of the molecule under study (Wesely and Hicks, 1977). Thus

$$\begin{aligned} r_a &= \rho u(z)/\tau + (Bu_*)^{-1} \\ &= u(z)/u_*^2 + (Bu_*)^{-1} \\ &= (ku_*)^{-1} [\ell n\ (z/z_o) + kB^{-1}] \end{aligned} \tag{4.12}$$

Here τ is the sheering stress or vertical momentum flux ρu_*^2, and u_* is the friction velocity. The third equation is obtained by using the familiar log profile of horizontal wind near the surface:

$$u(z) = u_* k^{-1}\ \ell n(z/z_o) \tag{4.13}$$

The value of kB^{-1} is chosen as 2.5 (Wesely et al. 1978). Wesely and Hicks (1977) show that an additional term involving the integrated ψ function must be included in (4.12) to correct for diabatic effects in the flux-gradient relationships. Following Hicks and Liss (1976) and making the approximation that ozone transfer is similar to that for sensible heat, $\psi_{O_3} = \psi_H$ and one obtains

$$\psi_{O_3} = \psi_H = \exp\ [0.598 + 0.39\ \ell n(-z/L) - 0.09\ (\ell n(-z/L))^2] \tag{4.14}$$

The stability parameter (-z/L) is obtained from data at the lowest altitude sampled. The Obukhov length L is

$$L = -u_*^3\ \bar{\theta}_v/(kg\ \overline{w'\theta_v'}) \tag{4.15}$$

Here $\bar{\theta}_v$ and $\overline{w'\theta_v'}$ are the mean virtual potential temperature and flux,

g is the acceleration of gravity and k the von Karman constant. The friction velocity u_* is calculated from momentum fluxes for each segment

$$u_* = [(\overline{w'u'})^2 + (\overline{w'v'})^2]^{1/4} \qquad (4.16)$$

The values of L and u_* for each segment at the lowest level are then averaged for the flight. The equation for the surface resistance then becomes

$$r_s = v_d^{-1} - (ku_*)^{-1}[\ln(z/z_o) - \psi_{o_s} + 2.5] \qquad (4.17)$$

In all calculations of these quantities the height of the measurement is adjusted by the displacement height,

$$z = z' - d \qquad (4.18)$$

where z' is the aircraft altitude above ground level (AGL). The radio altimeter which measures this altitude directly was not functioning properly during the forest flights. Therefore the altitude determined from the inertial data as described by Lenschow (1972) used in this analysis.

4.6 Net Radiation

The output of the radiometers is calibrated and temperature-corrected during the initial round of data processing done by NCAR. The outputs are reported as W m^{-2} on a horizontal surface parallel with the plane of flight of the aircraft over a field of view of 2π steradians. The data are recorded once per second. In order to compare radiative flux data taken at varying angles relative to the sun, several normalization procedures are necessary. The methods of calculation are as follows.

4.6.1 Angle Correction

The measured downward shortwave flux (SW↓) incident on the plane of the aircraft was normalized to a horizontal surface parallel to the surface of the earth at that latitude and longitude. According to methods developed in Robinson (1966), the direct solar irradiance on a tilted plane is related to the incoming irradiance by

$$E_{DIR} = E_o \cos \beta \tag{4.19}$$

where E_{DIR} is the direct component of irradiance on the tilted surface, E_o is the irradiance from the direction of the sun's rays and β is the angle between the normal to the surface and the sun's rays, which is given by:

$$\cos \beta = \cos AA \cos \Theta + \sin AA (\cos Az \tan \phi \cos \Theta - \cos Az \sin \delta \sec \phi - \sin Az \cos \delta \sin t_h) \tag{4.20}$$

The pitch angle is AA and Az is the heading of the aircraft. Here ϕ is latitude, Θ is the solar zenith angle for a horizontal plane, δ is the solar declination angle and t_h is the hour angle of the sun which increases 15° for every hour after local solar midnight. The roll angle of the airplane is assumed to be zero in these calculations. In practice the data analysis rejects data points for which the roll angle is greater than 5°. The values of AA, Az, and ϕ are recorded as data for each record of the flight. The solar zenith is calculated from

$$\cos \Theta = \sin \phi \sin \delta - \cos \phi \cos \delta \cos t_h \tag{4.21}$$

The solar declination angle is approximated by

$$\delta = -23.5 \cos [(JD + 9)(360/365)] \tag{4.22}$$

where JD is the Julian date. The hour angle t_h is calculated from the longitude and local time of day.

The measured irradiance at the aircraft (E_{OB}) is then the sum of the direct and diffuse (E_{DF}) components of irradiance

$$E_{OB} = E_{DF} + E_{DIR} = E_{DF} + E_o \cos \beta \quad (4.23)$$

The irradiance on a plane surface parallel to the earth's surface is

$$E_{TR} = E_{DF} + E_o \cos \theta \quad (4.24)$$

For a given ratio, x, of diffuse to total irradiance

$$x = E_{DF}/E_{TR} \quad (4.25)$$

substituted into 4.24

$$E_{TR} = xE_{TR} + E_o \cos\theta \quad (4.26)$$

and rearranging gives

$$E_o = E_{TR} (1-x)/ \cos \theta \quad (4.27)$$

Substituting (4.25) and (4.27) into (4.23) gives

$$E_{OB} = xE_{TR} + E_{TR} (1-x)(\cos \beta/\cos \theta) \quad (4.28)$$

and

$$E_{TR} = E_{OB}/[x + (1-x) \cos \beta/\cos \theta] \quad (4.29)$$

Equation (4.29) is used to normalize the flux on a tilted surface (E_{OB}) to that on a horizontal surface (E_{TR}). Note that if $\beta = \theta$, that is the aircraft is horizontal, $E_{TR} = E_{OB}$ and if there is no diffuse component, $x = 0$, then $E_{TR} = E_{OB} \cos\theta/\cos\beta$. This correction is applied only to the SW↓ measurements. The longwave and reflected shortwave SW↑ are assumed to be isotropic within the accuracy limits of the measurements. Note that as the diffuse component (x) approaches 100% the need for the angle correction goes to zero in Eq. (4.29). Equation (4.29) was applied to each data point.

4.6.2 Correction for Changing Zenith

The flux measurement portions of the flights lasted approximately three hours. Over this period of time the shortwave flux varied due to the varying solar zenith angle. To account for this the shortwave fluxes were normalized to a median solar zenith angle for the flight by

$$E_N = E_{TR} (\cos \theta_N / \cos \theta) \qquad (4.30)$$

Here E_N is the normalized irradiance incident on a plane surface and θ_N is the median solar zenith angle for the flight. Further detail of this procedure may be found in Ackerman and Cox (1981). This correction was applied to the SW↓ and SW↑ irradiances. It was applied to the calculated fluxes averaged over a period of two minutes.

4.6.3 Flux Divergence

The flux components for each two-minute average, normalized if necessary, were averaged together to give means over each leg. The legs at the same altitude were then averaged together to get a mean value for each component at each altitude. The net flux at each altitude was then calculated as

$$E_{net} = SW\downarrow + SW\uparrow + LW\downarrow + LW\uparrow \qquad (4.31)$$

where the downward fluxes are defined as positive. The heating of the air due to radiative flux divergence was calculated by

$$(\partial T/\partial t)_{rad} = (\rho c_p)^{-1} (\partial E_{net}/\partial z) \qquad (4.32)$$

where ρ is the average density in the boundary layer.

5. EXPERIMENTAL RESULTS AND DISCUSSION

The three main topics of interest in this study are ozone deposition parameters, scalar budgets, and radiation flux analysis. The results of this experiment yield values for the components of these topics. These values and discussion of their significance are presented in this section. Naturally these topics and some of the various subtopics are closely related. Also included in this section are observational results which are necessary to understand the boundary layer processes for the cases reported. These include discussion on the data time series, vertical profiles, spectra, and cospectra.

5.1 Time Series

The first step in data analysis is examination of raw time series data for parameters of interest during level flight legs. Examples of raw time series are shown in Fig. 6. Note the correlated excursions of higher upward vertical velocity, higher temperature and moisture, and lower ozone. These are examples of buoyant thermal plumes rising from near the surface. In the ozone time series, the additional variance in the signal contributed by the shot noise can clearly be seen. The time series are also plotted after removal of the mean and linear trend over the selected time interval (Fig. 7). At this point in the analysis, irregularities or 'spikes' in the data created by instrumental anomalies can be located in the time series and removed if necessary. The series are also examined for evidence of a faulty sensor or any atmospheric

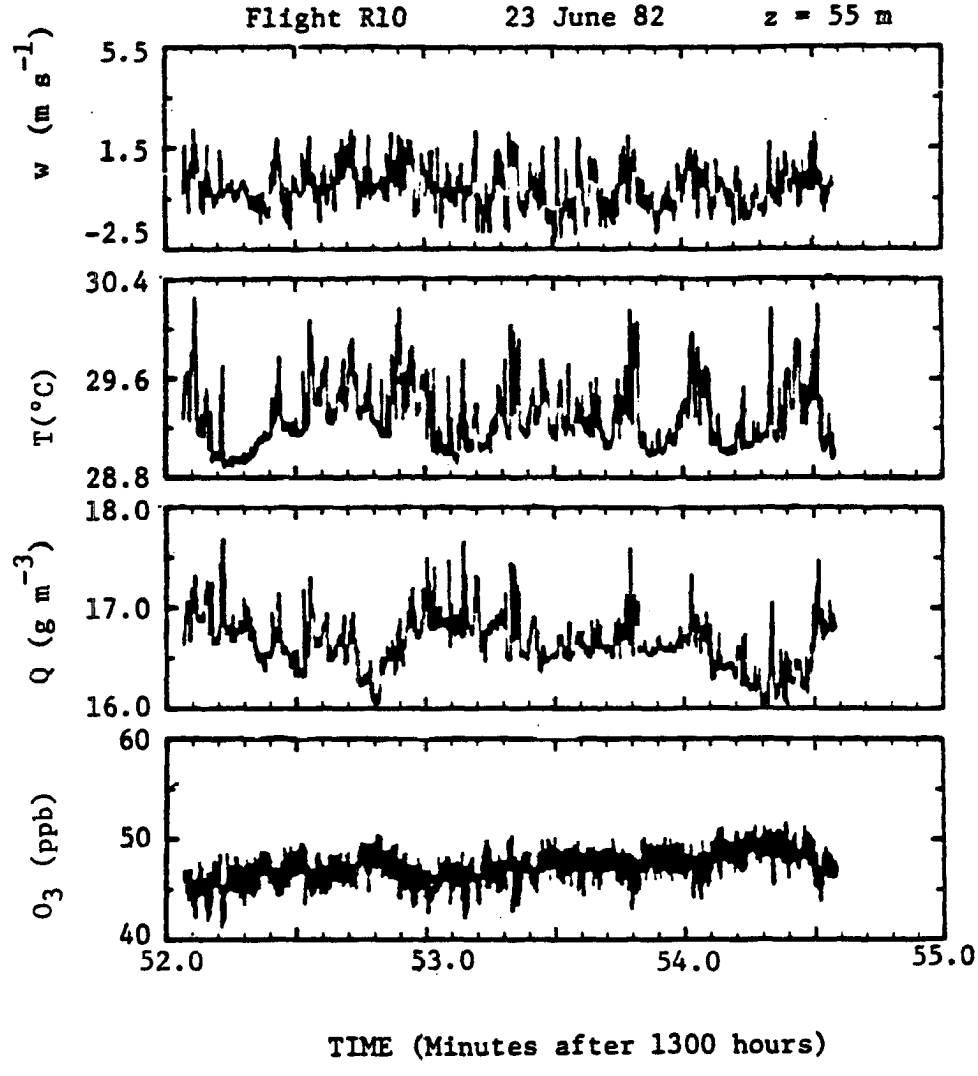

Fig. 6. Raw time series for 204 s of aircraft data.

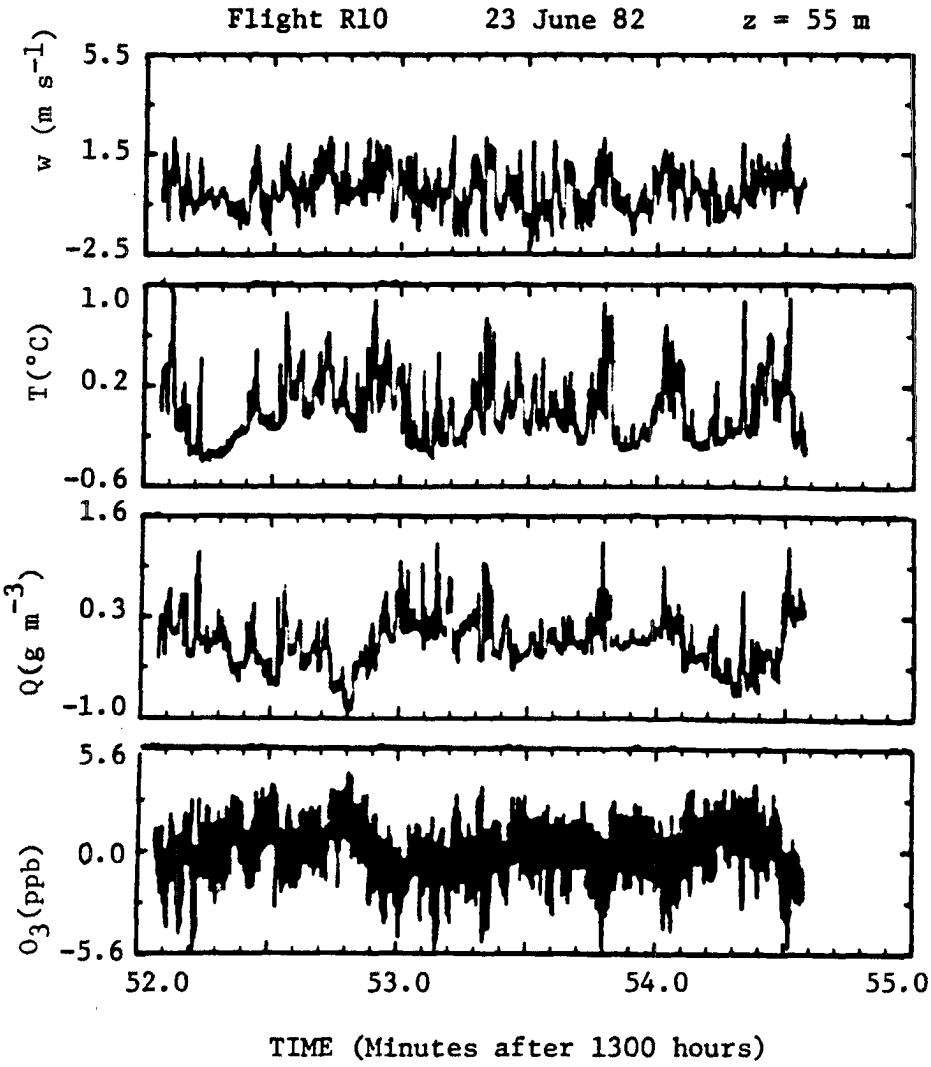

Fig. 7. Time series of data with mean and linear trend removed, same period as Fig. 6.

disturbance that could contaminate the measurements, such as a pollution plume. An additional operation, tapering the data at the ends of the time series, must be done for the spectral analysis in order to avoid introducing an artificial signal related to the averaging period (Bendat and Piersol, 1971 Chapter 9). The effect of tapering can be seen in the time series of Fig. 8.

5.2 Vertical Profiles

Data from the sounding portions of the flights are averaged over 10 m vertical depth and plotted versus altitude. These vertical profiles of mean quantities are essential components in a thorough case analysis. Also plotted are the sample variances over the 10 m averages which are useful in determining the precise depth of the mixed layer since the scalar variance decreases sharply above the mixed layer in most cases. Some examples of variance profiles are shown in Fig. 9 through 11. Notice that a different mixed layer would probably be inferred from examination of each of these profiles independently. The layer depth at this time was established to be about 1200 m using these, other variance, and mean profiles.

Figures 12 through 16 show the profiles of ozone, wind direction, wind speed, potential temperature, and water vapor mixing ratio at the midpoint of flight R10. The potential temperature and mixing ratio profiles indicate that at this time the depth of the mixed layer is about 1200 m. Ozone exhibits a fairly constant profile within the boundary layer and above there is only a slight discontinuity in ozone concentration across the inversion layer. Wind speeds in the boundary layer are very light and variable in direction, implying a fairly long residence time of the boundary layer over the forest.

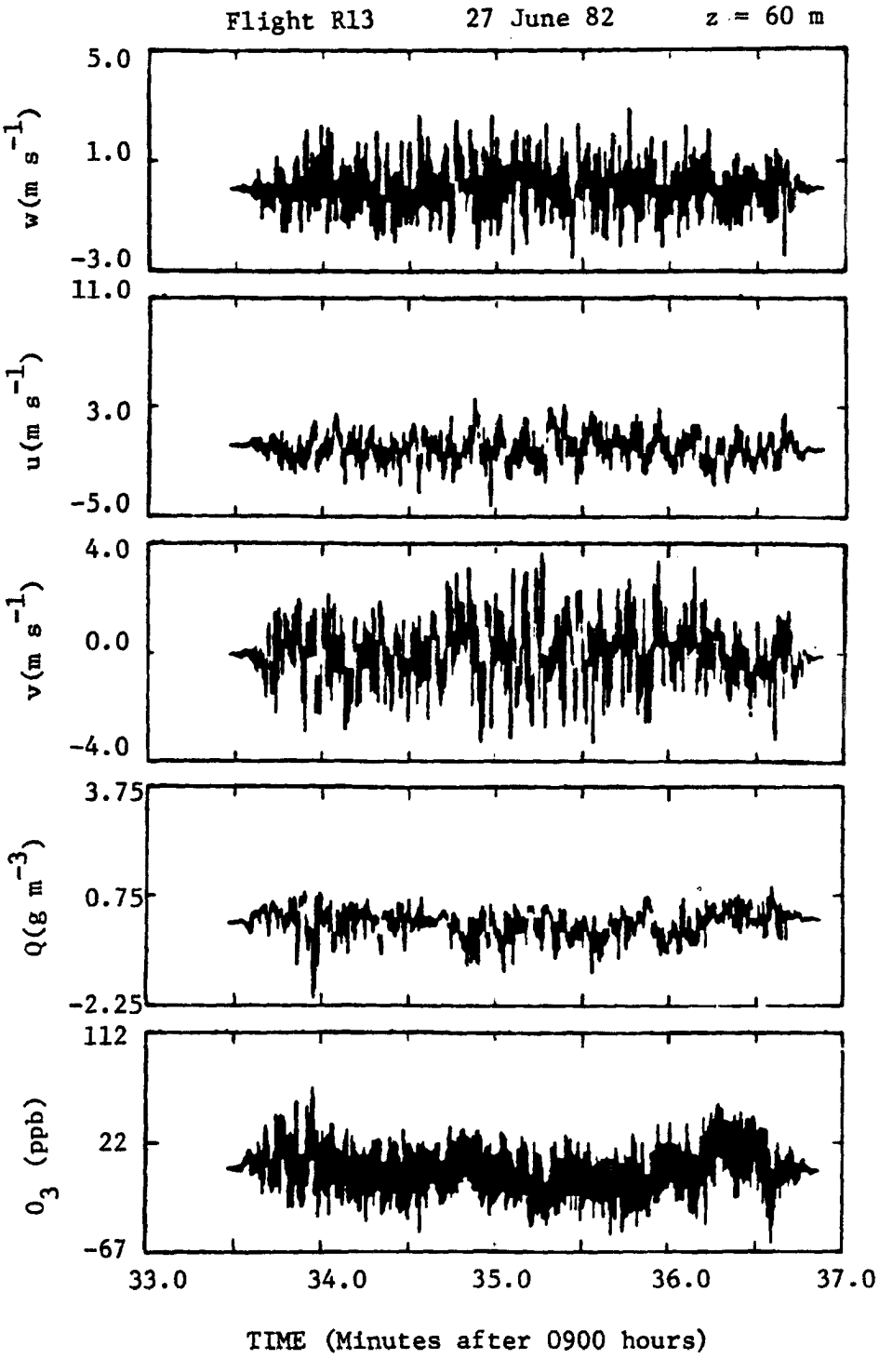

Fig. 8. Time series of detrended data with 10% of the data tapered at the ends with a cosine function.

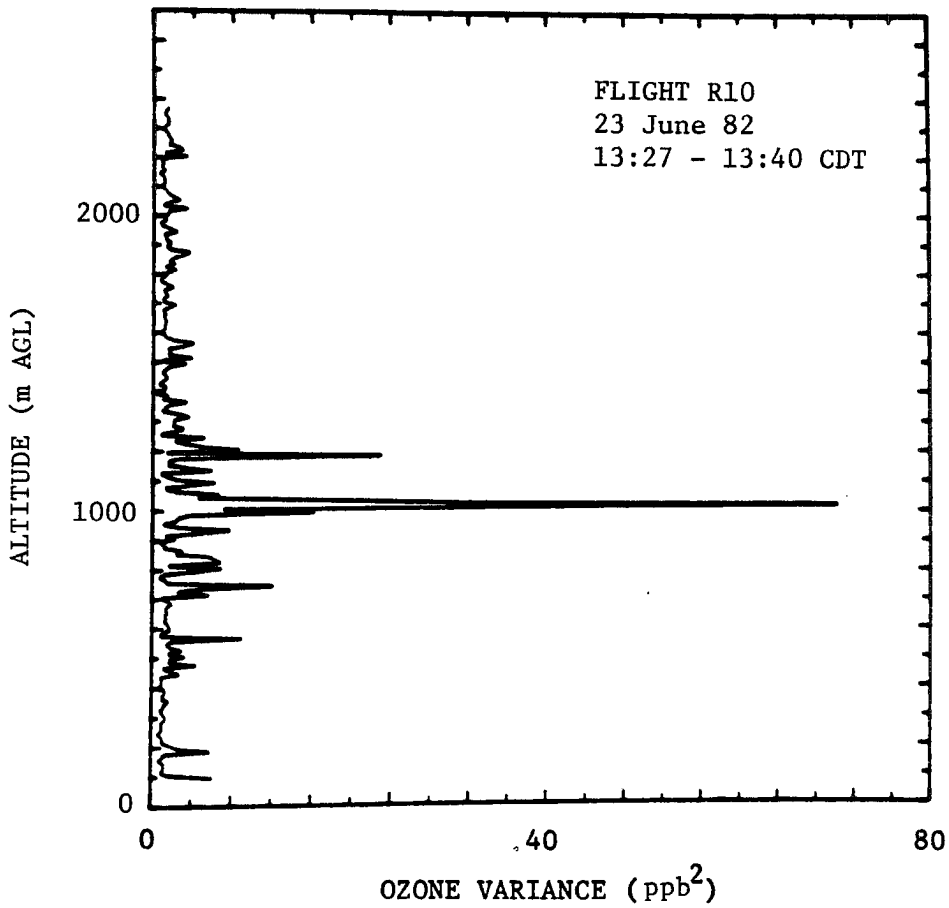

Fig. 9. Vertical profile of ozone variance.

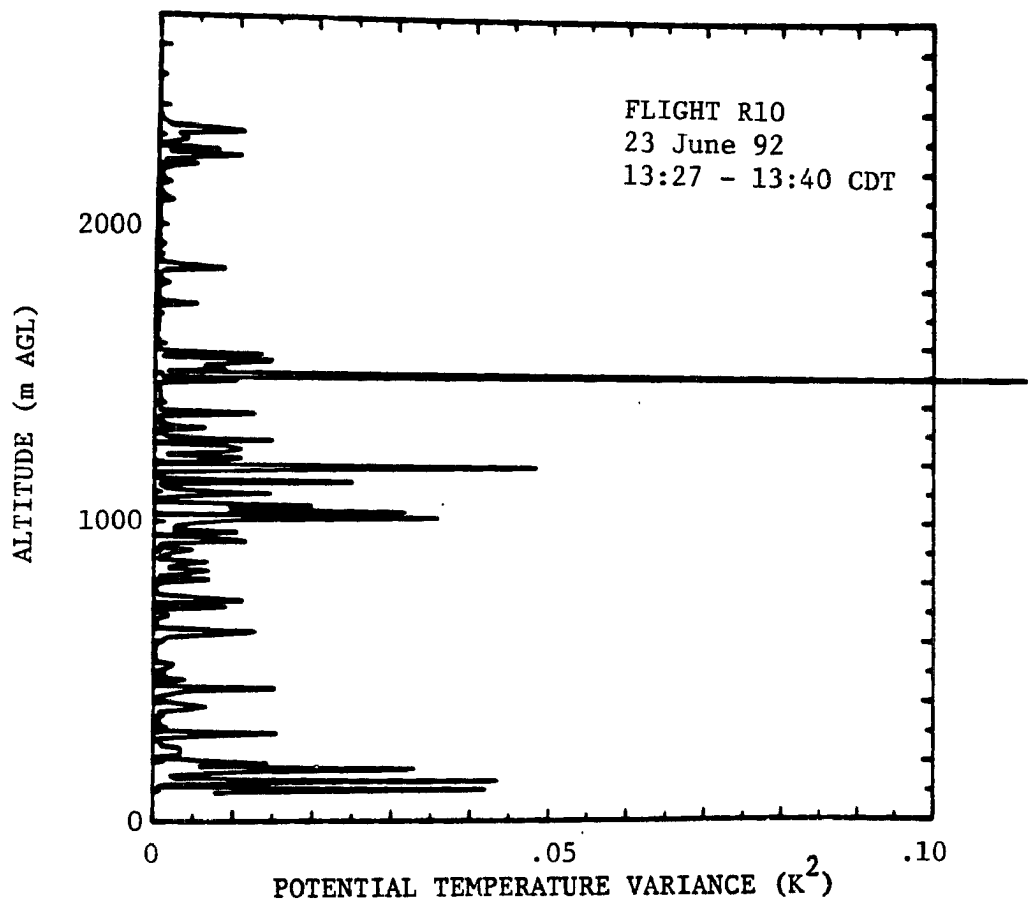

Fig. 10. Vertical profile of potential temperature variance for the same period as Fig. 9.

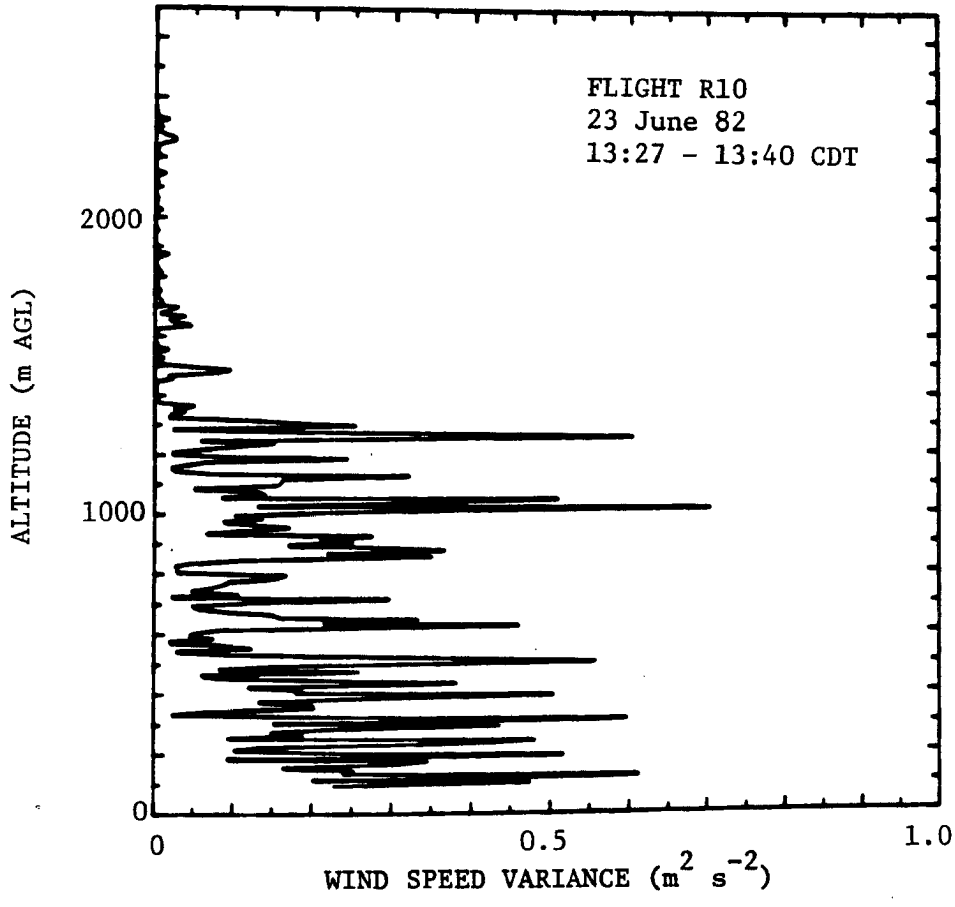

Fig. 11. Vertical profile of wind speed variance for the same period as Figs. 9 and 10.

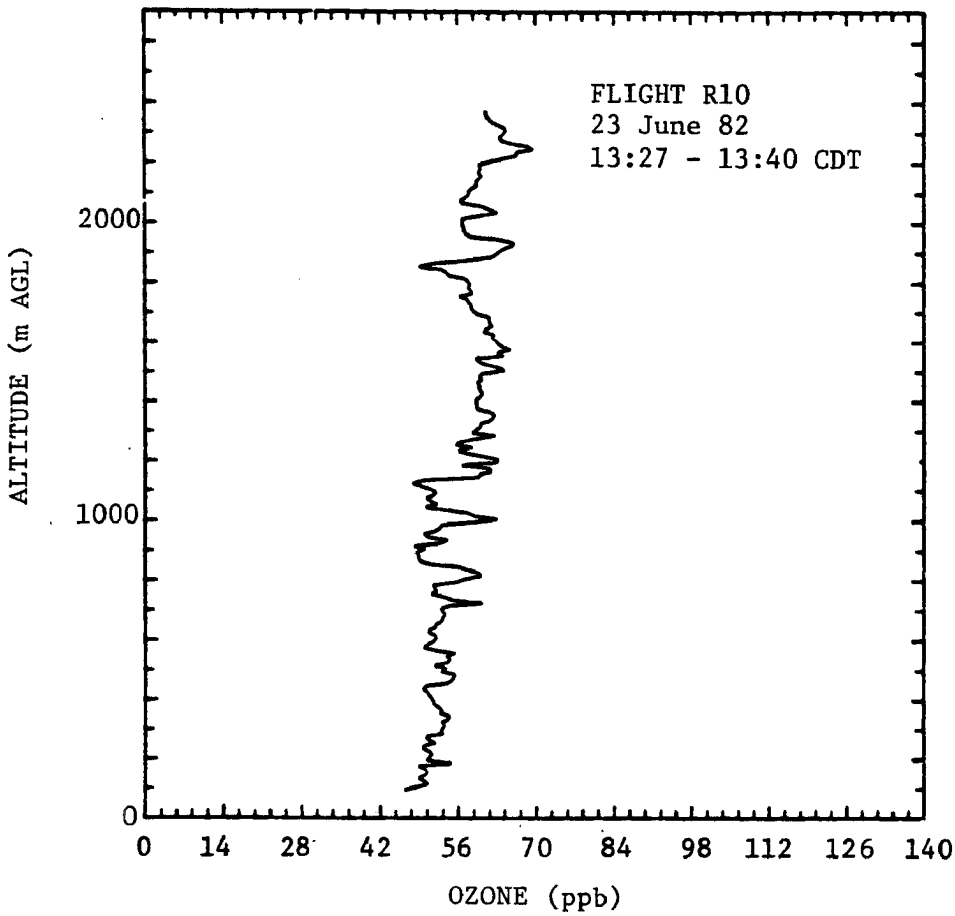

Fig. 12. Vertical profile of mean ozone concentration at the midpoint of flight R10.

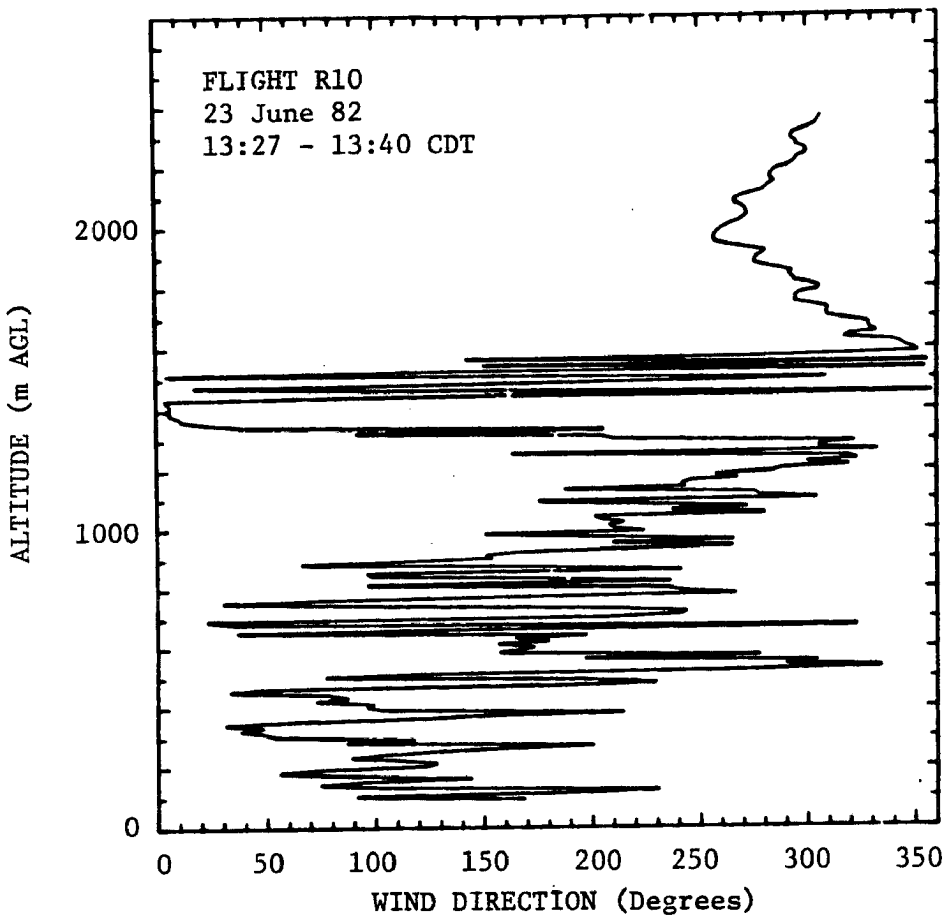

Fig. 13. Vertical profile of wind direction for flight R10.

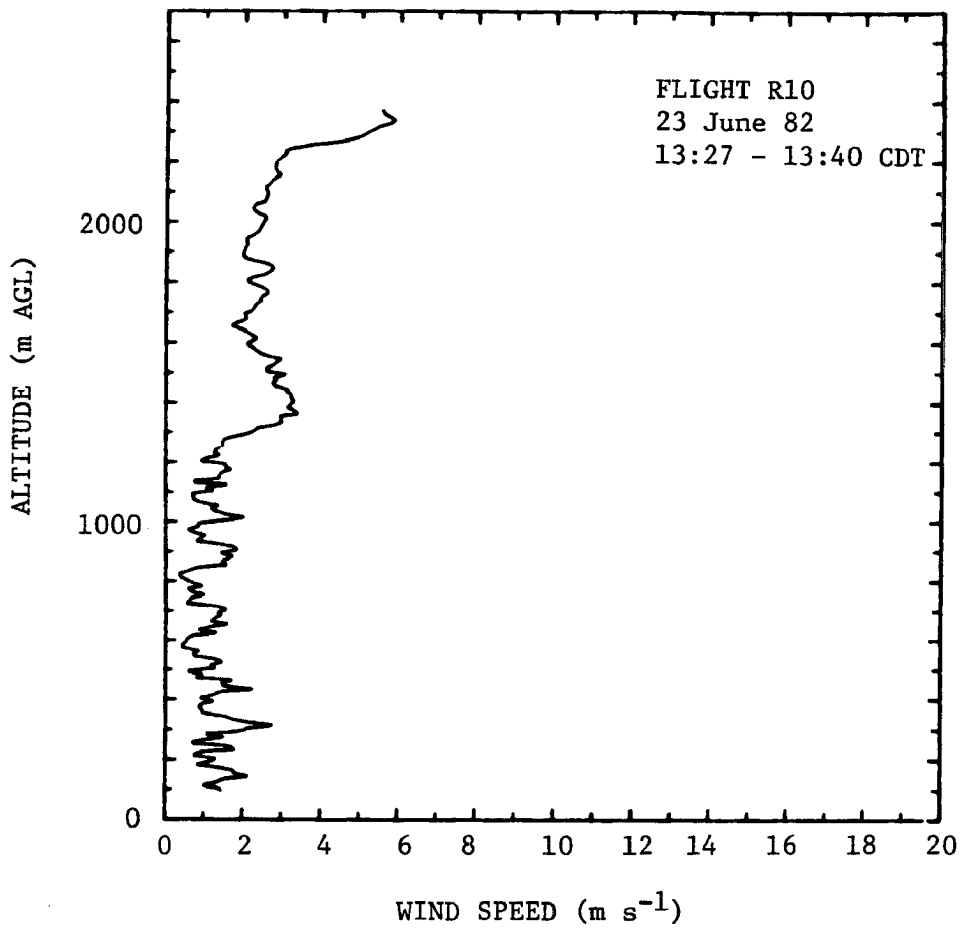

Fig. 14. Vertical profile of mean horizontal wind speed for flight R10.

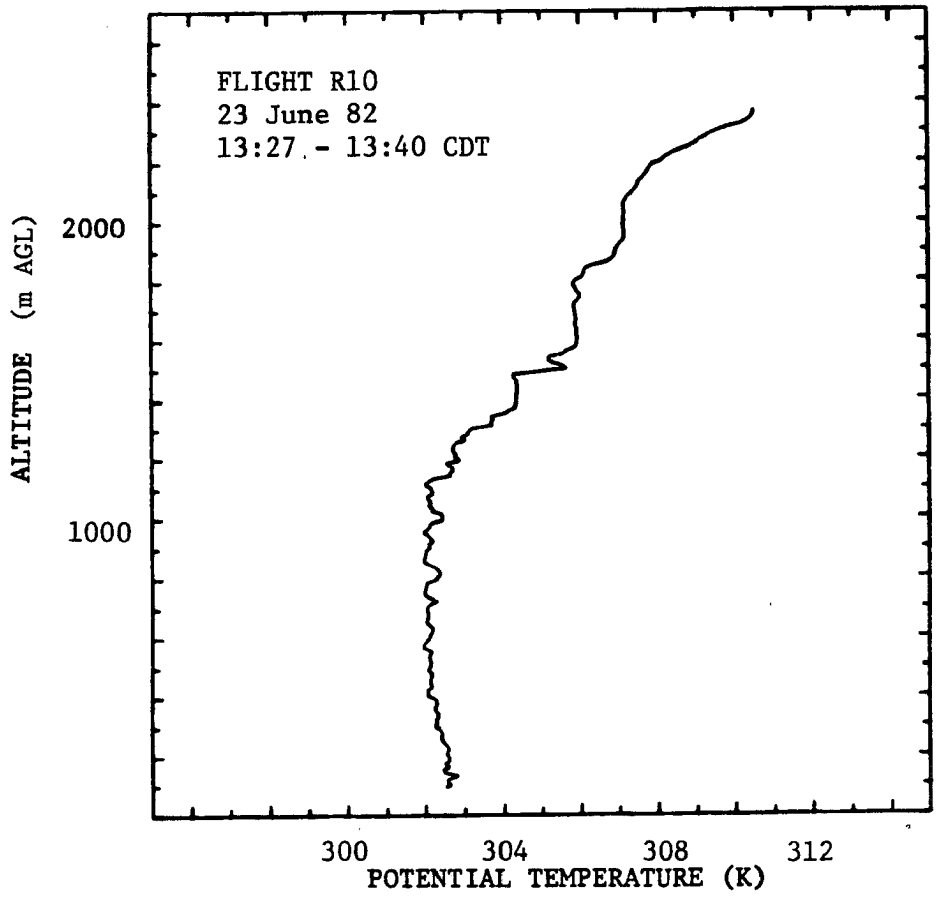

Fig. 15. Vertical profile of mean potential temperature for flight R10.

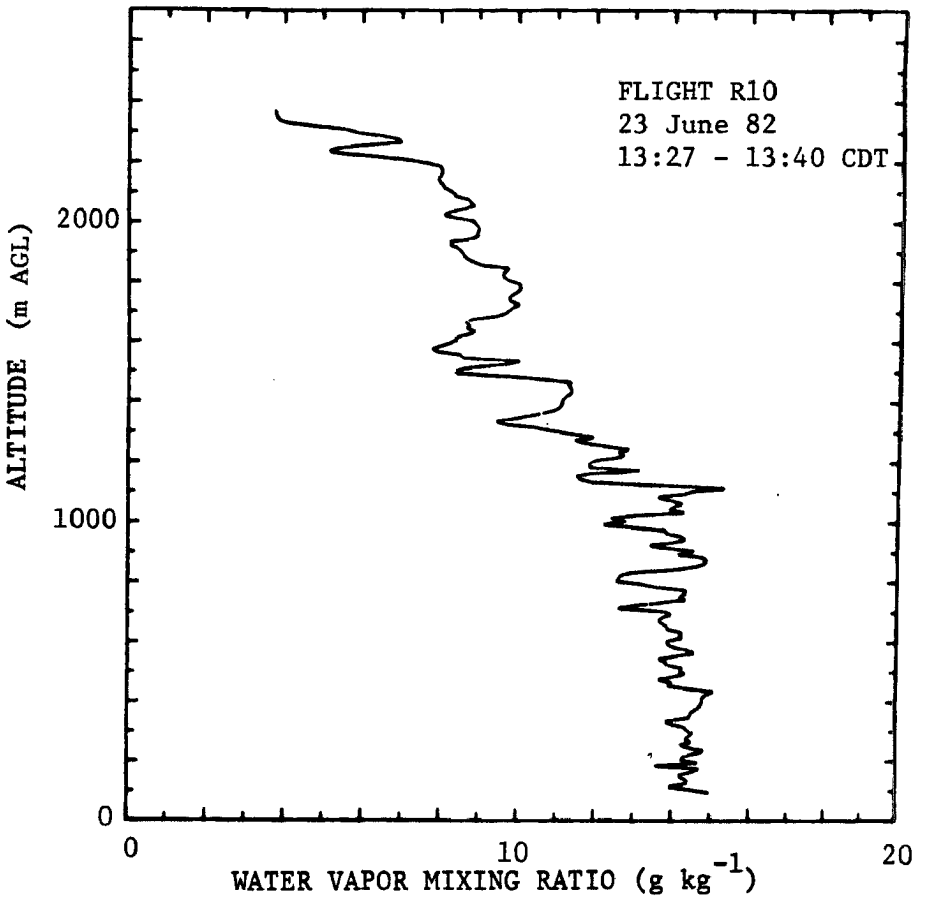

Fig. 16. Vertical profile of water vapor mixing ratio for flight R10.

Figures 17 through 21 show the profiles from a sounding near the end of flight R13. Potential temperature and mixing ratio in the boundary layer are similar to those in R10 but in this case the mixed layer extends to about 800 m. Wind speeds on this day are moderate throughout the boundary layer and consistently from the west-southwest direction. These winds imply advection from the Houston urban area on a time scale of 2 to 3 hours.

The profile for ozone on this day (Fig. 17) exhibits a quite remarkable distribution with height. The boundary layer concentration of about 55 ppb is similar to that of flight R10 but above the mixed layer an ozone-depleted layer exists, extending through a depth of almost 1000 m, with a concentration of about one half that above and below. It will be seen that this vertical distribution has a marked effect on the ozone flux profile for this day. It should be noted that the strongly layered structure in ozone concentration appearing at the top of the inversion layer should most likely be interpreted as horizontal as well as vertical inhomogeneities encountered by the aircraft along its slant path. The undulating nature of the inversion base and pronounced wind shear at that level create a region of large inhomogeneities (Kaimal et al., 1982). In view of the rather slow rate of climb of the aircraft little significance can be attributed to this structure.

The origin of the ozone depleted layer is puzzling. Ozone profiles on 23 and 25 June 1982 (Figs. 12 and 22) over the same area at the same time of day show no such behavior although the potential temperature and moisture profiles are very similar. Isentropic trajectory analysis may shed some light on this question.

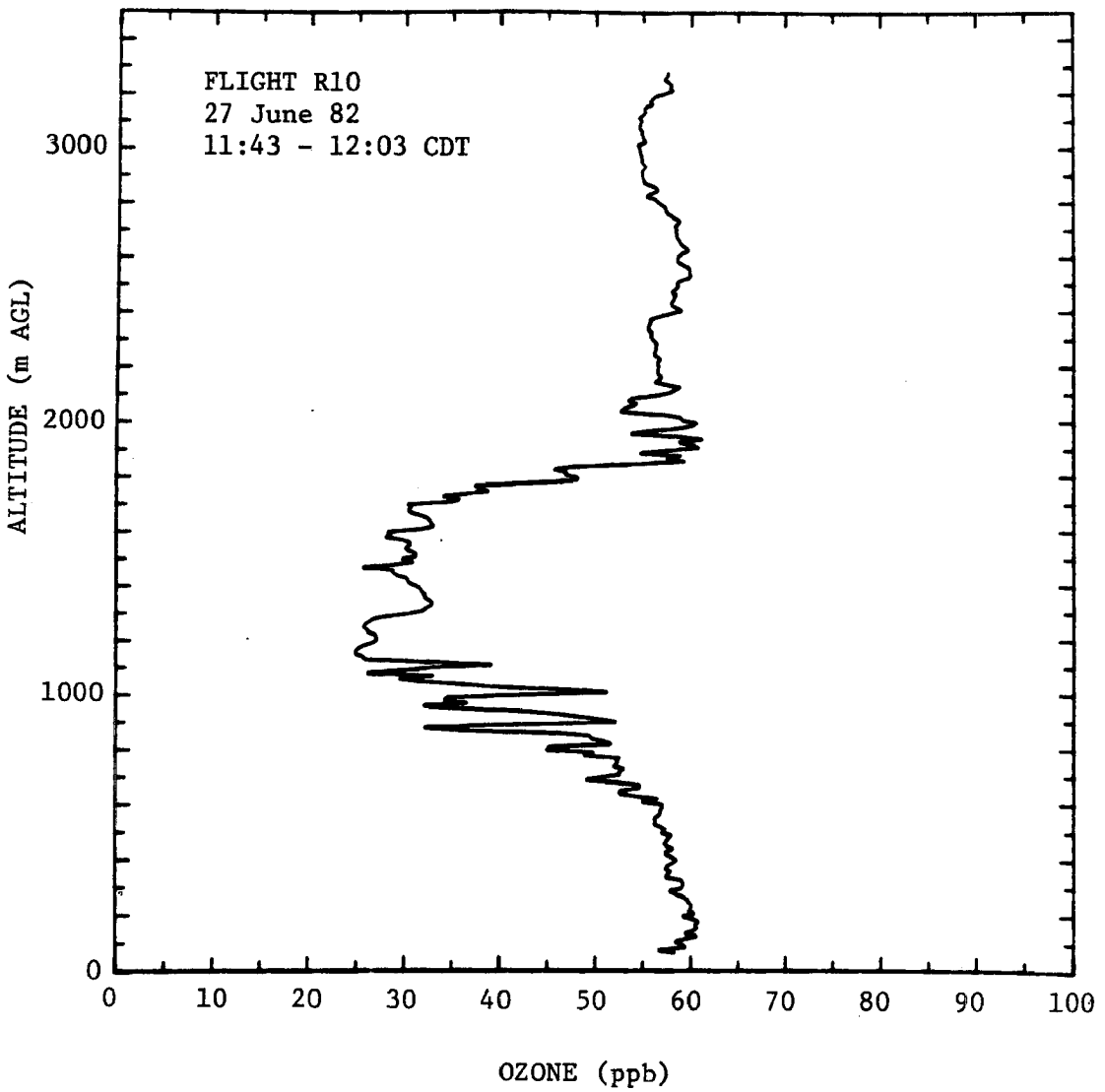

Fig. 17. Vertical Profile of mean ozone concentration taken near the end of flight R13.

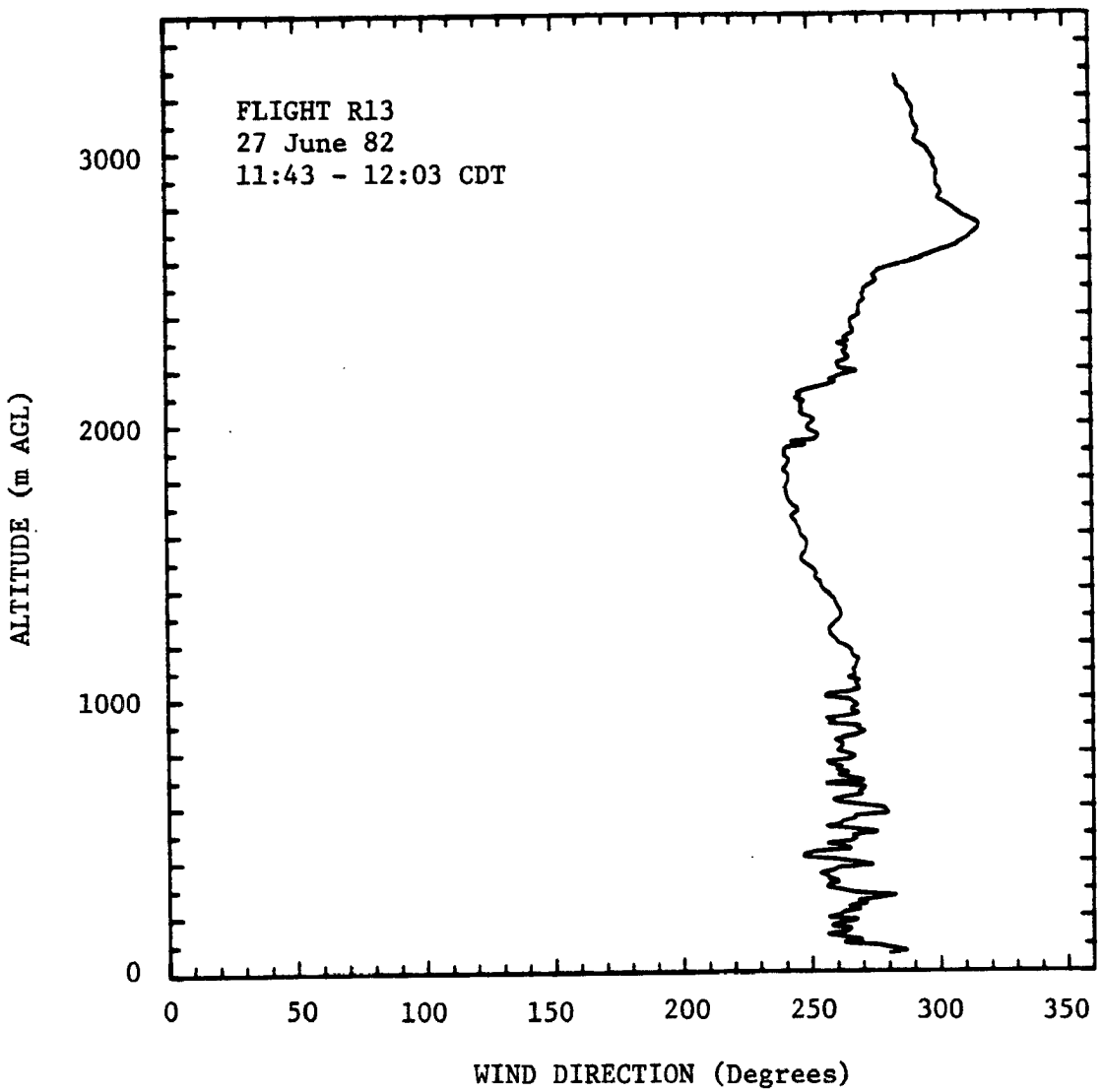

Fig. 18. Vertical profile of wind direction for flight R13.

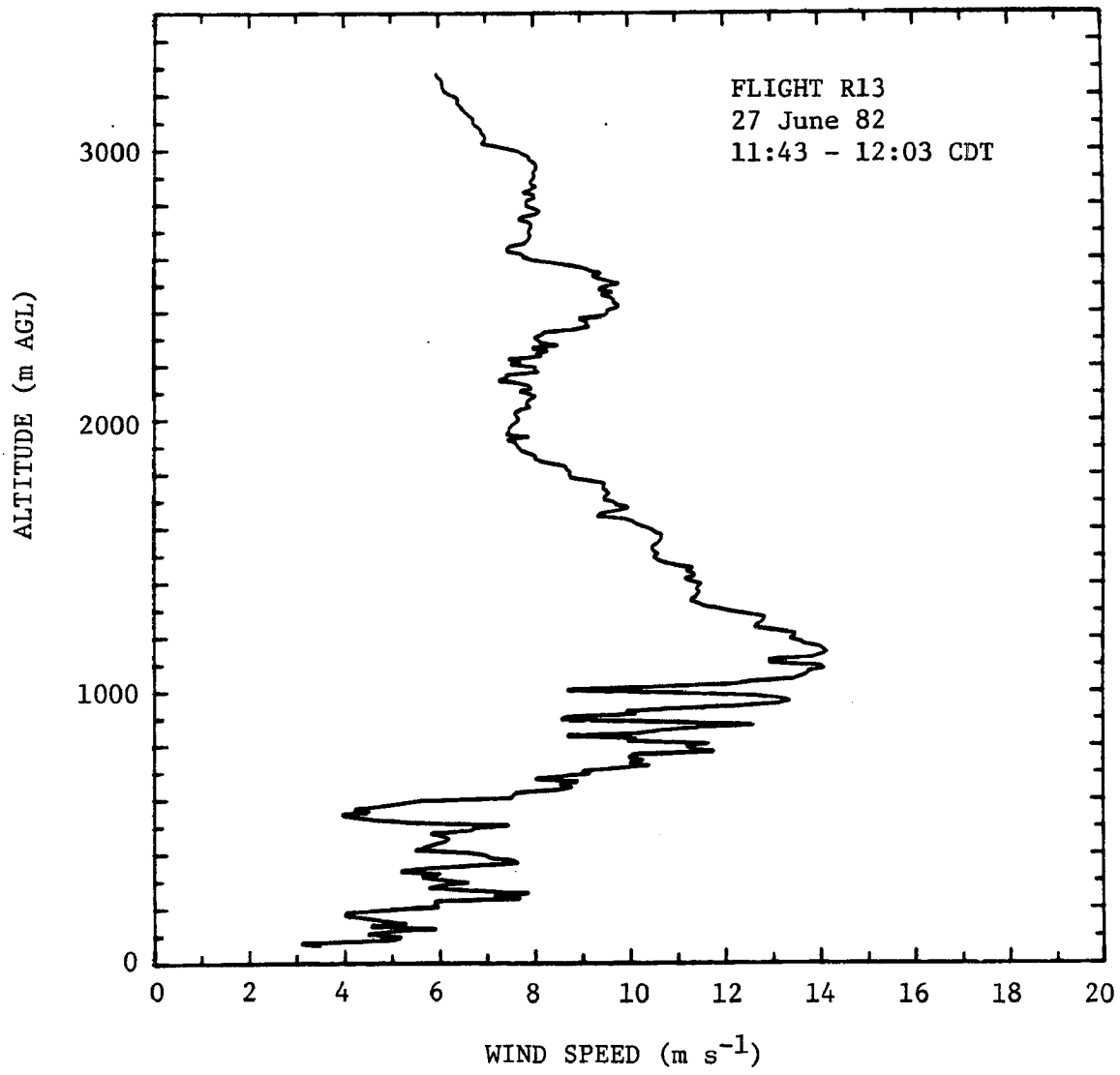

Fig. 19. Vertical profile of mean horizontal wind speed for flight R13.

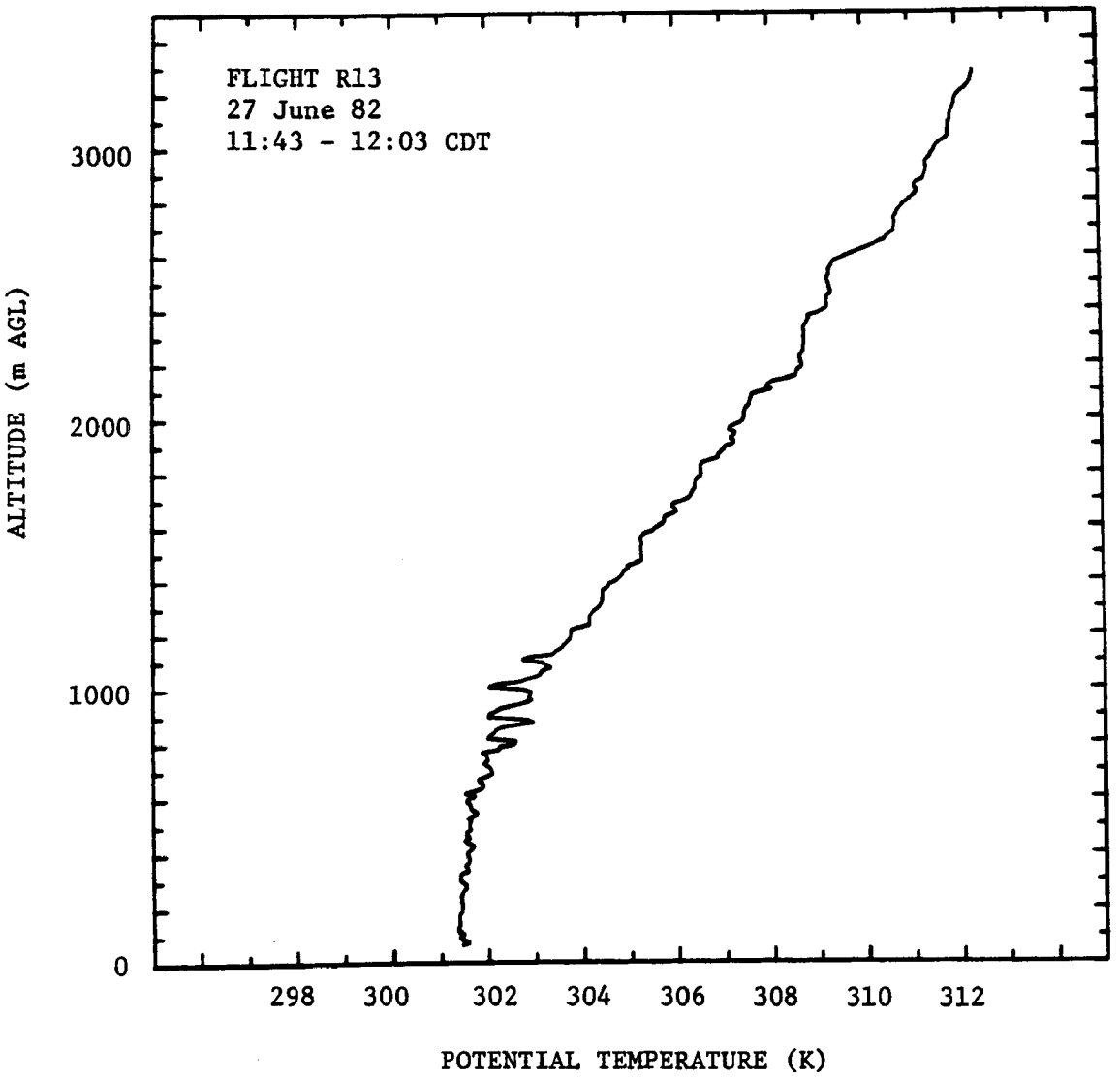

Fig. 20. Vertical profile of mean potential temperature for flight R13.

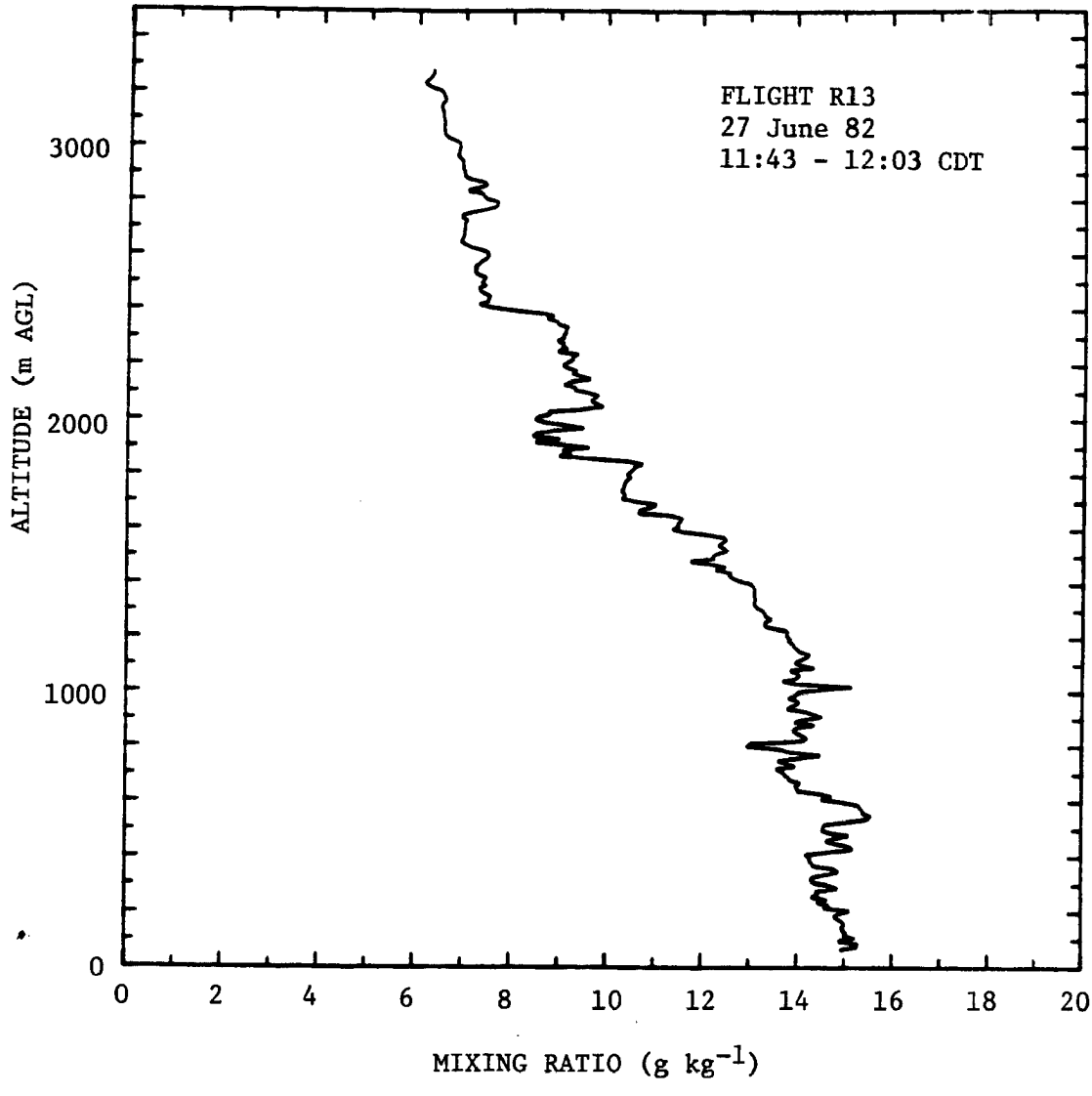

Fig. 21. Vertical profile of water vapor mixing ratio for flight R13.

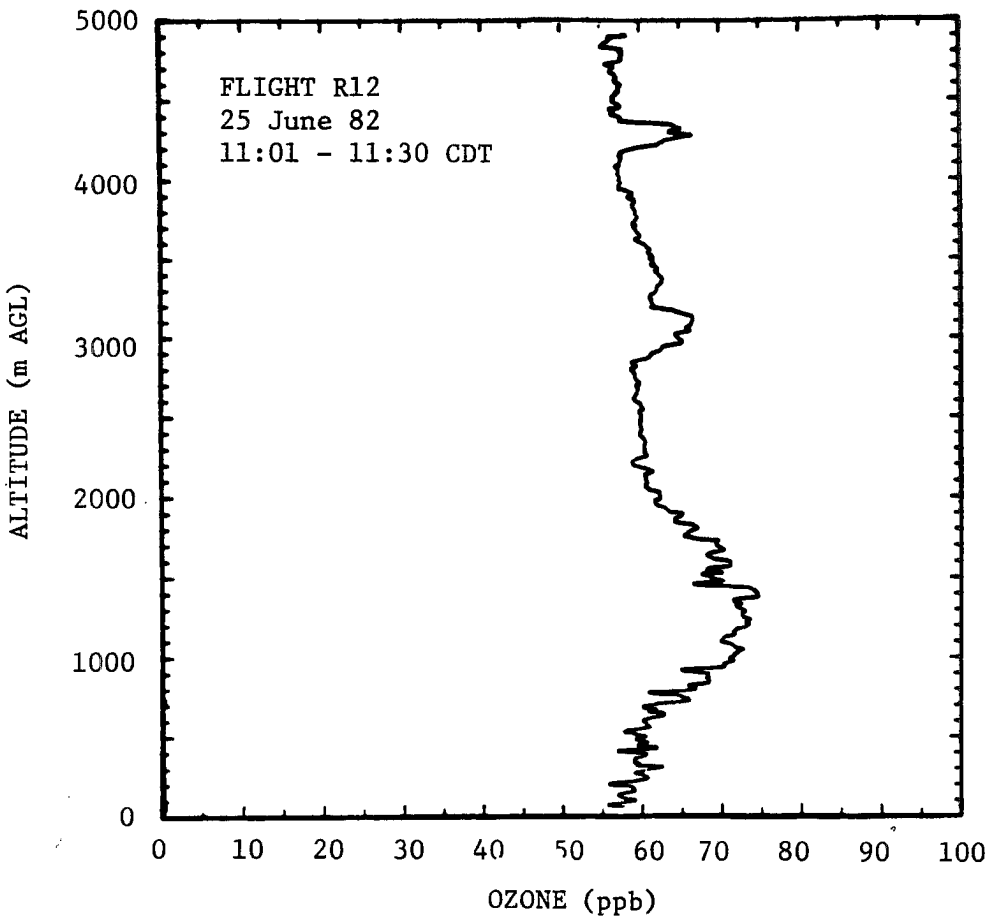

Fig. 22. Vertical profile of mean ozone concentration for flight R12.

5.2.1 Entrainment Velocity

Sounding plots are also useful in studying the growth of the mixed layer during the flight. Lenschow et al. (1981) have used this evolution to gain an estimate of the entrainment velocity for the case of an actively growing mixed layer in which the mean vertical velocity was assumed to be negligible. We can apply this type of analysis to flight R10 for which a full set of profiles is available. Figure 23 shows vertical profiles of potential temperature over the course of R10. The entrainment velocity estimated from the mixed layer growth of R10 is 6.3 cm s^{-1}. Lenschow et al. (1982) have shown that entrainment velocity estimated by the relation

$$(\overline{w'\theta'_3})_{z_i} = w_e \Delta \bar{\theta}_3 \qquad (5.1)$$

can be used to estimate the mean vertical velocity at the inversion height, w_{z_i}, for the case of a steady-state uniform boundary layer height. In Eq. (5.1), $(\overline{w'\theta'_3})_{z_i}$ is the ozone flux at the inversion height h, w_e is the entrainment velocity, and $\Delta\bar{\theta}_3$ is the change in ozone concentration across the top of the mixed layer. The ozone flux at the inversion height is obtained from extrapolation of the ozone flux profiles (Sec. 5.4.4) to $z=z_i$ and $\Delta\bar{\theta}_3$ is obtained from the mean ozone profiles. The resulting entrainment velocity, w_e, is 6.7 cm s^{1} for R13 and 6.5 cm s^{-1} for R10. This agrees very closely with w_e derived from the R10 boundary layer growth and probably represents a number typical of this regime (see also Lenschow et al., 1981). The close agreement between the entrainment velocity estimated by both methods for flight R10 indicates that the mean vertical velocity was in fact near

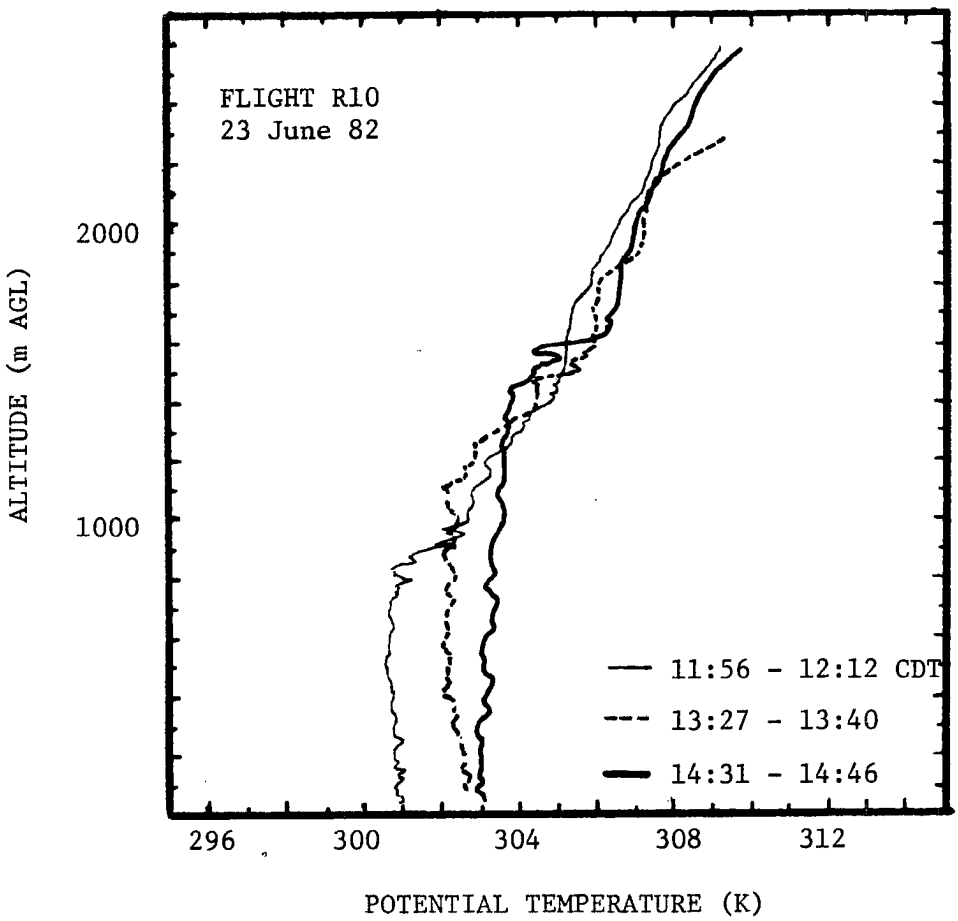

Fig. 23. Set of vertical profiles of potential temperature measured during flight R10 showing the increasing depth of the mixed layer with time.

negligible, a conclusion supported by the synoptic analysis in Sec. 3.4 and the weak inversions observed on the potential temperature profiles, Figure 23.

5.2.2 Surface Layer Gradients

Another interesting phenomenon that can sometimes be observed in the mean profiles is a positive gradient in ozone concentration near the surface. This would imply a very active sink for ozone at the surface and indeed the surface flux to the forest is found to be quite large. These departures from well-mixed ozone structure have been noted previously by Van Dop et al. (1977) below 500 m and attributed to enhanced photochemical destruction by pollutants as well as surface deposition. Lenschow (1982) has demonstrated how NO_x photochemistry can effect the ozone profile in the surface layer. Over the forest it is also possible that reactive hydrocarbons emitted by the vegetation are consuming ozone. Substantial ozone gradients can be seen below 200 m in Figs. 12 and 17. Gradients do not, however, always show up in the aircraft soundings. They seem to appear in about half the vertical profiles taken and usually those earlier in the day. The aircraft measurements, which are almost instantaneous and point specific, are not especially well-suited to measure gradients in the lower boundary layer. To consistently observe such gradients, longer averaging times are needed to remove rapid time and spatial variations. There is some evidence for the existence of this phenomenon in the aircraft data, however, which may merit further study.

5.3 Spectra and Cospectra

Data from the straight, level portions of the flights have been processed with a spectral analysis program package. The results of this analysis include power spectra, cospectra, autocorrelation of variance and co-variance, integral scales, means and higher order statistics. Generally this analysis is applied to vertical velocity, horizontal velocity components, temperature, absolute humidity, and ozone mixing ratio data. The spectral analyses from the Texas experiment comprise a very rich and interesting data set in themselves. A thorough investigation of this data set is, however, beyond the scope of this paper and only a brief discussion is included here.

The primary use of the spectra and cospectra is to determine what frequency response and averaging times are necessary to obtain reliable estimates of the vertical flux. At the high frequency end of the spectrum, the frequency response of the sensors is fixed so the spectra are used to assure ourselves that the observed spectral energy falls off well above the frequency limit dictated by the instrument response. On the low frequency end the spectra and cospectra are used to determine the averaging time necessary to include all significant contributions to the flux. Experience has shown that 205 s is generally a good time period in the fully convective planetary boundary layer.

An example set of spectra from flight R10 is shown in Fig. 24. In this example we see that the variance (area under the curve) dropsoff sharply above about 6 km and below about 60 m wavelength for each variable (except ozone in the high wavenumber region). The 205-s flux averaging time corresponds to a wavelength of about 14.5 km or wavenumber of about 0.4 radians km^{-1}. The bandwidth of the sensor

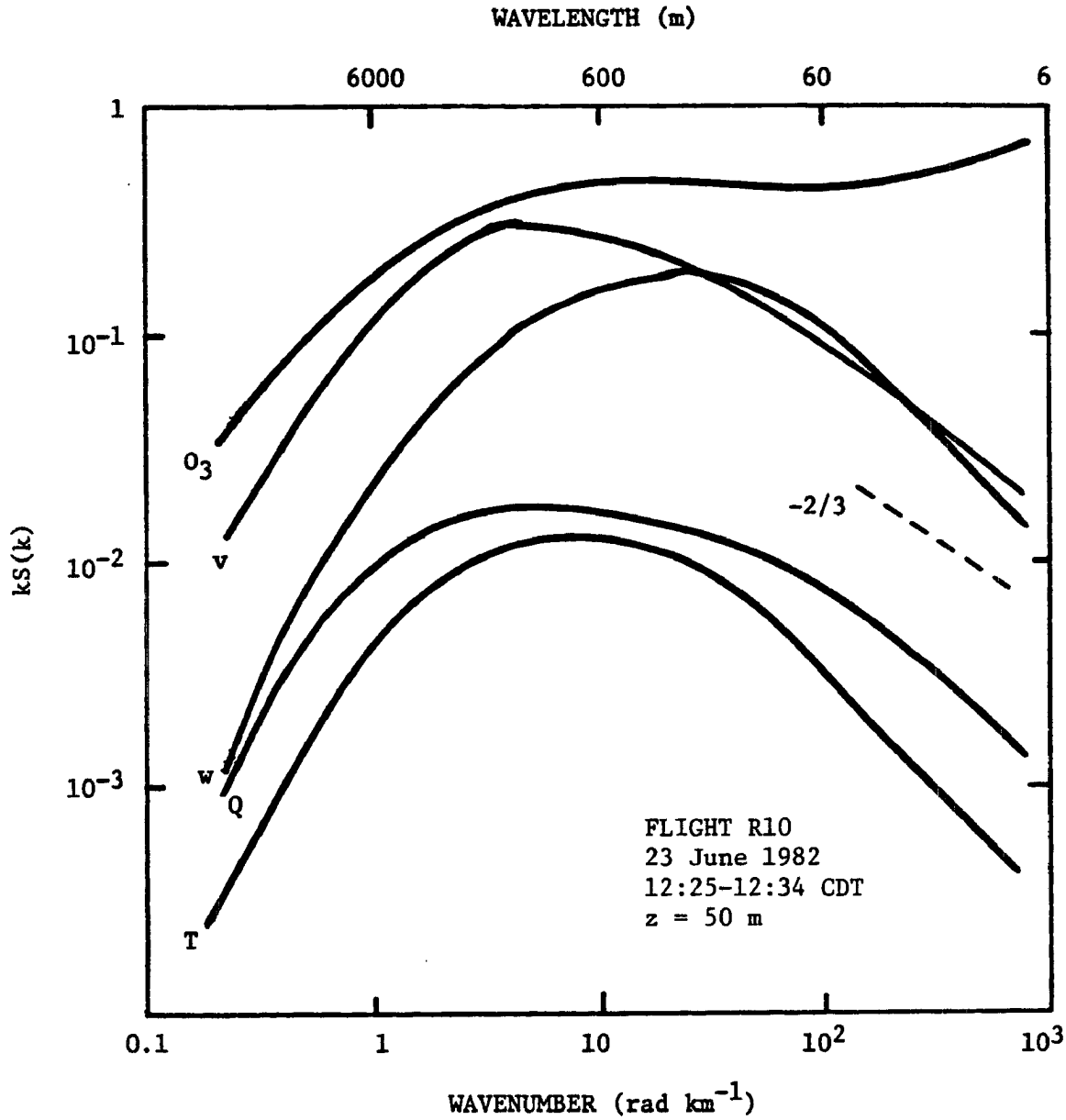

Fig. 24. Spectra from a portion of flight R10. The ordinate kS(k) is wavenumber times spectral density. The scalar variance units are: $O_3(ppb^2)$, $v(m^2\ s^{-2})$, $w(m^2\ s^{-2})$, $Q(g^2\ m^{-6})$, and $T(K^2)$.

response is limited to 10 Hz by a filter in the data recording. This frequency corresponds to a wavelength of less than 10 m at an average airspeed of 70 m s^{-1}. In this case we can feel confident that we are properly sampling the physical process that is creating most all of the boundary layer scalar variance. Clearly if all the significant scales contributing to the variance are included, the covariance estimates should be reliable as well.

The ozone spectrum in the high wavenumber region exhibits the variance in the ozone signal created by the random shot noise. This contribution to the ozone variance is not correlated with the vertical velocity and does not contribute to the measured vertical ozone flux as can be seen from the cospectrum of w and O_3. The spectra other than O_3 have the -5/3 slope in the inertial range which is that predicted by theory (the theoretical slope is -2/3 on a diagram of wavenumber times spectral density as in Fig. 24). The displacement of the wavelength of maximum amplitude for the w spectrum relative to the other scalars is consistent with spectra obtained by Kaimal et al. (1982) and Kaimal et al. (1976) near the surface in convective conditions. The spectra and cospectra shown in these figures are calculated in logarithmic block averages over wave number and smoothed by hand. This process is useful to obtain the general shape of the curves but confidence limits on any of the fine structure are not implied.

The cospectra with vertical velocity for this same period are shown in Fig. 25. It is apparent that essentially all of the vertical flux is occurring in the wavelength region from about 50 to 5000 m. The heat and moisture fluxes are clearly upward (positive), ozone downward (negative), while the momentum flux is mostly downward. Recall that the

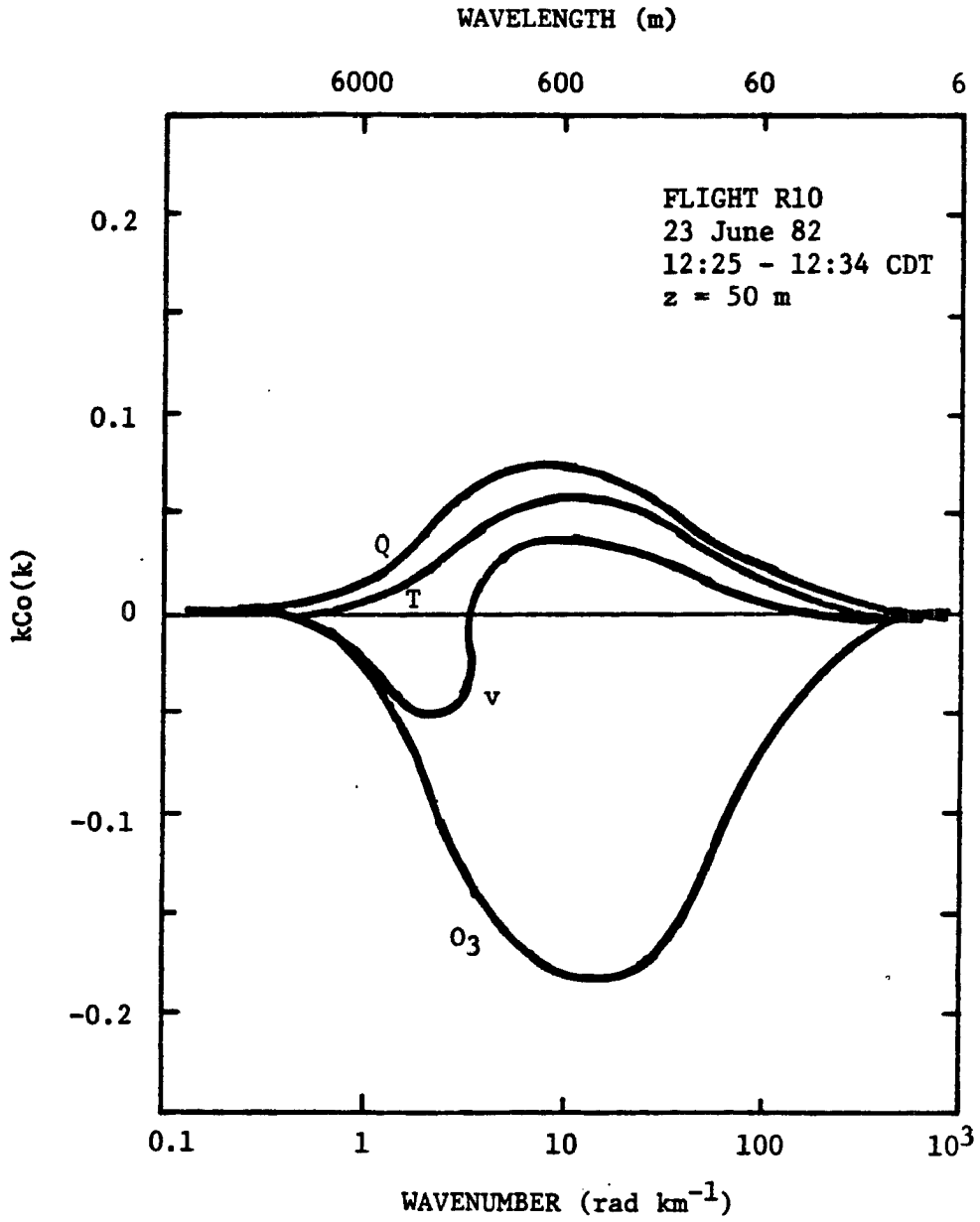

Fig. 25. Cospectra of vertical velocity with selected scalars. The ordinate kCo(k) is wavenumber times cospectrum. The units are: wQ(g m^{-2} s^{-1}), wT(K m s^{-1}), wv(m^2 s^{-2}), and wO_3(ppb m s^{-1}).

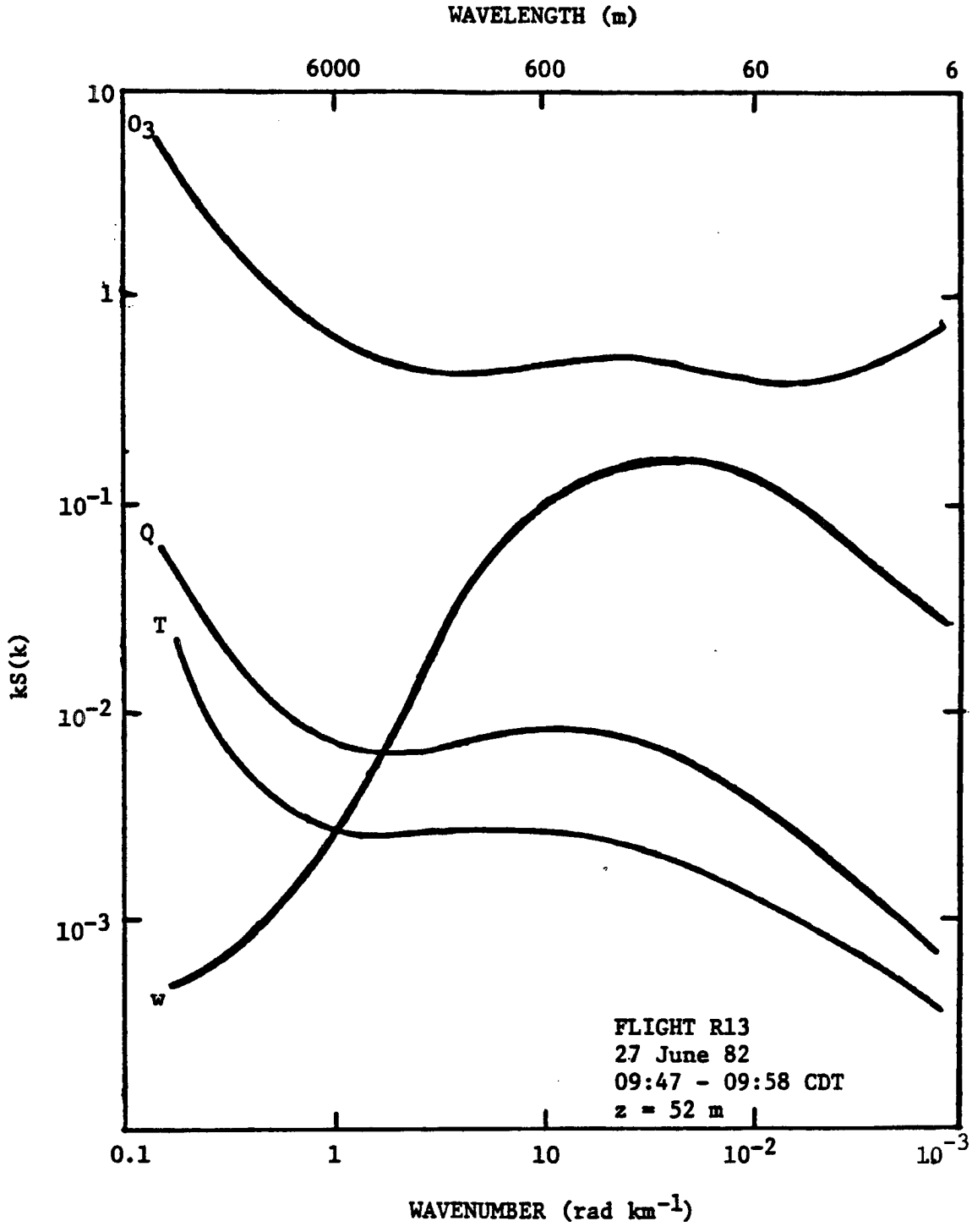

Fig. 26. Spectra measured early in flight R13. The ordinate kS(k) is wavenumber times spectral density. The scalar variance units are: O_3(ppb^2), Q(g^2 m^{-6}), T(K^2), and w(m^2 s^{-2}).

winds were very light on this day and that the momentum flux is nearly zero. The lack of correlation between w and the ozone shot noise can be seen here as well. Figure 26 shows a set of spectra from near the beginning of Flight R13. In this set it is apparent that there are large contributions to the scalar variances from scales of motion greater than 6 km. This effect is also seen in the time series for this period as a non-linear trend in the data with the turbulent fluctuations superimposed. Therefore we decided not to include the flux data from before 10:00 CDT since the aircraft, eddy correlation technique cannot accurately determine fluxes on these longer time scales. After that time the spectra are dominated by variance in the turbulent scale regions. Apparently, before the mixed layer has been established for some time, local effects such as terrain variation, vegetation differences or local water supply may be important factors at length scales of about 10 km or greater. Turbulence dominates the variances once the boundary layer has had time to mix up more completely.

An additional check on the suitability of the averaging period and the validity of the horizontal homogeneity assumption is the comparison of the leg-average flux (two or three 204-s segments) with the area under the cospectra over the entire leg. The agreement between these calculations is generally within 20%, and even better in most cases.

5.4 Fluxes

Vertical fluxes of horizontal wind components, absolute humidity, potential temperature, virtual potential temperature, and ozone mixing ratio are calculated by the eddy correlation method. The fluxes for

each 15-km segment at the same altitude are averaged and profiles are formed. The flux divergence is the slope of the profile determined by a least squares linear regression of the fluxes.

5.4.1 Sensible Heat Flux Profiles

Figure 27 shows profiles of sensible heat flux for Flights R5, R10, and R13 and the average flux at 60 m AGL for R12. The error bars are the uncertainty in the mean given by the student-t distribution at the 95% confidence level. These profiles show that the heat flux divergence for the two forest flights is about the same although the surface heat flux for R10 is almost twice that of R13. This is primarily because R13 was flown earlier in the day (median time is about 10:50 CDT) before maximum solar heating was attained while R10 was flown near local solar noon. Also more of the surface energy flux for R13 is going up as latent heat and cloudiness was more extensive. The heat flux over ocean (R5) is very small at all levels as most of the incoming solar energy is stored in the water (Sellers, 1965, Chapter 8). Note that only the lowest two levels are used in the divergence estimate for the R5 flux profile since the upper point is above the marine boundary layer (z_i = 500 m).

In all cases the heat flux changes sign near the middle of the boundary layer indicating entrainment of warmer air from above the inversion. The R10 and R5 heat fluxes are zero near 0.6 z_i which is close to the level of zero crossing found by Wyngaard et al. (1978) for AMTEX data (0.67 z_i). Lenschow and Stephens (1980) found that the thermal-scale heat flux went to zero at about 0.5 z_i and attributed the positive heat flux from 0.5 to 0.7 z_i to smaller scales. Thus it appears that the exact level of zero crossing for sensible heat flux may depend

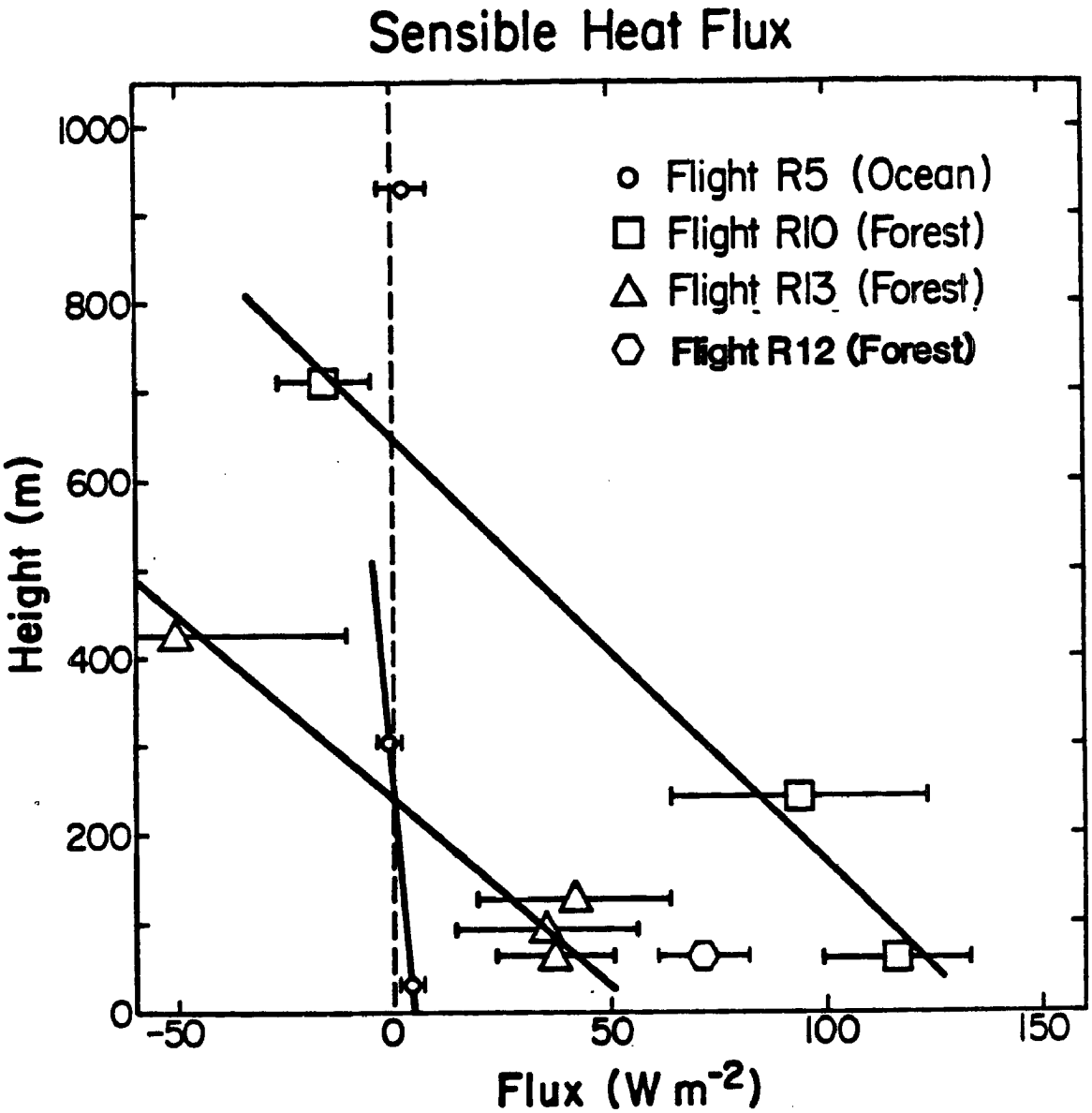

Fig. 27. Profiles of sensible heat flux ($\rho c_p \overline{w'\theta'}$) for flights R5, R10, R13, and the average heat flux for flight R12. Error bars are the 95% confidence limit on the mean flux based on a student-t distribution. The inversion height is 500 m for R5, 1200 m for R10, and 800 m for R13 and R12.

on the relative contribution to the flux by the various scales of motion which may vary over different surfaces. AMTEX data was gathered over ocean. The heat flux for flight R13 is zero at about 0.4 z_i but there is a large uncertainty in the value of the highest point.

5.4.2 Water Vapor Flux Profiles

The boundary layer profiles of water vapor flux over forest are shown in Fig. 28. The surface fluxes are similar, with R10 again the larger, while the flux divergences are about the same. The water vapor and sensible heat fluxes obtained by extrapolating the flux profiles down to the displacement height yield a Bowen ratio of 0.42 for R10 and 0.22 for R13. As observed earlier, proportionately more of the surface energy for R13 is going up as moisture than sensible heat compared to R10. This may be due to a greater availability of water at the surface during R13 from recent rains, the somewhat different geography and vegetation, or the fact that R13 took place earlier in the day. In any case, it is interesting that the divergences are almost exactly the same although the large uncertainties in the means caution against definitive statements. In general, water vapor is not very uniformly distributed in the boundary layer and the variability of the measurements reflect this fact. Also there were only a small number of segments flown for the upper levels of R13 so the student-t confidence limits are relatively large.

5.4.3 Flux Profiles of Virtual Potential Temperature

The virtual potential temperature flux profiles are shown in Fig. 29. Their behavior is consistent with the fluxes of sensible heat and moisture from which the virtual potential temperature is calculated.

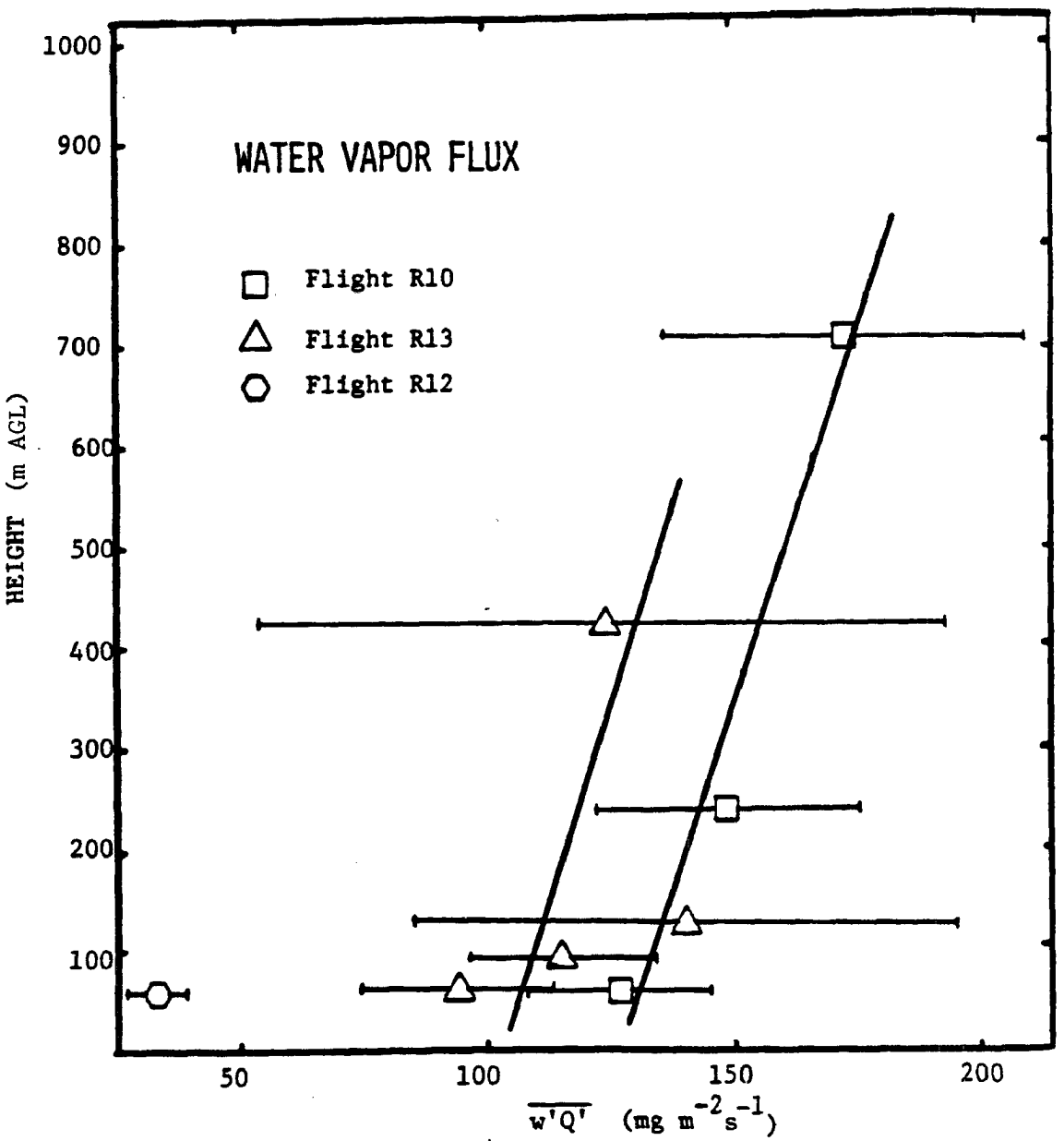

Fig. 28. Profiles of the water vapor flux over forest for flights R10 and R13, and the average flux for flight R12. Error bars are the 95% confidence limit on the mean flux based on a student-t distribution. The inversion height is 1200 m for flight R10 and 800 m for R13 and R12.

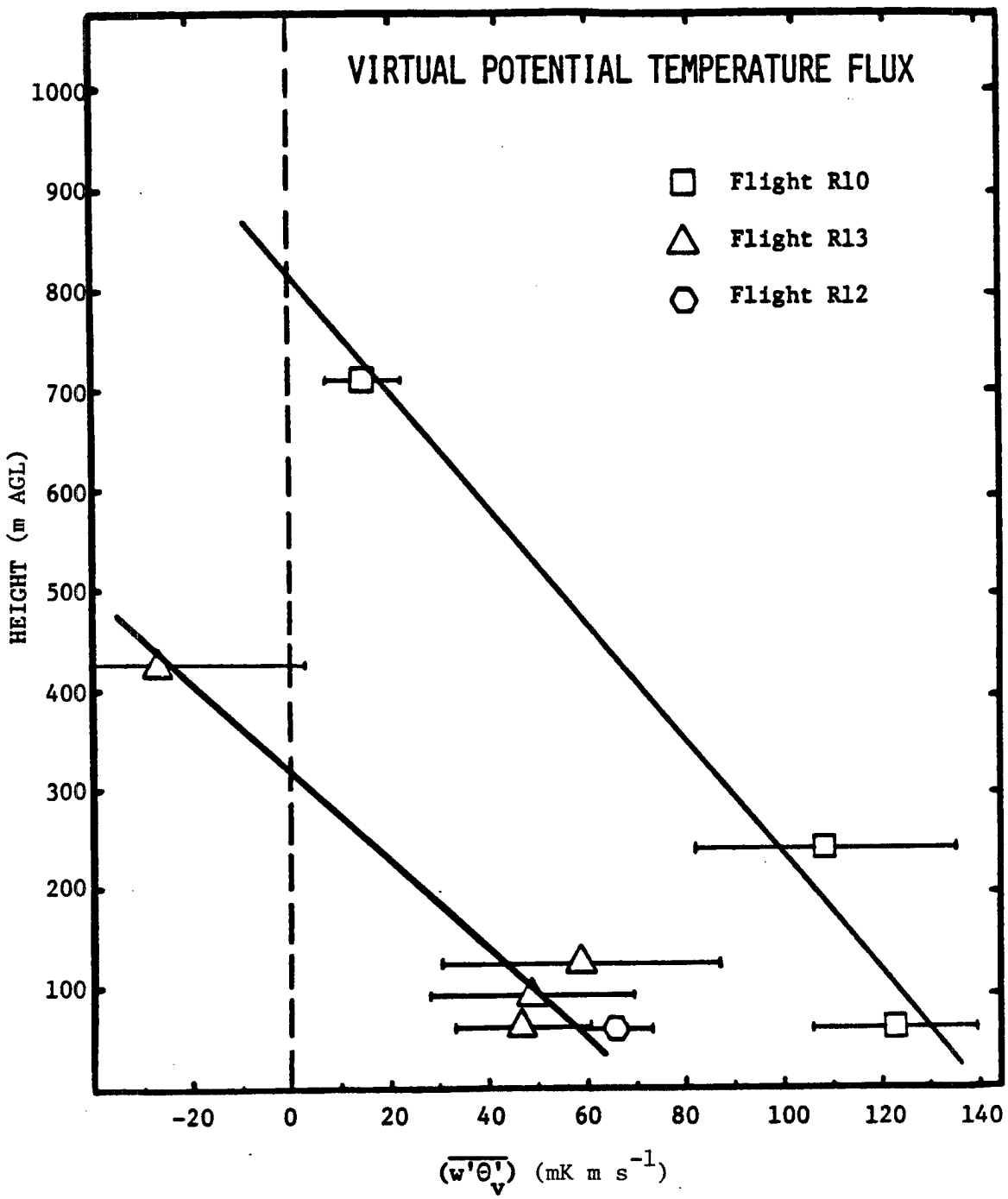

Fig. 29. Profiles of the flux of virtual potential temperature over forest for flights R10 and R13 and the average flux for flight R12. Error bars are the 95% confidence limit on the mean flux based on a student-t distribution. The inversion height is 1200 m for flight R10 and 800 m for R13 and R12.

5.4.4 Ozone Flux Profiles

Figure 30 shows the flux profiles for ozone. It is seen that the surface fluxes are almost the same for the two forest cases, but that the flux divergences are greatly different. This consistency of the magnitude of the surface flux suggests that it depends on the rate of destruction at the surface rather than the direct input of energy to the surface, as in the case of the heat flux. The surface destruction rate is a property of the surface itself, in these cases the forest. This is assuming, of course, conditions are such that there is sufficient sunlight, moisture, and ventilation for normal plant respiration. The slope of the flux profile is then determined by the entrainment flux at the inversion which depends on the entrainment velocity and change of ozone concentration across the inversion.

The ozone flux for R10 is downward throughout the mixed layer and nearly constant with height. This is consistent with the uniform vertical distribution of mean ozone observed in the sounding for this flight. In contrast, the flux profile from flight R13 has a large flux divergence. Ozone in the lower boundary layer is moving toward the surface while the flux in the upper part is upward, presumably reflecting the effect of the ozone depleted layer above. The ozone flux at the ocean surface is very small, even less than surface fluxes measured by Lenschow et al. (1982). This lower surface flux is probably due to the low windspeeds, the observed lack of wave action and a lower mean ozone concentration.

5.4.5 Horizontal Variablilty of Fluxes

The long horizontal track and number of low-level legs flown during R13 make it possible to look at the variation of the fluxes along the

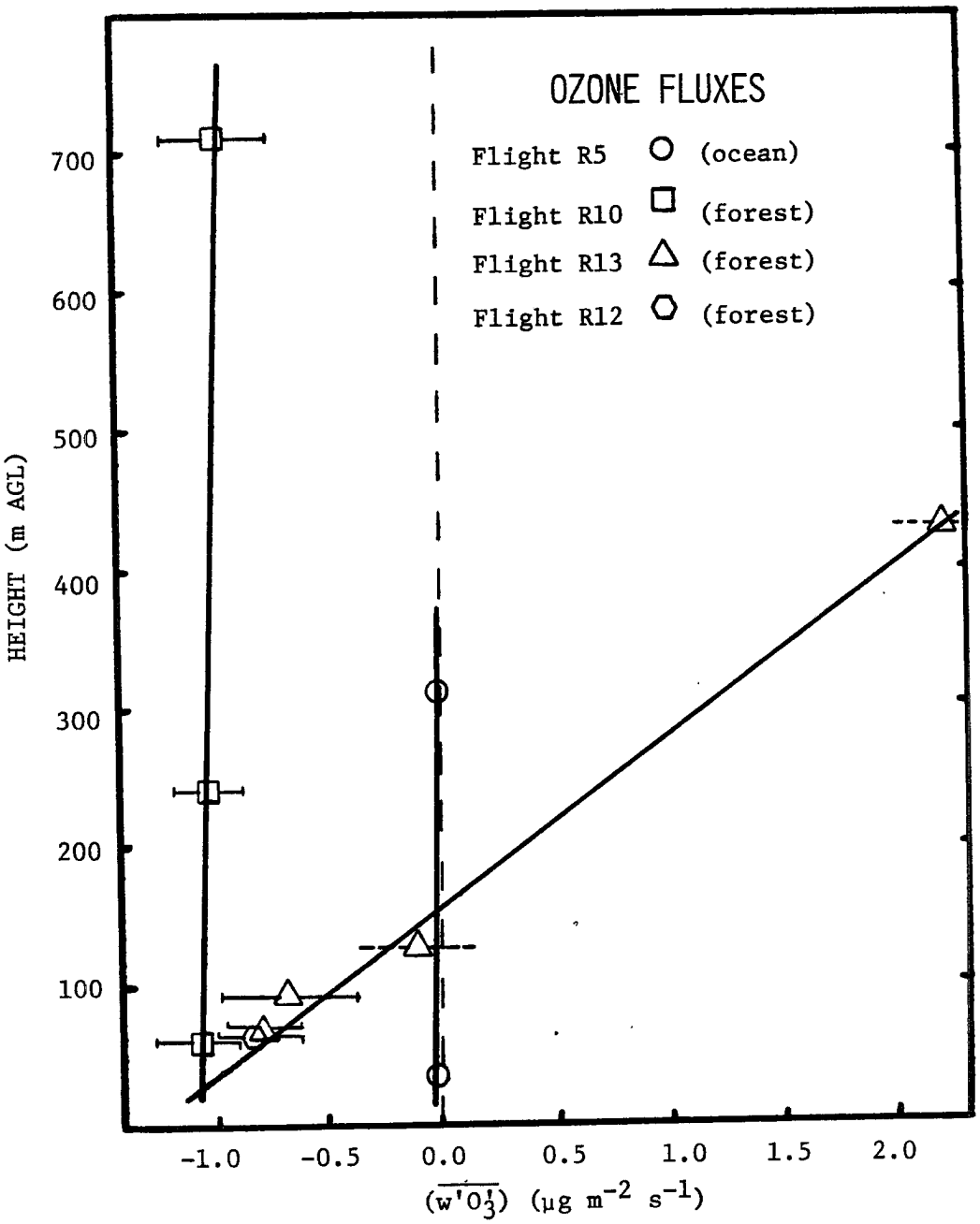

Fig. 30. Profiles of the ozone flux for flights R5, R10, R13, and the average flux for flight R12. Error bars are the 95% confidence limit on the mean flux based on a student-t distribution. The inversion height is 500 m for R5, 1200 m for R10, and 800 m for R13 and R12.

sampling path. Figures 31 through 33 show the horizontal distribution of the fluxes of water vapor, virtual potential temperature, and ozone. Potential temperature (or sensible heat) fluxes closely follow the pattern of the buoyancy fluxes. These legs are all flown at approximately 60 m AGL over a period of about 90 minutes. The length of the bars indicates the distance over which the eddy correlation fluxes are averaged. The different symbols indicate segments from the same leg and the order of observation. There is no correlation between the magnitude of the fluxes and the direction of aircraft flight. From this display of the measurements, it appears that the moisture flux (Fig. 31) is higher toward the western end of the track. The fluxes of virtual potential temperature (Fig. 32) and sensible heat (not shown) are uniform although the scatter is greater in the west. The ozone flux (Fig. 33) appears to be slightly lower on the west end although the variation among the points is greater than the change in the mean. Note that this trend to lower ozone flux in the west is opposite to the change in flux expected for an aircraft flying at constant altitude (MSL) over ground which slopes upward about 20 m over the track to the west. A larger downward ozone flux would be expected from the slope of the flux profile.

The horizontal flux profiles lead us to interesting observations on particular aspects of the exchange between the surface and the boundary layer. The virtual potential temperature flux at the surface should be controlled primarily by the solar heat input at the surface. If the storage and radiative properties of the forest are the same along the path and the solar input is the same, the virtual potential temperature flux should not vary. On the other hand, the ozone flux is controlled

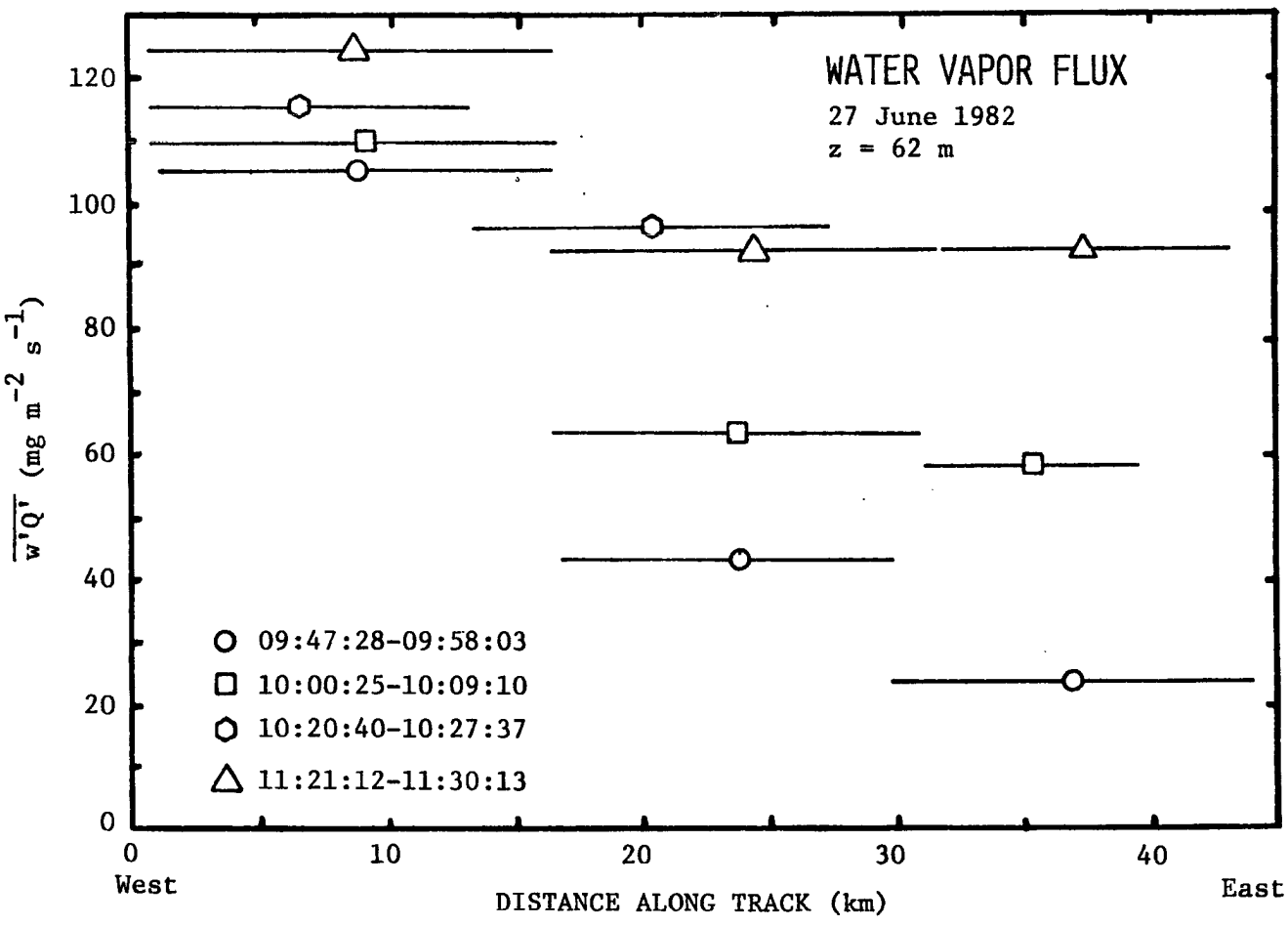

Fig. 31. Horizontal distribution of water vapor fluxes for flight R13 over forest. Length of segments represents the distance over which the flux is averaged. Symbols indicate the times of the segments.

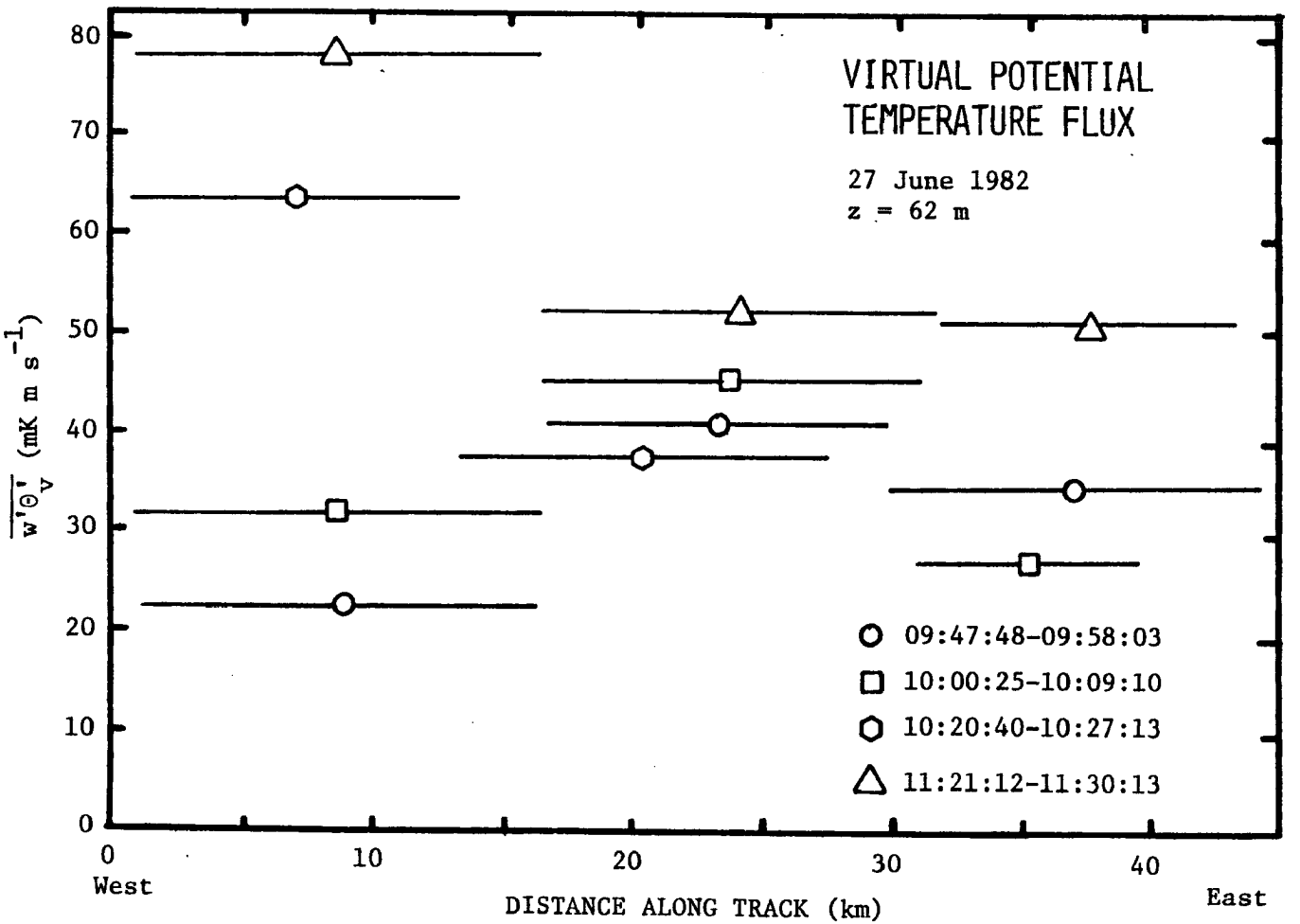

Fig. 32. Horizontal distribution of virtual potential temperature flux for flight R13 over forest. Length of segments indicates the distance over which the flux is averaged. Symbols represent the times of the segments.

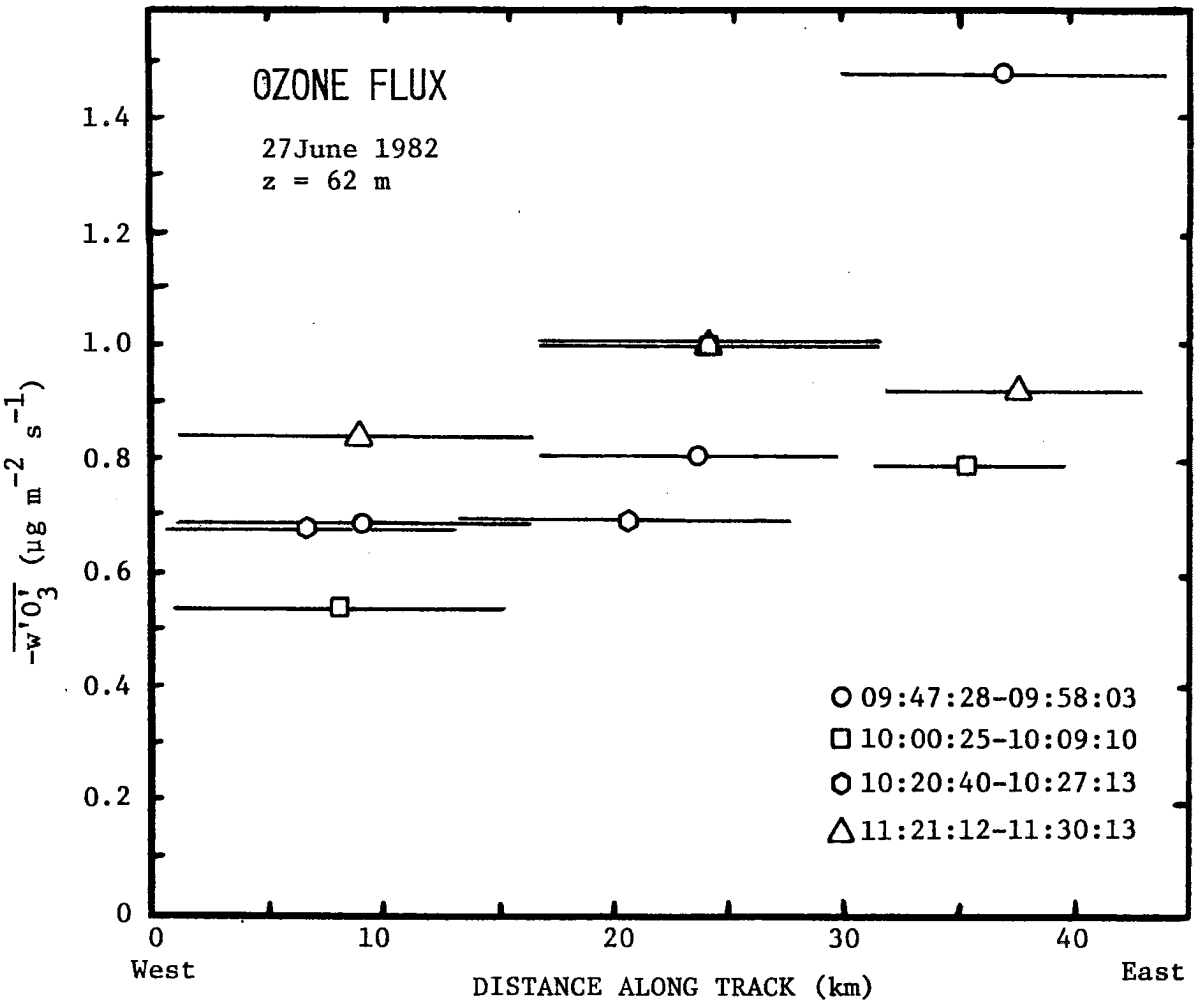

Fig. 33. Horizontal distribution of ozone fluxes for flight R13 over forest. Length of segments represents the distance over which the flux is averaged. Symbols indicate the times of the segments.

by the rate of destruction at the surface, while the moisture flux is controlled by distribution of water at the surface. Both of these factors are expected to have a strong dependence on the respiration of the vegetation. For example, different ecological group types or areas with different amounts of water available will transpire at different rates. It is generally accepted that destruction of ozone occurs on the cells in the stomatal openings of leaves. Observations in a chamber have demonstrated that ozone uptake is proportional to loss of water (Waggoner, 1975). This suggests that the magnitudes of ozone and water vapor flux ought to be highly correlated. Alternatively, as far as ozone variation is concerned, different plant types may emit characteristically different ozone-reactive hydrocarbons and modify the flux photochemically (Fitzjarrald and Lenschow, 1983). From study of a topographic map it appears that there are more streams at the west end. The western end is classified as flatland hardwood forest while the center portion is all lower slope hardwood/pine (Harcombe and Marks, 1979). Thus there is evidence here that flux measurements of this type may be useful in studying some of the finer points of the interaction between the forest and the overlying atmosphere.

5.5 Ozone Deposition

The aircraft flux measurements provide data for calculating the relevant ozone deposition parameters: surface flux, deposition velocity, aerodynamic resistance, and surface resistance. The methods of calculation are given in Sec. 4.5 above. Table 2 lists the deposition parameters measured in this experiment along with the results from several other experiments for comparison. The values calculated for Flight R12 (25 June 85) use a surface flux assumed to be 10% higher than

able 2. Ozone deposition parameters measured in the present study along with other measuremer
or comparison. Quantities are: surface flux $(\overline{w'O_3'})_o$, deposition velocity v_d, aerodynamic resi
a, and surface resistance r_s.

	$(\overline{w'O_3'})_o$ ($\mu g\ m^{-2}s^{-1}$)	v_d ($mm\ s^{-1}$)	r_a ($s\ m^{-1}$)	r_s ($s\ m^{-1}$)
exas Gulf Coast Forest				
3 June 82	-1.06	11	33.5	55.0
5 June 82	-0.87	11	37.8	55.7
7 June 82	-1.13	12	22.4	59.5
3 June 80*	-1.59	10	45	54
aize†	-0.2 to -1.2	2 to 8		90 to 370
oybeans#	-0.7	8	50	84
olorado Prairie				
June 80**	-0.58	6.7		
9 Sept 79††	-0.32	4.7	50	160
ulf of Mexico				
2 June 80*	-0.08	0.50	109	1890
orth Pacific				
Dec 80*	-0.05	0.57	60	1690

Lenschow et al., 1982; † Wesely et al., 1978; # Wesely et al., 1982; ** Pearson et al., 1982,
†† Lenschow et al., 1981.

the flux measured at 60 m. This was done since a complete flux profile was not available for this flight. The value of 10% was chosen as intermediate between values of the slopes measured on 23 and 27 June, but closer to that of 23 June since the mean profiles of 23 and 25 June are similar.

Over the forest, values for ozone surface flux and deposition velocity are relatively high while the surface resistance is low. The close agreement between all four forest measurements lends confidence to these values. These fluxes and deposition velocities are about twice that over crops and prairie, which are in turn about an order of magnitude larger than values over the ocean. This ordering is consistent with what would be expected from the large biomass and respiration of the forest crop canopy, and the low solubility of ozone in water.

5.5.1 Comparison to Previous Measurements

There are very few reported measurements of ozone deposition parameters over forest. The 1980 measurements (Table 2) reported by Lenschow et al. (1982) were obtained over the same general area as the present study. The remarkable agreement between those values, from 34 minutes of data, and the present study, obtained over roughly 7 hours, may, however, be fortuitous.

Greenhut (1983) has reported the results of a similar experiment, using the same ozone detector on a NOAA aircraft, over a pine forest in New Jersey. He found $r_s = 130$ s m^{-1} and $v_d = 6.4$ mm s^{-1} at 110 m AGL in daytime. Extrapolating his flux profile down nearer to the surface to better compare to these results might increase the deposition velocity

by 10 to 15% and decrease r_s by less than 10%. Thus most of the difference between measurements is likely due to different forest characteristics.

Hicks et al. (1982) did eddy correlation flux measurements over a pine plantation from a stationary tower. They mention that the daytime ozone deposition velocity was near 5 mm s^{-1} but put little emphasis on the ozone measurements. By comparison, Wesely et al. (1983) using a similar setup at a bare wintertime deciduous forest, report daytime deposition velocities from 2.3 to 4.5 mm s^{-1}. One might expect that ozone deposition would be significantly more rapid over an actively transpiring forest than other surfaces, due to the large amount of biomass and leaf area. In general the reported measurements agree with that trend (see Table 2), however, the values reported for other surfaces cover a range easily encompassing those for forests. Galbally (1971), using the profile method over dry soil with dry grass, and also over low, bush vegetation (z_o = 1.6 mm) reported deposition velocities ranging from 7 to 16 mm s^{-1} for 46 cases in near neutral conditions. He was unable to measure deposition velocities in unstable conditions with a satisfactory degree of confidence. As mentioned before, the profile method tends to fail in conditions of unmeasurably small vertical gradients. The conclusion of that paper holds that deposition velocity is approximately 10 mm s^{-1} for the considered surfaces in most conditions. Garland and Derwent (1979), find slightly lower mean values (v_d = 5.8 mm s^{-1}, r_s = 120 s m^{-1}) for 10-cm grass using the profile method. Van Dop et al. (1977) calculated still lower values (v_d = 1.3 mm s^{-1}) from measured profiles over dry grass. Note that this later value tends to agree with Galbally's measurements under stratification.

Ozone surface deposition parameters measured by the box method (Sec. 2.1) give an even wider range of values. Aldaz (1969) reports deposition velocities of 20 mm s^{-1} for juniper bush, 5 mm s^{-1} for sand or dry grass, and about 0.4 mm s^{-1} for sea water, while Hill (1971), finds v_d = 17 mm s^{-1} for alfalfa in a chamber with circulating air. Finally Galbally and Roy (1980) used the box method over grass to obtain values for the surface resistance ranging from 20 to 300 s m^{-1} (median value = 100 s m^{-1}) during daytime. In this same paper Galbally and Roy estimate the surface resistance to ozone uptake by forests to be 110 s m^{-1} in early morning, increasing to 380 s m^{-1} late in the day. These estimates assumed that the resistance to ozone uptake is the same as that for water vapor emission through the leaf stomata. The present study tends to support ozone deposition values lower than Aldaz (1969) and Hill (1971) but greater (lower resistance) than those of Galbally and Roy (1980).

5.6 Budgets

The scalar budgets for potential temperature, absolute humidity and ozone concentration are calculated according to the methods described in Sec. 4.4. In a cloud-free boundary layer it is expected that the net internal source/sink term for sensible heat and water vapor will be zero if the conditions of homogeneity and stationarity are met. Previous experiments (Lenschow et al., 1981, 1982; Pearson et al., 1982) have shown that this assumption is approximately true within measurement errors. The budgets over the Texas forest indicate, however, that this is not always the case.

The scalar budgets in Table 3 illustrate the different natures of the three cases. Clearly advection is not an important process for

TABLE 3

POTENTIAL TEMPERATURE BUDGETS (C hr^{-1})

Flight	$\frac{\partial \bar{\Theta}}{\partial t}$	$-\bar{u}\frac{\partial \bar{\Theta}}{\partial x}$	$\frac{\partial \overline{w'\Theta'}}{\partial z}$	Q_Θ
R5	0.08	-0.003	-0.06	0.01
R10	0.83	0.01	-0.66	0.18
R13	1.15	0.11	-0.79	0.47

ABSOLUTE HUMIDITY BUDGETS (mg m^{-3} s^{-1})

Flight	$\frac{\partial \bar{Q}}{\partial t}$	$-\bar{u}\frac{\partial \bar{Q}}{\partial x}$	$\frac{\partial \overline{w'Q'}}{\partial z}$	Q_Q
R5	0.01	0.01	0.003	0.02
R10	-0.16	-0.004	0.07	-0.09
R13	-0.26	0.13	0.06	-0.07

OZONE CONCENTRATION BUDGETS (ng m^{-3} s^{-1})

Flight	$\frac{\partial \bar{O}_3}{\partial t}$	$-\bar{u}\frac{\partial \bar{O}_3}{\partial x}$	$\frac{\partial \overline{w'O_3'}}{\partial z}$	Q_{O_3}
R5	-0.09	0.07	0.01	-0.01
R10	1.17	0.05	0.13	1.35
R13	2.38	-3.58	8.31	7.11

either Flight R5 or R10 in any of the budgets. The boundary layer wind speed on these days was very low, implying a fairly long residence time of the air in the boundary layer over the respective surfaces. For Flight R13 wind speeds and advection are significant from the direction of the Houston urban area. The advective term is of comparable magnitude with the other terms in each of the R13 budgets. Comparing the potential temperature budgets, we see in Flight R5 each of the terms is small and the budget is very close to balanced. Flight R10 would require an internal heat source of about 0.18 °C hr^{-1} to balance the time change and divergence terms. Flight R13 would require a heat source of 0.47 °C hr^{-1} to balance the time change, divergence, and additional cooling by advection. The heat source calculated for these two forest cases is not negligible, and may represent divergence of the net radiative flux in the planetary boundary layer.

Comparing the absolute humidity budgets, we find R5 is nearly balanced while the forest cases have residual sink terms which are roughly the same in magnitude as the measured terms. No explanation is available for the existence of these relatively large water vapor sinks. It is known that water vapor is very inhomogeneously distributed through-out the planetary boundary layer and consequently the horizontal gradients are difficult to measure. These could violate the assumption of horizontal homogeneity, or lead to an inaccurate estimation of the advection term. Water vapor budgets reported in Lenschow et al. (1981) and Pearson et al. (1982) balanced more closely than these but they were measured in a much drier climate in northeastern Colorado.

The source/sink term in the ozone budget represents the net production/destruction of ozone in the boundary layer. During daytime

this process is dominated by photochemistry. For the R5 case we find this term to be essentially zero. The R10 budget results in a source term equivalent to a production of about 2 ppb hr^{-1}. This is a relatively small rate, several times less than the other forest case, and about half that measured over eastern Colorado short grass prairie which is considered to be a fairly clean rural site (Lenschow et al., 1981, Pearson et al., 1982). The reason for this small source term in R10 appears to be the lack of both significant local sources of ozone-producing precursors and advection of them from the Houston urban area. The combination of an active surface sink together with a low concentration of precursors make this a relatively ozone-clean environment during the times of this study. The low net production exists in spite of the fact that emissions from the forest could be a major source of reactive hydrocarbons which are possible ozone-producing precursors (Dimitriades, 1981). The R13 ozone budget shows much more activity in all terms relative to the other flights. The mean concentration is increasing fairly rapidly (about 5 ppb hr^{-1}), higher ozone air is being advected in, and there is a large flux divergence. The resulting source term is a production of about 14 ppb hr^{-1}. This production rate is possible in air rich in the photochemical precursors of ozone such as oxides of nitrogen, reactive hydrocarbons, and free radicals, which are produced in a large metropolitan area. Thus it appears that the air in the boundary layer over the forest on this day is representative of a polluted urban air mass several hours downstream.

5.7 Radiation Flux Measurements

The research aircraft was equipped with radiometers to measure both upward and downward hemispheric longwave (terrestrial) and shortwave

(solar) radiative fluxes, thus allowing calculation of the net radiative flux and its divergence. A problem arises, however, when trying to do the measurements in a time varying or inhomogeneous cloud field, and steps must be taken to correct for the effects of cloud on the measurements. The flux component which most clearly shows the effect of clouds is the downward shortwave term (SW↓). Portions of the data from R5 and R10 taken in the immediate vicinity of clouds, as indicated by high variability in SW↓, were removed. Presumably this eliminated or minimized the effect of the evolving stratocumulus field observed during these flights. The dense cirrus cover during R13 was approximately steady state and homogeneous over the flight legs. To check this, variance statistics for two minute averaging times were compared for each flight, and in most cases they were close to constant during the flight.

An additional correction to the irradiance measurements arises from the fact that the aircraft flew at different angles of pitch and heading relative to the sun. The SW↓ irradiance measurements were normalized to a horizontal surface according to methods described in Sec. 4.6. The normalization was done assuming a range of diffuse/total fractions from 0 to 40% in order to test the sensitivity to this parameter. It was found that the difference in the solar fluxes was small, and the effect on the flux divergence almost zero. The results presented here use an assumed fraction of 20% diffuse sunlight for R5 and R10, and 40% for R13.

The flux measurement portions of the flights lasted about 3 hours so the solar flux to a plane surface also changed with the solar zenith

angle. To account for this, SW↑ and SW↓ were normalized to a median solar zenith angle for the flight. This procedure is detailed in Sec. 4.6.2.

5.7.1 Radiative Flux Data

Table 4 shows the resulting flux measurements averaged by altitude. Median flight times are given in parentheses. The trend of each flux with altitude is what would be expected in a well-mixed boundary layer with the exception of the two lower levels of the R13 longwave fluxes. These two levels are very close together, however, and the measurements are about the same within the error limits of the sensors. NCAR does not publish accuracy limits for these radiometers but is generally expected that they are within ± 5 to 10 W m^{-2}. From this it can be seen that the error in any net flux could be up to 40 W m^{-2}. If the instruments are stable and linear over the time and range of the measurements then the errors of accuracy will be small for the flux divergence which is the difference of the net flux. The flux at each altitude is the average over four legs of about 10 minute duration in most cases. The radiation time series are examined for any indication of a trend over the period which might be due to some instrument problem (e.g. salt buildup on the domes). Data are not included immediately after any change of altitude until the sensors have reached thermal equilibrium, which usually occurs within several minutes. One additional quality check is comparison of the LW↑ hemispheric sensor with the flux calculated from the measurement of the PRT-5. The PRT-5 measures the radiation temperature of the surface through a small acceptance angle

Table 4. Components of the radiative flux measured in June, 1982 in units of W m^{-2}. Median flight times are given in parentheses.

Flight	Alt (m)	$SW_{\downarrow}$	$SW_{\uparrow}$	Albedo	$LW_{\downarrow}$	$LW_{\uparrow}$	Net	Net Divergence
R5	939	705	43		342	442	562	.04 C hr^{-1}
(10:44)	314	656	31		385	460	550	
	41	645	30	.05	401	469	547	
R10	720	911	122		380	461	708	.11 C hr^{-1}
(13:27)	250	882	118		405	478	690	
	70	875	118	.14	411	483	685	
R13	437	643	88		385	462	477	.49 C hr^{-1}
(10:30)	113	605	86		398	471	446	
	73	564	82	.14	396	467	411	

and narrow bandwidth. The agreement between the two sensors is generally good, within 1% over uniform terrain at the lowest measured levels (15 to 70 m AGL).

Comparing Table 4 with Table 3 we see that the heating rate derived from the radiation profiles could account for a large part of the imbalance observed in the eddy flux budgets for each case. Including the measured radiative heating source term would bring the budgets for sensible heat much closer into balance.

5.7.2 Model Calculations

One mechanism of boundary layer heating arises from absorption of radiation by water vapor, carbon dioxide and ozone. This energy is rapidly transformed into heat. Radiative transfer calculations were made to estimate the magnitude of this heating. Aircraft sounding data for ozone, temperature, and moisture, nearby rawinsonde data and local climatology were input to the models of Cox and Griffith (1979). The forest flights used rawinsonde data from Lake Charles, LA. at 12 GMT (Greenwich Mean Time) and 00 GMT before and after the flights. The ocean flight used the sounding from Victoria, TX. The accuracy of this model in simulating radiative fluxes has been demonstrated by Cox and Griffith (1979) and Ackerman and Cox (1982). An updated parameterization of the water vapor continuum (Roberts, 1976) was incorporated into the IR transfer model to more accurately determine boundary layer fluxes.

The first runs were done for a cloud-free atmosphere. Even for this upper-limiting case the only possible heating at the level of the boundary layer was SW↓ absorption by water vapor. The highest calculated rate was 0.11 °C hr^{-1}. In all cases the calculated SW heating

was more than overcome by calculated LW cooling in the lower troposphere. The clear-sky calculations gave net cooling of 0.02 to 0.08 °C hr^{-1} for the three cases below 850 mb.

The model radiative fluxes did not agree well with the measurements except for LW↑ . This appears to be due to the presence of clouds during the experiment. In order to get a better comparison between modeled and measured fluxes cloud layers were introduced into the model as depicted in Fig. 35. Since there is no quantitative data on the physical composition, and very little information on the distribution of the clouds, the model cloud characteristics were adjusted until the flux components at the upper levels matched the measurements as well as possible. Sounding information and observations were used as guidelines where available. Both the model-generated profiles and observations are given in Figs. 34 and 35.

For flight R5 (ocean), both the model and the measurements suggest very small heating/cooling in the boundary layer, certainly well within the error limits of the respective values (Fig.34). The model net profile predicts a slight cooling, while the observations show no heating or cooling within the boundary layer. The difference between the modeled and observed net fluxes in the boundary layer is the result of a difference in the SW component as shown in Fig. 35. The likely cause of this difference is backscattering at the top of the boundary layer by clouds and possibly marine aerosol haze.

Flight R10 is a rural case. The slopes of the measured and calculated net profiles (Fig. 34) suggest a slight warming in the lower 700 m of the boundary layer, although the difference may not be significant. Inspection of the SW profile (Fig. 35) indicates that this heating is a

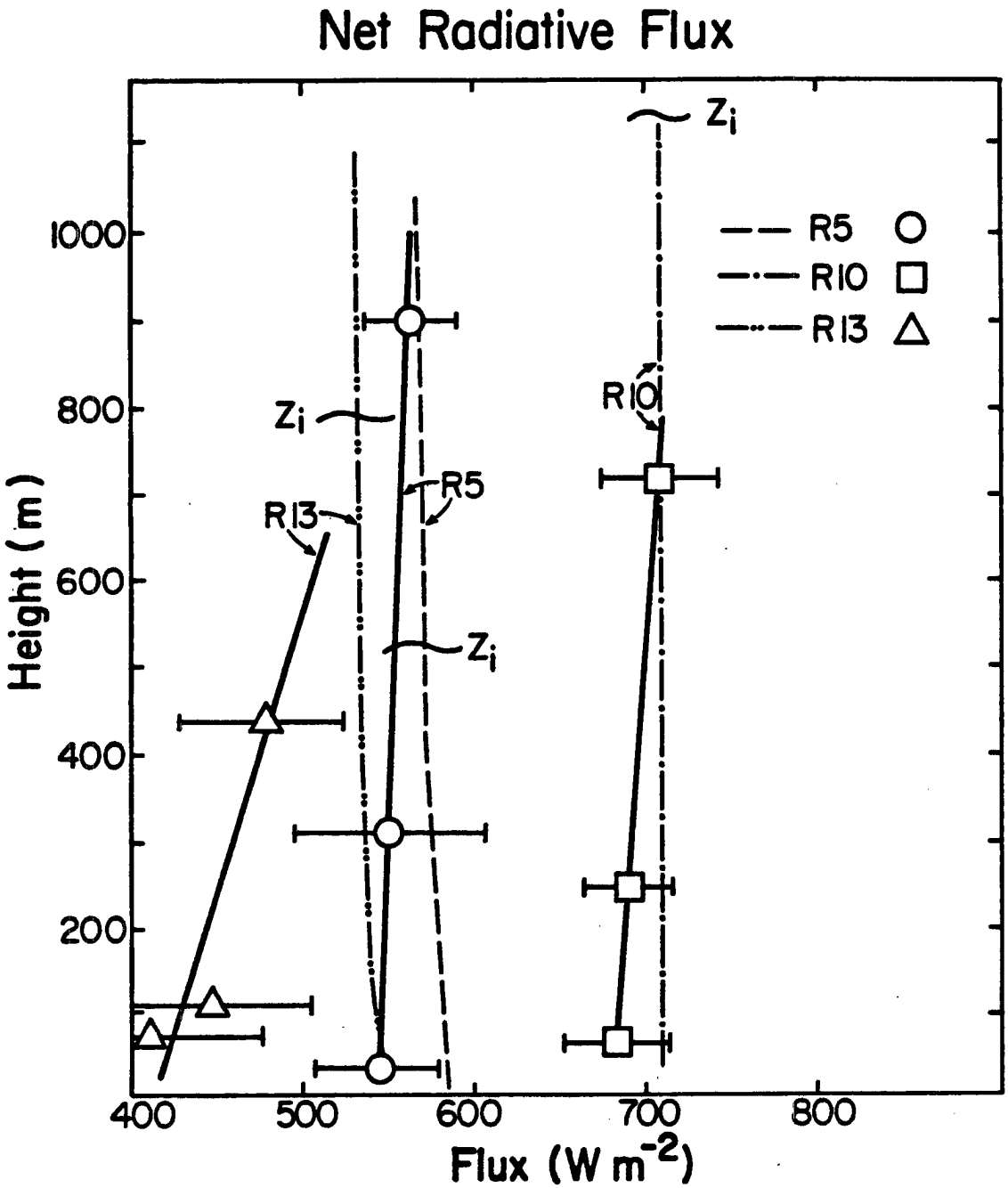

Fig. 34. Net radiative flux profiles for flight R5 over ocean and R10 and R13 over forest. Broken lines are model-generated profiles and solid lines are fit to the measured data points. z_i denotes the depth of the boundary layer for each flight. Error bars are ± 1 standard deviation from the mean measured flux.

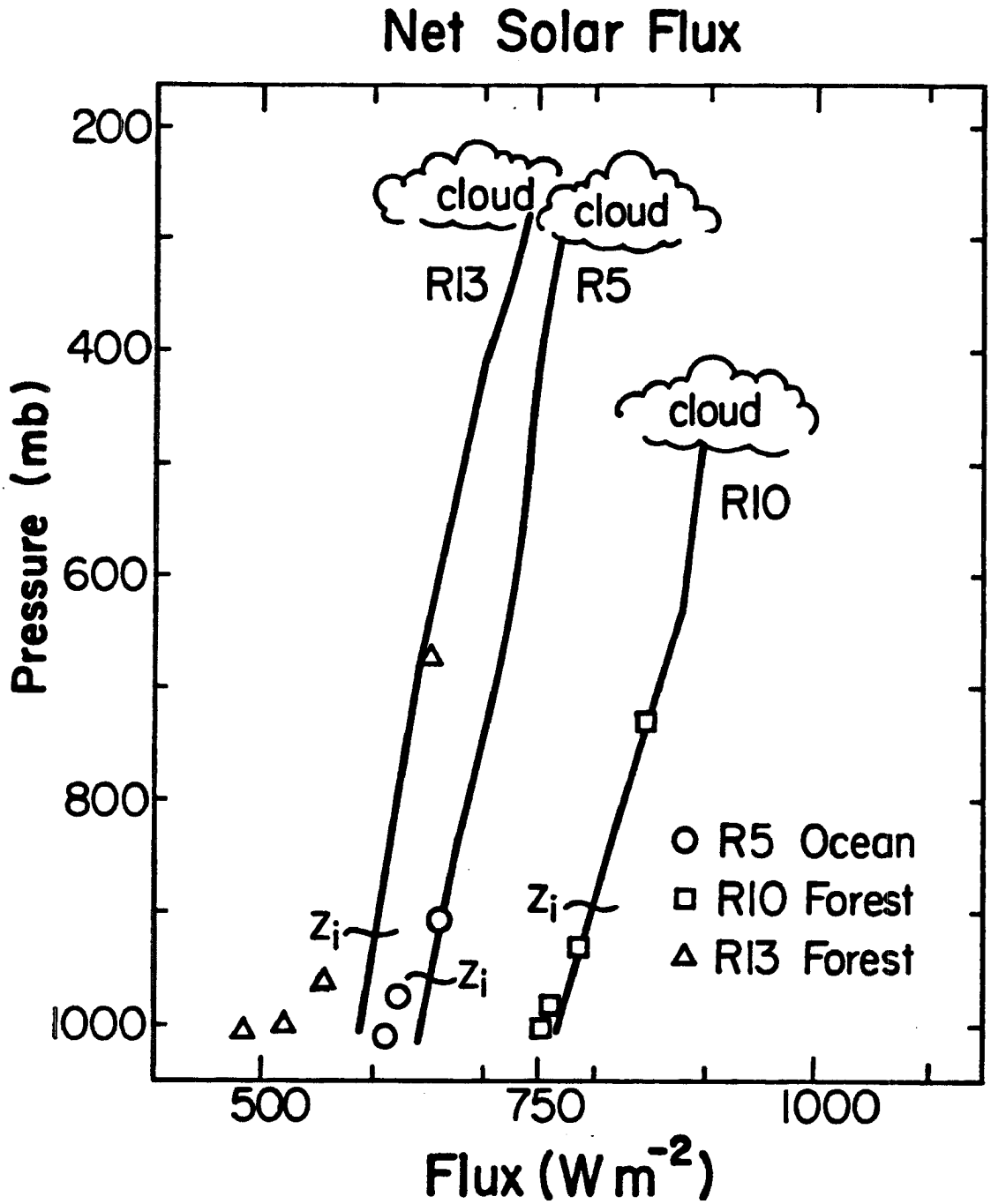

Fig. 35. Net solar component of the radiative flux in the troposphere. Solid lines are model-generated profiles.from the same run as Fig. 34 minus the longwave component. Symbols denote measured fluxes. z_i is the observed height of the boundary layer. Cloud symbols represent the location of cloud layers input to the radiative transfer model.

result of enhanced SW absorbtion. Note that there is good agreement between the measured and calculated SW fluxes at 925 mb, below cloud base, suggesting that cloud effects on the measurements were eliminated effectively.

Flight R13 is a rural case under the influence of an aged and diluted urban plume. Differences between the measured and modeled profiles are difficult to explain by measurement uncertainties. The substantial boundary layer heating appears to be the result of enhanced absorption at solar wavelengths as seen in Fig. 35.

5.7.3 Aerosol Characteristics

The key to understanding the results of this experiment may well lie in the radiative properties of the boundary layer aerosol. Unfortunately the aircraft could not support simultaneous chemical, meteorological, and aerosol measurements. Thus there are no data on composition, size, or distribution of the aerosol. General characteristics of the boundary layer aerosol for these flights can be inferred, however, from what we know about the meteorological condition at the time.

During the morning flight R5 winds throughout the boundary layer were 2 to 2.5 m s^{-1}, the nearest land was 180 km away and the nearest urban center was 240 km distant. The air in the flight area probably had a residence time of at least 24 hours over open ocean, since the wind direction varied from SW to NW. Pruppacher and Klett (1978) estimate a residence time of 0.5 to 2 days for aerosol below 1.5 km. We are concerned with only the lower 600 m and in a very humid atmosphere the residence time decreases rapidly with the increase in particle size (Hanel, 1977). The aerosol in the boundary layer of flight R5 was

probably marine in characteristics. It is unlikely that urban or rural aerosol made up a significant part of the particle inventory for this case. The maritime aerosol model of Shettle and Fenn (1979) consists of two components: a sea-salt component and a continental component similar to a rural aerosol without the larger particles assumed lost to fallout. It seems reasonable to assume such a distribution was present during flight R5. Shettle and Fenn give tables of single scatter albedo defined by:

$$a = \frac{\sigma_{scat}}{\sigma_{abs} + \sigma_{scat}} = \frac{\sigma_{scat}}{\sigma_{ext}}$$

Here σ_{ext} is the total extinction cross section equal to the sum of σ_{scat} the scattering cross section and σ_{abs} the absorption cross section. The relative humidity (RH) at 1000 mb, determined from the aircraft soundings, was about 80% for flight R5. At this humidity, values of $\underline{a}$ range from 0.89 to 0.99 for maritime aerosol at wavelengths 0.2 to 2.8 μm. For RH ranging from 0 to 0.99 the absorption by the maritime aerosol is at most only a few percent of the total extinction.

The opposite case appears in flight R13 over the forest. On 27 June boundary layer winds were moderate (4 to 10 m s^{-1}) from the direction of Houston 55 km to the west. The boundary layer on this day exhibited characteristics of an urban plume several hours old, as evidenced by the large source for ozone in Table 3. Using the 'urban' aerosol model of Shettle and Fenn at 70% RH we find $\underline{a}$ values range from 0.39 to 0.70. Absorption and scattering are roughly of the same magnitude for this 'sooty' model at solar wavelengths of radiation. The absorption attenuation coefficients range from 0.14 to 0.02 km^{-1} in the SW. Assuming that the incident solar radiation at the top of the

boundary layer is that given by the model calculations, and the spectral distribution is the same as at the top of the atmosphere (Thekaekara and Drummond, 1971), heating rates would be about 0.2 °C hr^{-1}. Also it should be noted that this model uses a 'sooty' component of 20% of the aerosol. The actual aerosol during the flight may well have a different composition or size distribution which could have a large effect on the actual attenuation. Hanel (personal communication) has estimated that heating rates over industrial Frankfurt are up to 1 hr^{-1} by aerosol absorption near noontime. Urban measurements by Waggoner et al. (1981) also agree with this range of absorption.

Flight R10 provides an intermediate case to the other two. On this day winds were very light (0 to 2 m s^{-1}) and variable in direction. The air probably had a fairly long residence time over the forest (12 to 24 hours) and was well-mixed and washed-out by a large thunderstorm in the area on the previous day. Advection terms in the budgets for sensible heat, water vapor, and ozone are all small. Photochemical activity, as indicated by ozone production, is low level, typical of a clean rural site. Shettle and Fenn's (1979) rural aerosol model at 50% RH gives $\underline{a}$ values near 0.9 for the measured spectral range. Absorption coefficients are an order of magnitude less than the urban case. This seems to indicate that there might be small heating by aerosol absorption in this case, which is what is observed.

5.7.4 Discussion

The logical source of boundary layer heating that would explain these observations is absorption of sunlight by the graphitic components of the atmospheric aerosol. Graphitic aerosol is known to be a highly

efficient absorber of sunlight and virtually 100% of the absorbed energy is transmitted to the surrounding air as heat (Frank, 1973, Gray et al., 1976). Each of the cases examined here supports this conclusion.

In flight R5 (ocean) the measurement of a near zero net radiative flux divergence and a zero heat source term is consistent with a non-absorbing marine aerosol.

For flight R13, the evidence from both the radiative flux measurements and the sensible heat budget indicate significant heating of the air in the boundary layer, nearly 0.5 °C hr^{-1}. Radiative transfer calculations show that gaseous components are unlikely to explain the observations. Aerosol characteristics deduced for this flight yield heating rates very consistent with the measurement results.

The results of flight R10 are consistent with the other two cases, although the magnitudes are small enough not to be conclusive. The combination of the small radiative heat source, the small imbalance of the sensible heat budget, the absence of significant advection, and low rate of ozone production all tend to support the conclusions of the other cases.

6. SUMMARY AND CONCLUSIONS

6.1 Summary

We have seen that the processes probed by this experiment have direct importance to the plants and animals living at our earth-atmosphere interface. Measurements of ozone deposition to various surfaces, ozone production inferred from boundary layer budgets, and radiative flux and divergence are all important to our understanding of atmospheric science and chemistry. They are necessary to validate the use of computer models, to formulate accurate model parameterizations, to assess the impacts of pollution producing activities, and as a basis for further scientific progress in many, often unforseen, areas. We have demonstrated the utility and effectiveness of the methods used in this experiment. The eddy-correlation technique has once again proven to be a highly useful method for measuring fluxes in the convective boundary layer. The use of an aircraft, and the accompanying fast response, high resolution instruments, is a particularly effective method to probe the depths of the planetary boundary layer above forest surfaces. The capacity to make measurements throughout the depth of the boundary layer allows us to calculate the significant terms in the budget of an atmospheric scalar including the in situ source/sink term. This budget-flight method has been used successfully for budgets of ozone, sensible heat and water vapor. We have also been able to measure the major components of the atmospheric radiative flux and divergence with reasonable confidence, in spite of the many difficulties associated

with this method. Further, we have demonstrated with these results that the analogies and methods used to determine deposition parameters for ozone yield consistent results for a variety of conditions. The success we have had using the methods and techniques of this experiment is very encouraging for further study of a similar nature.

The experimental findings discussed above are quite numerous and very interesting. The vertical profiles have shown us that ozone concentration may be very inhomogeneously distributed even while potential temperature and water vapor vary in a more typical manner. The vertical profiles have also allowed us to calculate an entrainment velocity typical for the convective boundary layer and to observe occasional gradients in mean ozone concentration near the surface. Using spectral analysis we have found that in one case the boundary layer over the forest has apparently not yet evolved into well-mixed conditions before about 10:00 A.M. CDT. We have found, by analysis of flux profiles, that for the forest cases the heat and moisture flux divergences are very similar. The flux throughout the boundary layer for either case could be determined by specification of a surface flux and a slope. This surface flux appears to be closely related to the solar energy flux arriving at the surface. The ozone flux profiles in contrast, have shown that the flux above the surface may be very different for two cases even though the surface fluxes are similar. The very different divergences seem to occur in response to the mean vertical ozone distribution and possibily to interaction between advective and photochemical processes. The ozone flux over the ocean is found to be very nearly zero throughout the boundary layer.

Examination of the horizontal distribution of fluxes along a path over the forest has led to other findings. It has confirmed the fact that water vapor fluxes are not homogeneously distributed in the horizontal and decreased our confidence in the possiblility of accurately measuring water vapor budgets in such a moist region. Sensible heat and ozone fluxes are found to be better behaved in the horizontal but significant variability is still present. These fluxes at the lowest level, when averaged together, have given values for ozone surface deposition to forest that are consistent with each other and previous measurements.

The findings of the budget analysis for these flights are also significant. We have found that the sensible heat budgets do not necessarily balance to a source term near zero. We have found that advection from an urban area may have a large effect on the budgets of both heat and ozone. The ozone budgets over forest led to very different net source terms, one typical of a "clean" atmosphere and the other polluted.

The findings of the sensible heat budget led us to undertake analysis of the radiative fluxes measured during the experiment. The findings from this analysis show that the net flux may be divergent within the planetary boundary layer. We found the magnitude of heating implied by this divergence very nearly balanced the source term in the sensible heat budgets for each case. Use of a radiative transfer model predicted that the measured radiative flux divergence was not due to absorption by the gaseous components of the atmosphere. A model for optical

characteristics of atmospheric aerosol predicted heating amounts by aerosol absorption of sunlight that are consistent with the observations for each case.

6.2 Conclusions

The various findings of this experiment lead to several conclusions. In general one may conclude that a forest of the nature of the Big Thicket interacts strongly with processes occuring in the overlying planetary boundary layer. It is a very active sink for ozone, often more so than previously thought at least in convective conditions. It is also a large source of sensible heat and moisture and possibly other chemical species. Our findings show that the forest itself does not entirely determine the state of the boundary layer above and we may conclude that vertical distribution of scalars in and above the boundary layer as well as horizontal gradients created by the conditions surrounding the area are important influences.

In particular one of the most important conclusions of this experiment results from the findings in the heat budgets and radiative flux divergences. The net radiative source term in the heat budget may be significant in certain cases. The principle component of this heat source appears to be divergence of the solar radiative flux. Measurements of this type are not only possible but may be essential to a complete understanding of the energy budget in the planetary boundary layer.

The forest is a complicated case. The horizontal flux analysis and the spectral analysis lead us to several conclusions regarding the accuracy of the flux measurements. Caution must be used in interpretation of the flux measurements. Time series and spectra are necessary

to determine which data will give reliable flux estimates under the fundamental assumptions. Our analysis of the horizontal flux variation recommends that several, on the order of three to six individual flux estimates must be averaged together to get the mean. The consistent results for ozone surface deposition confirms this application. Also it appears that simple relationships such as ozone flux being proportional to negative water vapor flux may not hold for all cases. We may also conclude that data from the full depth of the boundary layer and above are needed to make sense of a given case.

6.3 Recommendations For Further Study

The findings of this experiment have raised several questions that naturally lead to recommendations for further research. The first of these is to determine the role of aerosol in determining the components of the boundary layer energy budget. Sampling for aerosol size, number distribution, and chemical composition, along with the existing measurements is needed.

Another unanswered question, which may be closely related to aerosol compositon and distribution, is the role of natural organic compounds emitted by trees versus the emission of man-made hydrocarbons. The proposal for inclusion of hydrocarbon and aerosol sampling has been addressed by the Clear Air Boundary Layer Experiment (CABLE) done in the same area of Texas in 1983. The results of this experiment should help answer these questons.

The high rate of ozone deposition to forest suggests that this surface may be a very active sink for other chemicals and aerosols as well. At present, instruments capable of measuring eddy fluxes of

nitric oxide from an aircraft have been developed, but have not been flown on light platforms due to weight and space limitations. Specific and fast response sensors for nitrogen dioxide are likely to be available in the near future. Including fluxes of these species would greatly enhance measurements of photochemically reactive trace gases. Other species of interest and importance, including reactive hydrocarbons and sulfure dioxide present formidible problems to developing fast response instrumentation, and eddy fluxes of these gases are not likely to be possible in the near future.

The variation among budgets for these cases indicates that a more systematic study of the differences between marine, rural, and urban cases should be attempted. Such an experiment would contribute greatly to our understanding of the relative impact of man-made and "natural" pollution. An area like the Big Thicket is nearly ideally situated to encounter advection from these three major air types.

The success of the measurements over ocean and forest naturally leads to the possibility of similar experiments over a wide variety of surfaces. Further work over oceans has been done in CABLE and will be done in the Chemistry, Dynamics, and Microphysics of the Stratocumulus Capped Mixed Layer off the California Coast (DYCOMS) experiment. DYCOMS will also provide many other mean chemistry measurements. Other forest surfaces of interest would be rain-forest or jungle, hardwood typical of northeast U.S. or any type with a large coverage globally. The only restraint appears to be finding enough terrain that is sufficiently flat. World-wide, the measurement possibilities for other surfaces are almost endless.

Halpern, P. and K. L. Coulson, 1976: A theoretical investigation of the effect of aerosol pollutants on shortwave flux divergence in the lower troposphere, J. Appl. Meteorol. 15, 464-469.

Hanel, G. 1977: Humidity effects on motion and Brownian Diffision of atmospheric particles computed from measured physico-chemical aerosol data, Pure Appl. Geophys., 115, 775-797.

Harcombe, P. A., and P. L. Marks, 1979: Forest vegetation of the Big Thicket National Preserve, Report to Office of Natural Sciences, Southwestern Region National Park Service, Sante Fe, NM.

Hicks, B. B. and M.L. Wesely, 1982: Some direct measurements of atmospheric sulfur fluxes over a pine plantation, Atmos. Environ., 16, 2899-2903.

Idso, S. B., 1981: An experimental determination of the radiative properties and climatic consequences of atmospheric dust under nonduststorm conditions,Atmos. Environ. 15, 1251-1259.

Junge, C. E., 1962: Global ozone budget and exchange between stratosphere and troposphere, Tellus, 14, 363-377.

Kaimal, J. C., J. C. Wyngaard, Y. Izumi, and C. R. Cote, 1972: Spectral characteristics of surface layer turbulence, Q. J. R. Meteorol. Soc., 98, 503-589.

Kaimal, J. C., J. C. Wyngaard, D. A. Haugen, O. R. Cote', Y. Izumi, S. J. Caughey, and C. J. Readings, 1976: Turbulence structure in the convective boundary layer, J. Atmos. Sci., 33, 2152- 2169.

Lamb, B., H. Westberg, G. Allwine, and T. Quarles, 1985: Biogenic hydrocarbon emissions from deciduous and coniferous trees in the United States, J. Geophys. Res., 90, 2380-2390.

Lenschow, D. H. 1970: Airplane measurements of planetary boundary layer structure, J. Appl. Meteorol., 9, 874-884.

Lenschow, D. H., 1982: Reactive trace species in the boundary layer from a micrometeorological perspective, J. Meteorol. Soc. Jpn., 60, 472-480.

Lenschow, D. H., 1972: The measurement of air velocity and temperature using the NCAR Buffalo Aircraft Measuring System, NCAR Technical Notes, National Center for Atmospheric Research Boulder, CO (Revised and reprinted November, 1981). NCAR-TN/EDD-74.

Lenschow, D. H., and P. L. Stephens, 1980: The role of thermals in the convective boundary layer, Boundary-Layer Meteorol., 19, 509-532.

Lenschow, D. H., A. C. Delany, B. B. Stankov, and D. H. Stedman, 1980a: Airborne measurements of the vertical flux of ozone in the boundary layer, Boundary-Layer Meteorol., 19, 249-265.

Lenschow, D. H. J. C. Wyngaard, and W. T. Pennell, 1980b: Mean-field and second-moment budgets in a baroclinic, convective boundary layer, J. Atmos. Sci., 37, 1313-1326.

Lenschow, D. H., R. Pearson, Jr., B. B. Stankov, 1981: Estimating the ozone budget in the boundary layer by use of aircraft measurements of ozone eddy flux and mean concentration, J. Geophys. Res., 86, 7291-7297.

Lenschow, D. H., R. Pearson, Jr., B. B. Stankov, 1982: Measurements of ozone vertical flux to ocean and forest, J. Geopys. Res., 87, 8833-8837.

Lenschow, D. H. and L. Kristensen, 1984: Uncorrelated noise in turbulence measurements, J. Atmos. Oceanic Technol., 2, 68-81.

Levy, H. II, J. D. Mahlman, W. J. Moxim, and S. C. Liu, 1985: Tropospheric Ozone: The role of transport, J. Geophys. Res., 90, 3753-3772.

Liou, K-N, and T. Sasamori, 1975: On the transfer of solar radiation in aerosol atmospheres, J. Atmos. Sci., 32, 2166-2177.

Liu, S. C., D. Kley, M. McFarland, J. D. Mahlman, and H. Levy II, 1980: On the origin of tropospheric ozone, J. Geophys. Res., 85, 7546-7552.

Matthews, R. D., R. F. Sawyer, R. W. Shefer, 1977: Interference in chemiluminescent measurements of NO and NO2 emissions from combustion systems Environ. Sci. Technol., 11, 1092-1096.

McBean, G. A., and M. Miyake, 1972: Turbulent transfer mechanisms in the atmospheric surface layer, Q. J. R. Meteorol. Soc., 98, 383-398.

Method, T. J., and T. N. Carlson, 1982: Radiative heating rates and some optical properties of the St. Louis aerosol, as inferred from aircraft measurements, Atmos. Environ., 16, 53-66.

Panofsky, H. A. and J. A. Dutton, 1984: Atmospheric turbulence: models and methods for engineering applications, Wiley-Interscience, New York.

Pearson, R. Jr., and D. H. Stedman, 1980: Instrumentation for fast response ozone measurements from aircraft, Atmos. Technol., 12, 51-55.

Pearson, R. Jr., B. F. Weber, D. H. Lenschow, and B. B. Stankov, 1982: Ozone flux and mean concentration budget over short-gras prairie, Second Syposium Nonurban Troposphere, AMS/AGU/NASA, Williamsburg, Virginia, May 25-28. Reprint Volume published by the American Meteorological Society, Boston, Massachusetts.

Pielke, R. A., 1984: Mesoscale Meteorological Modeling, Academic Press, Orlando, FL.

Prupacher, H. R. and J. D. Klett, 1978: Microphysics of Clouds and Precipitation, D. Reidel Publishing Company, Dordrecht, Holland.

Quarles, T., B. Lamb, and E. Robinson, 1980: Measurements of isoprene fluxes from a northeastern deciduous forest, presented at the Air Pollution Control Associating Meeting, March 17, 1980.

Raupach, M. R., 1979: Anomalies in flux-gradient relationships over forest, Boundary-Layer Meteorol., 16, 467-486.

Regener, V. H., and L. Aldaz, 1969: Turbulent transport near the ground as determined from measurements of the ozone flux and ozone gradient, J. Geophys. Res., 74, 6935-6942.

Roach, W. T., 1961: Some aircraft observations of fluxes of solar radiation in the atmosphere, Q. J. R. Meteorol. 87, 346-363.

Roberts, R. E., J. E. A. Selby, and L. M. Biberman, 1976: Infrared continuum absorption by atmospheric water vapor in the 8-12 ≤m window, Applied Optics, 15, 2085-2089.

Robinson, N. Ed, 1966: Solar radiation, Elsevier Publishing, Amsterdam, Netherlands.

Seiler, W., and P. J. Crutzen, 1980: Estimate of gross and net fluxes of carbon between the biosphere and the atmosphere from biomass burning, Clim. Change, 2, 208-247.

Sellers, W. D., 1965: Physical Climatology, The University of Chicago Press, Chicago.

Shettle, E. P. and R. W. Fenn, 1979: Model for the aerosols of the lower atmosphere and the effects of humidity variations on their optical properties, report # AFGL-TR-79-0214.

Singh, H. B., F. L. Ludwig, and W. B. Johnson, 1978: Tropospheric ozone: Concentrations and variabilities in clean remote atmospheres, Atmos. Environ., 12, 2185-2196.

Spyers-Duran, P. and D. Baumgardner, 1983: In flight estimation of the time response of airborne temperature sensors, 5th Symposium on Meteorological Observations and Instrumentation. April 11-15 1983. Toronto, Ont., Canada, Published by the American Meteorological Society, Boston, MA.

Tajchman, S. J., 1982: Comments on measuring turbulent exchange within and above forest canopy, Bull. Am. Meteorol. Soc., 62, 1550-1559.

Thekaekara, M.P. and A. J. Drummond, 1971: Standard values for the solar constant and its spectral components. Nature (London) Phys. Sci., 229, 6-9.

Waggoner, P. E., 1975: Micrometeorological Models, in Vegetation and the Atmosphere, J. L. Monteith, ed., Academic Press, London, 205-227.

Waggoner, A. P., R. E. Ness, N. C. Ahlquist, D. S. Covert, S. Will, R. J. Charlson, 1981: Optical characteristics of atmospheric aerosols, Atmos. Environ., 15, 1891-1909.

Welch, R. and W. Zdunkowski, 1976: A radiation model of the polluted atmospheric boundary layer, J. Atmos. Sci., 33, 2170-2184.

Wesely, M. L. and B. B. Hicks, 1977: Some factors that affect the deposition rates of sulphur dioxide and similar gases on vegetation, J. Air Pollut. Control Assoc., 27, 1110-1116.

Wesely, M. L., J. A. Eastman, D. R. Cook, and B. B. Hicks, 1978: Daytime variations of ozone eddy fluxes to maize, Boundary-Layer Meteorol., 15, 361-373.

Wesely, M. L., D. R. Cook, and R. M. Williams, 1981: Field measurements of small ozone fluxes to snow, wet, bare soil, and lake water, Boundary-Layer Meteorol., 20, 459-471.

Wesely M. L., J. A. Eastman, D. H. Stedman and E. D. Yalvac, 1982: An eddy-correlation measurement of NO2 flux to vegetation and comparison to O3 flux, Atmos. Environ., 16, 815-820.

Wesely, M. L., D. R. Cook, and R. L. Hart, 1983: Fluxes of gases and particulates above a deciduous forest in wintertime, Boundary-Layer Meteorol. 27, 237-255.

Wyngaard, J. C., W. T. Pennell, D. H. Lenschow and M. A. Le Mone, 1978: The temperature humidity covariance budget in the convective boundary layer, J. Atmos. Sci., 35, 47-58.

Zimmerman, P. R., 1979a: Testing of hydrocarbon emissions from vegetation, leaf litter, and aquatic surfaces, and development of a methodology for compiling biogenic emission inventories, Final Report, EPA-460/4-79-004, U. S. E.P.A., Office of Air Quality Planning and Standards, Research Triangle Park, N.C.

Zimmerman, P. R., 1979b: Determination of emission rates of hydrocarbons from indigenous species of vegetation in the Tampa/St. Petersburg, FL area, EPA 904/9-77-028, U. S. E.P.A, Region 4, 345 Courtland St., NE, Atlanta, GA, 30308.